Doctoral Dissertation
博士論文

Microscopic Theory of Thermoelectric Transport in Magnetic Fields: Application to Dirac Systems

（磁場中の熱電輸送に関する微視的理論：ディラック系への応用）

A Dissertation Submitted for the Degree of Doctor of Philosophy
July 2020
令和２年７月博士（理学）申請

Department of Physics, Graduate School of Science,
The University of Tokyo
東京大学大学院理学系研究科物理学専攻

Könye Viktor Arthur
コニェ　ヴィクトル　アートル

Abstract

In this dissertation we study the magnetotransport of Dirac systems. We present a microscopic formalism to calculate transport coefficients in finite magnetic fields in the framework of linear response theory. We distinguish the cases of low magnetic fields and high magnetic fields and study them separately.

At low magnetic fields, we show how the magnetoconductivity can be calculated in the linear order of the magnetic field. Assuming small scattering rates and treating the magnetic field as perturbation we give formulas for the Hall conductivity and longitudinal conductivity. In the lowest order of the scattering rate, we recover the result of the semiclassical Boltzmann transport theory. At the subleading order, we get quantum corrections in terms of the Berry curvature and the orbital magnetic moment. The terms containing the Berry curvature are consistent with the semiclassical theories that include the anomalous velocity, but the terms containing the orbital magnetic moment can not be described with the anomalous velocity. We apply this formalism to tilted Weyl semimetals and study the effects of the tilting on the magnetoconductivity. We show the appearance of a finite linear longitudinal magnetoconductivity and we discuss how the orbital magnetic moment affects this result.

At high magnetic fields, we describe a microscopic theory to calculate thermoelectric transport coefficients using impurity Green's functions calculated in the first Born approximation using screened charged impurities. We employ this formalism to study the transverse magnetoconductivity and magnetothermopower of three-dimensional massive Dirac materials in high magnetic fields. We focus on the effects of the mass term and we show the main differences that arise compared to the massless Dirac fermions. The different behavior is shown to be relevant at high magnetic fields or low charge carrier densities. We show that the electric conductivity is proportional to $\propto B^{-1}$ and this behavior does not change qualitatively in the case of a finite mass term. On the other hand we find that the mass term causes significantly different behavior in the Seebeck and Nernst coefficients that show a $\propto B^2$ dependence at high fields.

Acknowledgements

First of all, I would like to extend my deepest gratitude to my supervisor Prof. Masao Ogata for all his support and guidance during these three years of PhD research. Thank you for your patience and for always taking the time to discuss things with me. I am extremely grateful to Dr. Hiroyasu Matsuura, for all his help and insightful suggestions. I am deeply indebted to Mr. Ikuma Tateishi, who extended tremendous assistance with numerical calculations and all aspects of academic life. Special thanks to Dr. Kunio Tokushuku for helping me with both academic and everyday matters. I also wish to thank all the other members of the Ogata group. It was a great pleasure attending our weekly seminars and I appreciate all the fruitful discussions. Thank you for accepting me in the group and switching to English just for me.

Immeasurable thanks are extended to my dear friends Mr. Troy Stade and Mr. István Vona for helping me in proofreading this dissertation and related works.

I would like to acknowledge the financial support of the Ministry of Education, Culture, Sports, Science and Technology (MEXT) of Japan, which made my stay in Japan possible.

Last but not least, I would like to thank my family and friends for all their moral support and encouragement throughout my PhD. All my accomplishments would not have been possible without the relentless support of my parents and their profound belief in my abilities.

List of publications

- Part of Chapter 5 was published in
  V. Könye and M. Ogata, "Magnetoresistance of a three-dimensional Dirac gas," Phys. Rev. B 98, 195420 (2018).

- Part of Chapter 5 was published in
  V. Könye and M. Ogata, "Thermoelectric transport coefficients of a Dirac electron gas in high magnetic fields," Phys. Rev. B 100, 155430 (2019).

- Part of Chapter 4 was submitted to Phys. Rev. Research and posted in
  V. Könye and M. Ogata, "Microscopic theory of magnetoconductivity at low magnetic fields in terms of Berry curvature and orbital magnetic moment," arXiv:2006.15882, (2020)

Contents

Abstract **iii**

Acknowledgements **v**

List of publications **vi**

1 Introduction **1**
1.1 Theory of magnetotransport 1
1.1.1 Boltzmann transport theory 2
1.1.2 Linear response theory 3
1.1.3 Linear response theory in low magnetic fields 3
1.1.4 Linear response theory in high magnetic fields 4
1.2 Magnetotransport of Dirac systems 4
1.2.1 Experimental studies 5
1.2.2 Theoretical studies in low magnetic fields 8
1.2.3 Theoretical studies in high magnetic fields 9
1.3 Structure of the dissertation 10

2 Quantum systems in magnetic fields **13**
2.1 Clean system 13
2.1.1 General Hamiltonian and Green's function 13
2.1.2 Landau problem of a general Hamiltonian 15
2.1.3 Densities and currents 16
2.1.4 Chemical potential 19
2.2 Impurities 19
2.2.1 Dyson equation 19
2.2.2 Self-energy and scattering rate 21
2.2.3 Impurity potential screening 22

3 Transport in magnetic fields **25**
3.1 Current operators under external fields 25

3.2 Transport coefficients in magnetic fields . . . 26
3.2.1 Current-current correlation function . . . 27
3.2.2 Magnetization and Energy magnetization . . . 30
3.2.3 Transport coefficients . . . 30
3.3 Vertex correction . . . 33

4 Conductivity in low magnetic fields 37
4.1 Conductivity at zero magnetic field . . . 37
4.2 Linear order of the magnetic field . . . 39
4.2.1 Hall conductivity . . . 39
4.2.2 Longitudinal conductivity . . . 42
4.3 Tilted Weyl node . . . 45
4.4 Summary . . . 49

5 Relativistic electron gas 51
5.1 Model . . . 51
5.1.1 Chemical potential . . . 54
5.2 Impurity Green's function . . . 57
5.2.1 Screening . . . 57
5.2.2 Scattering rate . . . 59
5.3 Magnetoconductivity . . . 63
5.3.1 Hall conductivity σ_{xy} . . . 63
5.3.2 Conductivity σ_{xx} . . . 65
5.3.3 Vertex correction . . . 71
5.3.4 Magnetoresistance . . . 74
5.4 Magnetothermopower . . . 75
5.5 Summary . . . 80

6 Summary and outlook 85

A Matsubara summations 89
A.1 Matsubara summation with branch cuts . . . 89
A.2 Integrals of Green's functions . . . 91
A.3 Summations in Chapter 4 . . . 93

B Low field magnetoconductivity 95
B.1 Low magnetic field approximation . . . 95
B.2 Luttinger-Kohn representation . . . 97
B.3 Current-current correlation . . . 98

Bibliography 101

Chapter 1

Introduction

In this dissertation we study thermoelectric transport in magnetic fields. We develop a microscopic formalism to calculate magnetoconductivity and magnetothermopower in solid state systems. We apply this formalism to study the magnetotransport of Dirac systems in both low and high magnetic fields. Thermoelectric transport plays an essential role in solid state physics. Measuring transport properties of a material is one of the main tools used to get a deeper insight into the material. In a magnetic field these properties can be studied in a diverse manner (the basic transport effects in a magnetic field are reviewed in Fig. 1.1). The presence of a magnetic field gives rise to many exotic phenomena (e.g. quantum Hall effect, linear magnetoresistance and magnetothermopower in Dirac systems, chiral anomaly in Weyl semimetals etc.) This makes magnetotransport interesting to study and useful for both fundamental and applied research. Therefore, the theoretical understanding of magnetotransport is crucial for the study of solid state systems. This topic is extensively discussed in the literature with a long history of experimental and theoretical studies. Even recently, a lot of research is carried out in this area in connection with topological systems and the effects of the Berry curvature. In this chapter we review the theoretical and experimental work done to study magnetotransport, and clarify how these relate to the present dissertation.

1.1 Theory of magnetotransport

In this section we review the theoretical methods used to study magnetotransport in the literature. We point out the research relevant to our study, and discuss how our formalism fits into this picture. We divide the discussion into the low magnetic field

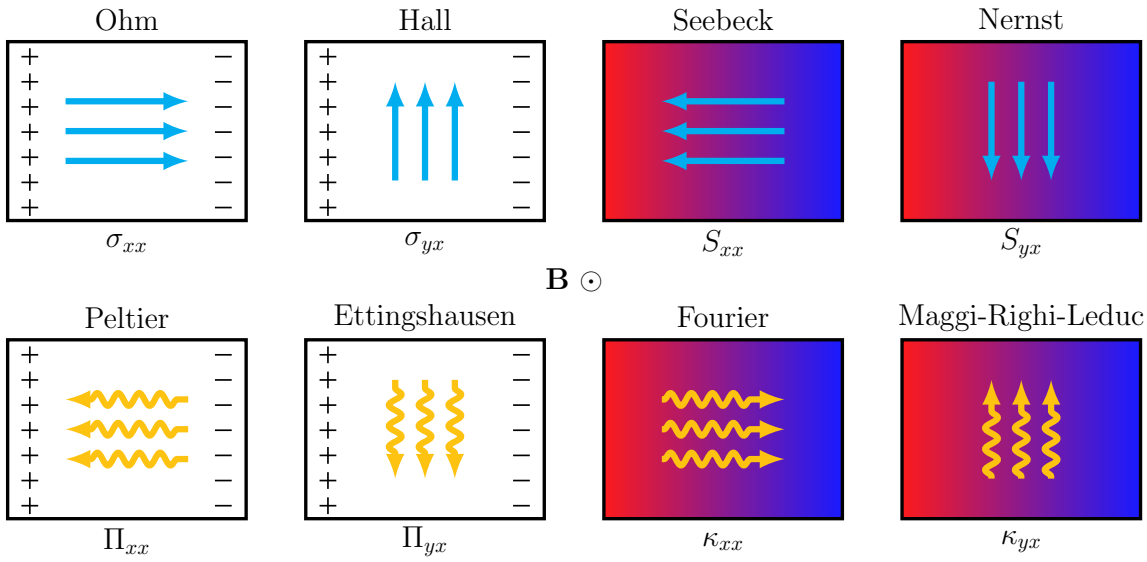

Figure 1.1: Transport effects in a magnetic field.

and high magnetic field methods, as these consist of significantly different approaches.

1.1.1 Boltzmann transport theory

A widely used and very successful theory to calculate transport is the semiclassical Boltzmann transport theory with relaxation time approximation [1, 2]. This was further improved after realizing the importance of the Berry curvature [3] in electric transport [4–8]. By introducing the so called anomalous velocity related to the Berry curvature, this theory had great success in describing several phenomena (e.g. anomalous Hall effect [9, 10] and quantum Hall effect [8]).

In finite magnetic fields the Boltzmann transport theory can be used to study the magnetoconductivity at low magnetic fields. If the anomalous velocity is taken into account, in a magnetic field several effects appear connected to the Berry curvature. In Ref. [11] they showed that in magnetic fields the Berry curvature modifies the phase-space density of states. Furthermore, the magnetoconductivity was shown to have a contribution coming from the Berry curvature [12–17], which can lead to a planar Hall effect [16], or a negative magnetoresistance without chiral anomaly [15].

1.1.2 Linear response theory

A very effective formalism to study transport in solid state systems is the linear response theory [18, 19]. A microscopic description of the electric conductivity using linear response theory was formulated by Kubo [20], where the conductivity is expressed using the current-current correlation. The extension of this theory to thermal transport coefficients was developed by Luttinger [21]. Following Luttinger's argument the calculation in magnetic fields had to be slightly modified by Smrčka and Středa [22] to include the magnetization and the so called energy magnetization [23]. In this work we base our formalism on these theories and extend it to multi-band Hamiltonians with random impurities. The details of this will be explained in Chapter 3.

In usual systems the thermoelectric transport coefficients can be expressed using only the zero temperature conductivity as a function of the chemical potential. These relations, from now on referred to as Sommerfeld-Bethe (SB) relations [24, 25], can be obtained from the Boltzmann transport equation. It was Jonson and Mahan [26] who first showed these relations microscopically for the case of a single-band Hamiltonian with static random potentials and static phonons. They also discussed the violation of the SB relations in the presence of electron-phonon interaction. The validity of the SB relations has been discussed in the presence of mutual interactions between electrons [24, 27]. In this dissertation we show that the SB relations are valid for a multi-band Hamiltonian in case of an external magnetic field and impurities.

In the absence of a magnetic field Karplus and Luttinger [28] showed that a finite magnetic moment leads to an anomalous Hall conductivity that is expressed by what we call Berry curvature nowadays. It was later shown that the same result can be achieved with the semiclassical Boltzmann theory with anomalous velocity [9, 10]. In the case of no magnetic field the connection of the microscopic theory to the Boltzmann theory was discussed in Ref. [29].

1.1.3 Linear response theory in low magnetic fields

Using linear response theory in magnetic fields is more challenging. For small magnetic fields a microscopic theory was developed by Fukuyama [30, 31]. The magnetoconductivity in linear order of the magnetic field is given as a formula containing velocity operators and Green's functions. In this thesis we start from this formalism, and evaluate it in a general manner and show how this leads to the Boltzmann result and

quantum corrections connected to the Berry curvature and orbital magnetic moment.

The formalism we describe in this dissertation shares similarities with the problem of orbital susceptibility. A well known method to calculate the orbital susceptibility is the Landau-Peierls formula [32, 33]. The same problem can be treated with microscopic calculations using linear response theory [34–37]. The microscopic theory was shown to contain the Landau-Peierls contribution with additional corrections [38–40]. This is analogous to our problem, but a big difference is that in the case of orbital susceptibility the scattering rate can be ignored, while in the case of magnetoconductivity it is essential to have finite results.

1.1.4 Linear response theory in high magnetic fields

In the case of high magnetic fields, the perturbative approach can no longer be applied. In order to have a quantum description the system has to be solved in the magnetic field and the Landau levels [32, 41] have to be utilized. One of the difficulties is that the magnetic field breaks the translational symmetry, so the Green's function is no longer diagonal in the momentum space. Furthermore, in the magnetic field impurities play an important role, and the proper treatment of the self-energy is crucial. A successful method to do this is the Born approximation. Using this formalism, the high magnetic field conductivity of graphene [42] and the Weyl Hamiltonian [43] was calculated. We detail these results in Dirac systems in the next section.

1.2 Magnetotransport of Dirac systems

In this section we review previous studies on three-dimensional Dirac systems. Almost a century passed since Dirac wrote down the equation named after him in 1928 [44], which played a very important role in understanding relativistic fermions in particle physics. Shortly after this, Weyl [45] showed that to describe massless fermions a simpler equation with two component fields can be used. These so called Weyl fermions were not yet found among the known elementary particles. However, in solid state systems electrons in a periodic potential can behave effectively as Weyl fermions. These effective massless electrons were first found in graphene after it was isolated in 2004 [46]. Following the discovery of several other two-dimensional massless fermions [47], they were also theoretically proposed in three dimensions [48–50] and later found exper-

imentally (for recent reviews see Ref. [51, 52]). Three-dimensional materials exhibiting massless fermions are topologically classified as Dirac or Weyl semimetals [53]. A simple continuum model to study Dirac and Weyl semimetals is the Weyl Hamiltonian with an effective speed of light [48–51].

In several Dirac systems the nodal point is gapped out, and this translates to a finite mass term in the effective model described by the 4×4 massive Dirac Hamiltonian [54–58]. These materials, hosting massive Dirac fermions are sometimes referred to as gapped Dirac materials, or massive Dirac materials in the literature [59–61]. A schematic representation for the different Dirac systems is shown in Fig. 1.2

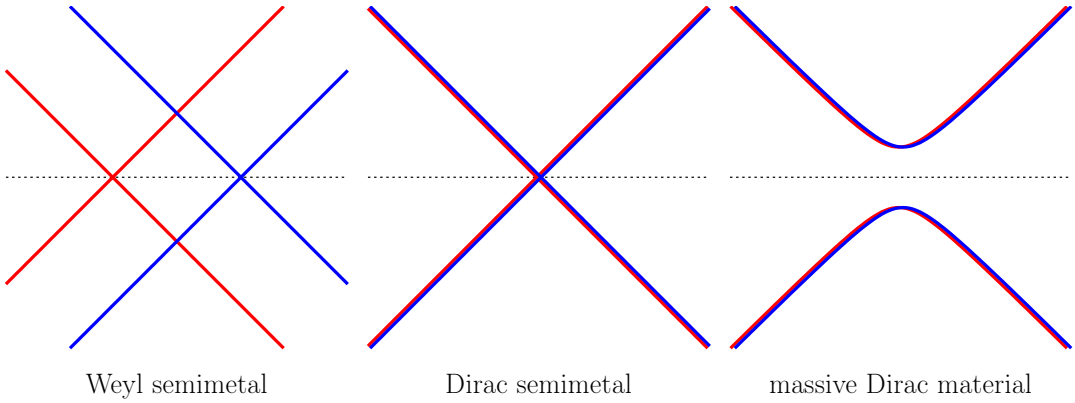

Figure 1.2: Schematic dispersion relation of Weyl semimetals, Dirac semimetals, and massive Dirac materials.

The thermoelectric transport in Dirac systems is an old problem, with the first studies carried out in connection with graphite [62] and bismuth [54]. Recently, with the discovery of new materials and experimental observation of interesting phenomena (e.g. negative magnetoresistance, linear magnetoresistance and magnetothermopower) there is a renewed interest in Dirac systems. In the last decade extensive research was carried out both experimentally and theoretically to understand three-dimensional Dirac systems. In the following we review these materials and the exotic transport properties associated with them.

1.2.1 Experimental studies

Some of the experimentally studied three-dimensional Dirac materials include Dirac semimetals: Cd_3As_2 [63–70], Na_3Bi [71–74], Weyl semimetals: TaAs [75, 76], NbAs [77], and massive Dirac materials: bismuth [55], $ZrTe_5$ [60, 78–80], Sr_3PbO [81],

$Pb_{1-x}Sn_xSe$ [82, 83].

Three-dimensional Dirac materials show a lot of exotic transport phenomena that are not present in usual systems nor in two-dimensional Dirac systems (for recent reviews see Refs. [84, 85]). One of these interesting features is the chiral anomaly and as a consequence negative magnetoresistance in Weyl semimetals. In Weyl semimetals Weyl nodes come in pairs with opposite chirality. In a magnetic field parallel to the electric field the chiral symmetry is broken leading to the chiral anomaly [86] (also called Adler-Bell-Jackiw anomaly [87, 88]). In transport measurements this leads to a negative longitudinal magnetoresistance [89, 90].

Another interesting and unique feature that seems to be present in all three-dimensional Dirac materials is a non-saturating linear transverse magnetoresistance [68, 69, 81, 90–95]. The linear magnetoresistance of the Dirac semimetal Cd_3As_2 measured in Ref. [68] is shown in Fig. 1.3. The effect persists to room temperature and shows no signs of saturation with the magnetic field. They also studied the Subnyikov de-Haas oscillations at low temperatures and showed that they are consistent with massless relativistic fermions.

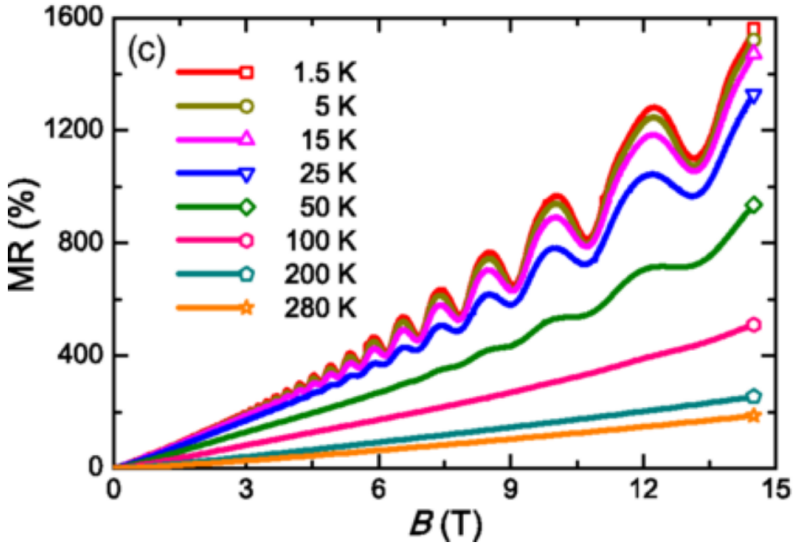

Figure 1.3: Linear magnetoresistance of Cd_3As_2 measured in Ref. [68] (Reprinted figure from Physical Review Letters).

This effect is not only present in massless Dirac systems but also appears in massive Dirac systems. The magnetoresistance of the massive Dirac material Sr_3PbO measured in Ref. [81] is shown in Fig. 1.4. They found the magnetoresistance to be large and

non-saturating with very little temperature dependence[1].

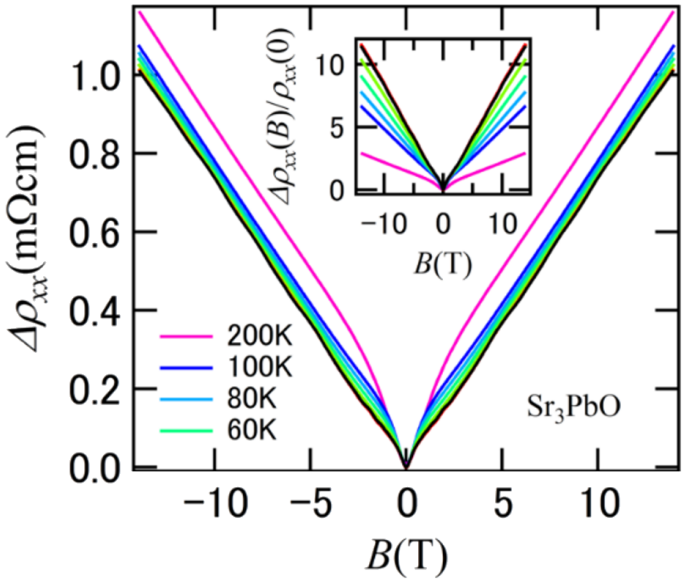

Figure 1.4: Linear magnetoresistance of Sr_3PbO measured in Ref. [81] (Reprinted figure from Physical Review B).

Furthermore, several thermoelectric experiments were carried out in an external magnetic field. Similarly to the magnetoresistance, the magnetothermopower at high magnetic fields was found to be increasing linearly with the magnetic field [80, 83, 96]. This results in a high thermoelectric figure of merit [97], which has very valuable applications in thermoelectric devices. The magnetothermopower of the massive Dirac material $Pb_{1-x}Sn_xSe$ measured in Ref. [83] can be seen in Fig. 1.5.

After reaching the quantum limit at $B \approx 10\,\mathrm{T}$ they found that the magnetothermopower increases linearly. The first Landau level manifests as a big jump in the magnetothermopower when the magnetic field is lowered below the quantum limit. The temperature dependence of the thermopower is close to linear at low temperatures.

At lower magnetic fields, the Nernst coefficient is found to be large, with an anomalous contribution [98–100]. This effect is predicted to be directly caused by the finite Berry curvature associated with the Weyl nodes [101, 102].

[1]This is also true for massless Dirac systems. The temperature dependence in Fig. 1.3 is due to the temperature dependence of the zero field resistivity which normalizes the magnetoresistance.

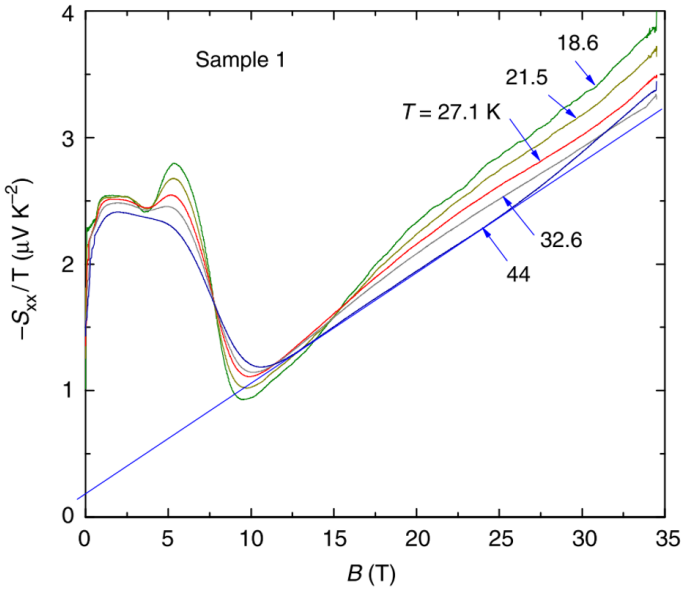

Figure 1.5: Linear magnetothermopower of $Pb_{1-x}Sn_xSe$ measured in Ref. [83] (Reprinted figure from Nature Communications).

1.2.2 Theoretical studies in low magnetic fields

The theoretical study of thermoelectric transport of three-dimensional Dirac systems is a diverse and extensively discussed problem in the literature. In the absence of a magnetic field several semiclassical and microscopic theoretical studies were carried out [103–105]. In a finite magnetic field the calculation becomes more challenging and in this section we review the methods and results found in the literature.

At low magnetic fields the most frequently used method to calculate transport of Dirac systems is the semiclassical Boltzmann theory with anomalous velocity. Several papers study the magnetoconductivity of Dirac and Weyl semimetals [12–14, 106, 107]. It was shown that the finite Berry curvature causes unusual phenomena in Dirac systems such as the negative magnetoresistance without the chiral anomaly [15, 17, 106] and the planar Hall effect [16, 107].

Furthermore, the semiclassical theory was also applied to study thermoelectric coefficients at low magnetic fields. For example the anomalous behavior of the Nernst coefficient is intensively studied with this method [101, 102, 108–111].

As for a microscopic calculation in low magnetic fields, linear response theory was used to study the Hall conductivity of two-dimensional Dirac systems [112, 113].

In this dissertation we employ the microscopic theory to study three-dimensional Dirac materials. We compare the formalism with the results of the Boltzmann theory, and study the quantum corrections that are not present in the semiclassical formulation. The details of this are described in Chapter 4

1.2.3 Theoretical studies in high magnetic fields

Next, we talk about the calculations performed in high magnetic fields. A formalism that was able to describe the linear magnetoresistance for Weyl semimetals was proposed by Abrikosov [43]. He used the first Born approximation to calculate the scattering rate and the Kubo formula for the conductivity. The important assumption of taking screened Coulomb potentials as impurities led to his result of linear magnetoresistance. He only studied the case with zero chemical potential and at very high magnetic fields where only the zeroth Landau level contributes to the conductivity.

More recent studies [114–116] revisited this calculation in more detail. It was shown that the screened Coulomb impurities used by Abrikosov are crucial for reproducing the linear behavior [115], since a completely different behavior is achieved for the simple case of short-range scatterers. In Ref. [114] Xiao et al. calculated the scattering rates for different Landau levels, and they showed that there is a Landau level dependence of the scattering rate. In their result they recovered the linear magnetoresistance for high magnetic fields, but at low fields they obtained a $B^{1/3}$ behavior. Also the effect of the first Landau level is very strong and gives a strong jump in the magnetoresistance. Klier et al. [115, 116] gave an analytic argument using the self-consistent Born approximation and several other approximations. They determined the scaling of the conductivity in the different magnetic field regimes. They recovered the linear background with Subnyikov de-Haas oscillations. The vertex correction in the massless case was investigated in Ref. [115], where they found that close to the Weyl point the effect of the vertex correction is negligible.

For the case of high magnetic fields, the Seebeck coefficient for the Weyl Hamiltonian was studied by Skinner and Fu [117] and was found to be linear and non-saturating at high fields. Their calculation is based on expressing the thermopower using the entropy density.

The above studies only discussed the massless case using the Weyl Hamiltonian. In the case of massive fermions, some older references [118, 119] discussed the prob-

lem in the context of astrophysics and thus the formalism and approximations are not exactly applicable for solid state systems. On the other hand, a recent study of the transverse magnetoresistance in gapped Dirac semimetals only used short-range scatterers and a very simple model for the scattering rate [120]. In the case of longitudinal magnetoresistance the self-consistent Born approximation was discussed in the case of short-range impurities in Ref. [61, 121]. However, as explained before, the choice of impurity potential is crucial. Therefore, in order to have a proper description for the massive Dirac fermions, the inclusion of the screening is inevitable.

Basing our research on Abrikosov's work we extend the formalism to thermoelectric transport and massive Dirac fermions. This gives a unified microscopic approach to study the transport coefficients of Dirac systems in high magnetic fields. In particular, we will give analytic formulas for the scalings in high magnetic fields which give novel predictions for the experiments. Our results are described in detail in Chapter 5.

1.3 Structure of the dissertation

First, in Chapter 2 we describe the basic formalism to study quantum systems in magnetic fields. This chapter creates the framework to the rest of the thesis and includes the necessary definitions and notations. We define the Hamiltonian, the Green's functions, the current operators and the chemical potential. We describe the method to calculate the impurity Green's function, using finite temperature Feynman diagrams. We give explicit expressions to calculate the screened impurity potential using the random phase approximation, and the scattering rate using the first-order Born approximation.

In Chapter 3 we discuss linear response theory in magnetic fields. We present a formalism to calculate the transport coefficients in terms of the current operators and Matsubara Green's functions. We discuss how the effect of impurities can be treated using the impurity Green's function, and give explicit expressions to calculate the vertex correction. We show that the Sommerfeld-Bethe relations hold, even in the presence of magnetic fields, thus the Mott formula and Wiedemann-Franz law are valid.

In Chapter 4 we derive a formula that expresses the magnetoconductivity at low magnetic fields. The contents of this chapter were published in Ref. [122]. We show how the microscopic theory of low field Hall conductivity developed by Fukuyama [30, 31] can be extended and used for general models. We evaluate the Hall conductivity and longitudinal magnetoconductivity in the low scattering rate limit in the linear order of the magnetic field. We discuss, how this result relates to the Boltzmann transport

theory, and show that in the microscopic calculation quantum corrections appear, that are not present in the Boltzmann theory.

In Chapter 5 we study the thermoelectric transport of a massive relativistic electron gas. The results of this chapter were published in Refs. [123] and [124]. We apply the formalism described in Chapters 2 and 3 to Dirac materials, using the Dirac Hamiltonian as a simple model. First, we solve the Landau problem of the system in a finite magnetic field. Then, we calculate the chemical potential, the screened impurity potential, and the scattering rate. Finally, we study the magnetic field and mass term dependence of the transverse components of the conductivity, and thermopower.

Throughout the dissertation we use units where $\hbar = 1$ (in some instances the $\hbar$ dependence will be shown explicitly).

Chapter 2

Quantum systems in magnetic fields

2.1 Clean system

In this section we discuss solid state systems in a finite magnetic field without any impurities. The effect of impurities will be discussed in the next section. We show how the Landau problem of a general Hamiltonian can be solved. We give expression to the Green's function, current operators, and chemical potential which will be extensively used in later parts of the dissertation.

2.1.1 General Hamiltonian and Green's function

As a general model for electrons in solid state systems under the influence of a magnetic field we can start with the Dirac Hamiltonian with periodic potential $V(\mathbf{x})$ and magnetic field $\mathbf{B}$ introduced using the vector potential $\mathbf{A}$ with minimal coupling ($\mathbf{p} \to \mathbf{p} + e\mathbf{A}$):

$$\mathbb{H}(\mathbf{p}, \mathbf{x}) = \gamma_0 \left[mc^2 + c\boldsymbol{\gamma}(\mathbf{p} + e\mathbf{A}) \right] + V(\mathbf{x}) \,, \tag{2.1.1}$$

where γ_μ are the Dirac matrices, m is the electron rest mass, c is the speed of light, and $e > 0$ is the elementary charge. Using the Foldy-Wouthuysen transformation [125] up to quadratic order in momentum, the Hamiltonian in a magnetic field becomes:

$$\mathbb{H}(\mathbf{p}, \mathbf{x}) = \frac{(\mathbf{p} + e\mathbf{A})^2}{2m} + V + \mu_B \boldsymbol{\sigma} \cdot \mathbf{B} + \frac{\hbar}{4m^2c^2} \boldsymbol{\sigma} \cdot [\boldsymbol{\nabla} V \times (\mathbf{p} + e\mathbf{A})] + \frac{\hbar^2}{8m^2c^2} \nabla^2 V \,, \tag{2.1.2}$$

where the first two terms are the classical Hamiltonian in a magnetic field, then there is the Zeeman term ($\mu_B = e\hbar/2m$ is the Bohr magneton), the spin orbit interaction, and finally the Darwin term.

In the absence of a magnetic field the Hamiltonian is periodic in real space and the system can be expressed with the following Bloch Hamiltonian:

$$\mathbb{H}_{\mathbf{k}}(\mathbf{p},\mathbf{x}) = \frac{(\mathbf{p}+\mathbf{k})^2}{2m} + V + \frac{\hbar}{4m^2c^2}\boldsymbol{\sigma}\cdot[\boldsymbol{\nabla}V\times(\mathbf{p}+\mathbf{k})] + \frac{\hbar^2}{8m^2c^2}\nabla^2 V\,. \tag{2.1.3}$$

This Hamiltonian acts on Bloch wave functions as:

$$\mathbb{H}_{\mathbf{k}}(\mathbf{p},\mathbf{x})\mathbf{u}_{a\mathbf{k}}(\mathbf{x}) = E_{a\mathbf{k}}\mathbf{u}_{a\mathbf{k}}(\mathbf{x})\,, \tag{2.1.4}$$

where, $\mathbf{u}_{a\mathbf{k}}(\mathbf{x})$ is a two-component vector which is periodic with the same period as $V(\mathbf{x})$, a denotes the band index, and the wave vector $\boldsymbol{k}$ is within the first Brillouin zone.

There are several methods to approximate this Hamiltonian with effective Hamiltonians [2], and in general the Bloch Hamiltonian becomes an $n\times n$ Hermitian matrix which is a function of only the quasi momentum:

$$\mathbb{H}(\mathbf{k})\,|a,\mathbf{k}\rangle = E_{a\mathbf{k}}\,|a,\mathbf{k}\rangle\ . \tag{2.1.5}$$

From this we can make an effective continuum model by substituting the quasi momentum with the real momentum $\mathbb{H}(\mathbf{p})$.

In effective models like these we can introduce the magnetic field in two ways. For small magnetic fields we can use the (2.1.2) Hamiltonian and treat the magnetic field as a perturbation. Then for the zeroth order Hamiltonian we can use the effective model. For high fields we can create a continuum model for the effective model and use minimal coupling ($\mathbf{p}\to\mathbf{p}+e\mathbf{A}$) directly on the effective model to introduce the magnetic field.

After solving the $\mathbb{H}(\mathbf{p},\mathbf{x})\,|a\rangle = E_a\,|a\rangle$ eigenvalue problem, the Matsubara Green's function can be expressed as [19]:

$$\mathbb{G}(i\omega_m) = \sum_a \frac{|a\rangle\langle a|}{i\omega_m+\mu-E_a}\,. \tag{2.1.6}$$

In later sections we will use several representations of this Green's function. Using the wave functions defined as $\boldsymbol{\phi}_a(\mathbf{x}) := \langle\mathbf{x}|a\rangle$, the Green's function in the coordinate

representation becomes:

$$\mathbb{G}(\mathbf{x},\mathbf{x}',i\omega_m)=\sum_a \frac{\boldsymbol{\phi}_a(\mathbf{x})\boldsymbol{\phi}_a^\dagger(\mathbf{x}')}{i\omega_m+\mu-E_a}\,. \tag{2.1.7}$$

Using the Fourier transform of the wave functions $\boldsymbol{\phi}_{a\mathbf{q}}=\int \mathrm{d}^3x\,\mathrm{e}^{-i\mathbf{qx}}\boldsymbol{\phi}_a(\mathbf{x})$ the Green's function in the momentum representation is expressed as:

$$\mathbb{G}_{\mathbf{qq}'}(i\omega_m)=\sum_a \frac{\boldsymbol{\phi}_{a\mathbf{q}}\boldsymbol{\phi}_{a\mathbf{q}'}^\dagger}{i\omega_m+\mu-E_a}\,. \tag{2.1.8}$$

Finally, in the eigenstate representation the Green's function is diagonal:

$$G_{ab}(i\omega_m)=\frac{\delta_{ab}}{i\omega_m+\mu-E_a}=:\delta_{ab}G_a(i\omega_m)\,. \tag{2.1.9}$$

The connections between these representations are:

$$\mathbb{G}(\mathbf{x},\mathbf{x}',i\omega_m)=\frac{1}{V^2}\sum_{\mathbf{q},\mathbf{q}'}\mathrm{e}^{i\mathbf{qx}}\mathbb{G}_{\mathbf{qq}'}(i\omega_m)\mathrm{e}^{-i\mathbf{q}'\mathbf{x}'}\,, \tag{2.1.10a}$$

$$\mathbb{G}(\mathbf{x},\mathbf{x}',i\omega_m)=\sum_{a,b}\boldsymbol{\phi}_a(\mathbf{x})G_{ab}(i\omega_m)\boldsymbol{\phi}_b^\dagger(\mathbf{x}')\,, \tag{2.1.10b}$$

$$\mathbb{G}_{\mathbf{qq}'}(i\omega_m)=\int \mathrm{d}^3x\,\mathrm{d}^3x'\,\mathrm{e}^{-i\mathbf{qx}}\mathbb{G}(\mathbf{x},\mathbf{x}',i\omega_m)\mathrm{e}^{i\mathbf{q}'\mathbf{x}'}\,, \tag{2.1.10c}$$

$$\mathbb{G}_{\mathbf{qq}'}(i\omega_m)=\sum_{a,b}\boldsymbol{\phi}_{a\mathbf{q}}G_{ab}(i\omega_m)\boldsymbol{\phi}_{b\mathbf{q}'}^\dagger\,, \tag{2.1.10d}$$

$$G_{ab}(i\omega_m)=\int \mathrm{d}^3x\,\mathrm{d}^3x'\,\boldsymbol{\phi}_a^\dagger(\mathbf{x})\mathbb{G}(\mathbf{x},\mathbf{x}',i\omega_m)\boldsymbol{\phi}_b(\mathbf{x}')\,, \tag{2.1.10e}$$

$$G_{ab}(i\omega_m)=\frac{1}{V^2}\sum_{\mathbf{q},\mathbf{q}'}\boldsymbol{\phi}_{a\mathbf{q}}^\dagger\mathbb{G}_{\mathbf{qq}'}(i\omega_m)\boldsymbol{\phi}_{b\mathbf{q}'}\,. \tag{2.1.10f}$$

2.1.2 Landau problem of a general Hamiltonian

We assume a Hamiltonian expressed as an $n\times n$ Hermitian matrix which is a function of the momentum $\mathbb{H}(\mathbf{p})$. The magnetic field points in the z direction $\mathbf{B}=(0,0,B)$ and we fix the gauge to the Landau gauge, with the vector potential expressed as $\mathbf{A}=(0,Bx,0)$. In the magnetic field the momentum is $\boldsymbol{\pi}=\mathbf{p}+e\mathbf{A}$. Using this momentum and the canonical commutation relations $[x_\alpha,p_\beta]=i\delta_{\alpha\beta}$ the following bosonic operator

can be defined:

$$a := \frac{\ell_B}{\sqrt{2}}(\pi_x - i\pi_y)\,, \qquad \left[a, a^\dagger\right] = 1\,, \tag{2.1.11}$$

where $\ell_B = \sqrt{\hbar/eB}$. The backwards relations are:

$$\pi_x = \frac{1}{\sqrt{2}\ell_B}(a + a^\dagger)\,, \qquad \pi_y = \frac{i}{\sqrt{2}\ell_B}(a - a^\dagger)\,, \qquad \pi_z = p_z\,. \tag{2.1.12}$$

This representation can be used in several systems to diagonalize the Hamiltonian easily. The $a^\dagger a$ combination can be diagonalized in the usual way for bosonic operators ($a^\dagger a\,|n\rangle = n\,|n\rangle$). Every $\mathbb{H}(\boldsymbol{\pi})$ Hamiltonian can be expressed as $\mathbb{H}(a, a^\dagger, p_z)$, and the $|n, p_y, p_z\rangle$ states can be used to find the solution to the eigenvalue problem using:

$$a\,|n, p_y, p_z\rangle = \sqrt{n}\,|n-1, p_y, p_z\rangle\ , \quad a^\dagger\,|n, p_y, p_z\rangle = \sqrt{n+1}\,|n+1, p_y, p_z\rangle\ . \tag{2.1.13}$$

The normalized wave functions of the $|n, p_y, p_z\rangle$ states can be expressed as:

$$\langle x|n, p_y, p_z\rangle = \frac{i^n}{L} h_n\left(x + \ell_B^2 p_y; \ell_B\right) \mathrm{e}^{ip_y y} \mathrm{e}^{ip_z z}\,, \tag{2.1.14}$$

where $L^3 = V$ is the volume of the system and h_n are the orthonormal Hermite-functions:

$$h_n(x; \ell_B) := \frac{(\ell_B^2\pi)^{-1/4}}{\sqrt{2^n n!}} \exp\left(-\frac{x^2}{2\ell_B^2}\right) H_n\left(\frac{x}{\ell_B}\right)\,, \tag{2.1.15}$$

where $H_n(x)$ are the Hermite-polynomials. As the Hamiltonian does not depend on p_y it can be shown that each Landau level is $L^2/2\pi\ell_B^2$-fold degenerate in p_y.

2.1.3 Densities and currents

In this section, we derive the current operators of a general non-interacting multi-band Hamiltonian based on the continuity equation (a similar derivation can be found in Ref. [18]). For an arbitrary single-particle Hamiltonian ($\mathbb{H}$) the many-body Hamiltonian can be written as:

$$\mathcal{H} = \sum_{a,b} \int \mathrm{d}^3x\, \Psi_a^\dagger(\mathbf{x}) H_{ab}(\mathbf{p}, \mathbf{x}) \Psi_b(\mathbf{x})\,, \tag{2.1.16}$$

where $\Psi_a(\mathbf{x})$ is the field operator. From now on for the summations over indices the Einstein summation convention will be used. In the coordinate representation the

momentum is a differential operator which can be expressed using an integral transform with a singular kernel, thus the Hamiltonian can always be written as[1]:

$$\mathcal{H} = \int \mathrm{d}^3x\, \mathrm{d}^3x'\, \Psi_a^\dagger(\mathbf{x}) H_{ab}(\mathbf{x},\mathbf{x}') \Psi_b(\mathbf{x}')\,. \tag{2.1.17}$$

The particle ($\mathbf{j}$) and energy currents ($\mathbf{j}_E$) are connected to the particle (ϱ) and energy (h) densities through the continuity equation:

$$\partial_t \varrho + \mathrm{div}\mathbf{j} = 0\,, \qquad\qquad \partial_t h + \mathrm{div}\mathbf{j}_E = 0\,. \tag{2.1.18}$$

The particle and energy density operators are defined to be Hermitian as:

$$\varrho(x) = \Psi_a^\dagger(\mathbf{x})\Psi_a(\mathbf{x})\,, \quad h(x) = \int \mathrm{d}^3x'\, \frac{1}{2}\left[\Psi_a^\dagger(\mathbf{x}) H_{ab}(\mathbf{x},\mathbf{x}')\Psi_b(\mathbf{x}') + (x \leftrightarrow x')\right]\,. \tag{2.1.19}$$

From now on $\mathbf{j}_1 \equiv \mathbf{j}$, $\mathbf{j}_2 \equiv \mathbf{j}_E$, $\varrho_1 \equiv \varrho$, and $\varrho_2 \equiv h$. The many body current operators ($\boldsymbol{\mathcal{J}}_i$) can be expressed with the density operator using Eq. (2.1.18) as:

$$\begin{aligned}\mathcal{J}_\alpha^{(i)} &:= \int \mathrm{d}^3x\, j_\alpha^{(i)}(\mathbf{x}) = \int \mathrm{d}^3x \sum_\beta (\partial_\beta x_\alpha) j_\beta^{(i)}(\mathbf{x}) \\ &= -\int \mathrm{d}^3x \sum_\beta x_\alpha \partial_\beta j_\beta^{(i)}(\mathbf{x}) = \int \mathrm{d}^3x\, x_\alpha \partial_t \varrho_i(\mathbf{x})\,,\end{aligned} \tag{2.1.20}$$

where we neglected surface terms during the partial integrations. Introducing the polarization operators ($\boldsymbol{\mathcal{P}}_i$) the current operators are:

$$\boldsymbol{\mathcal{P}}_i := \int \mathrm{d}^3x\, \mathbf{x}\varrho_i(\mathbf{x})\,, \qquad\qquad \boldsymbol{\mathcal{J}}_i = \partial_t \boldsymbol{\mathcal{P}}_i = i[\mathcal{H}, \boldsymbol{\mathcal{P}}_i]\,. \tag{2.1.21}$$

Using the previous definitions and the anticommutator of fermionic field operators $\left\{\Psi_a(\mathbf{x}), \Psi_b^\dagger(\mathbf{x}')\right\} = \delta_{ab}\delta(x-x')$ the current operators become:

$$\boldsymbol{\mathcal{J}}_1 = i\int \mathrm{d}^3x\, \mathrm{d}^3x'\, \Psi_a^\dagger(\mathbf{x}) H_{ab}(\mathbf{x},\mathbf{x}')(\mathbf{x}'-\mathbf{x})\Psi_b(\mathbf{x}')\,, \tag{2.1.22a}$$

$$\boldsymbol{\mathcal{J}}_2 = \frac{i}{2}\int \mathrm{d}^3x\, \mathrm{d}^3x'\, \mathrm{d}^3x''\, \Psi_a^\dagger(\mathbf{x}) H_{ac}(\mathbf{x},\mathbf{x}'')(\mathbf{x}'-\mathbf{x}) H_{cb}(\mathbf{x}'',\mathbf{x}')\Psi_b(\mathbf{x}')\,. \tag{2.1.22b}$$

[1] We use this form because it makes it easier to understand what should be derivated and what should not. Usually, this is done with differential operators acting to the right and to the left, which can make the formalism confusing.

Using differential operators these can be expressed as:

$$\boldsymbol{\mathcal{J}}_i = \int \mathrm{d}^3x\, \Psi_a^\dagger(\mathbf{x},t)\mathbf{J}_{ab}^{(i)}(\mathbf{p},\mathbf{x})\Psi_b(\mathbf{x},t)\,, \tag{2.1.23}$$

where (using $[f(\mathbf{p}),\mathbf{x}] = -i\boldsymbol{\nabla}_{\mathbf{p}} f(\mathbf{p})$):

$$\mathbf{J}_{ab}^{(1)}(\mathbf{p},\mathbf{x}) = \boldsymbol{\nabla}_{\mathbf{p}} H_{ab}(\mathbf{p},\mathbf{x})\,, \tag{2.1.24a}$$

$$\mathbf{J}_{ab}^{(2)}(\mathbf{p},\mathbf{x}) = \frac{1}{2}\left[\mathbf{J}_{ac}^{(1)}H_{cb} + H_{ac}\mathbf{J}_{cb}^{(1)}\right]\,. \tag{2.1.24b}$$

If the Hamiltonian includes impurities in the form of $V(\mathbf{x})$ we can see that it doesn't affect the particle current, but it appears in the energy current. Thus, in order to calculate the energy current the matrix elements of the impurity potential would be necessary. This can be avoided by expressing the energy current with the particle current operator. A similar argument for a single-band Hamiltonian can be found in Refs. [126] and [24]. We start by defining:

$$\boldsymbol{\mathcal{J}}_1(\tau,\tau') := \int \mathrm{d}^3x\, \boldsymbol{\Psi}^\dagger(\mathbf{x},\tau)\boldsymbol{\mathbb{J}}_1\boldsymbol{\Psi}(\mathbf{x},\tau')\,, \tag{2.1.25}$$

where we use the τ imaginary times of the Matsubara formalism. The many-body current operator can be expressed with a limit as:

$$\boldsymbol{\mathcal{J}}_1(\tau) = \lim_{\tau'\to\tau^-} \boldsymbol{\mathcal{J}}_1(\tau,\tau')\,. \tag{2.1.26}$$

Using the grand canonical Hamiltonian ($\mathcal{K} = \mathcal{H} - \mu\mathcal{N}$) the τ derivative of an arbitrary A operator is:

$$\partial_\tau A(\tau) = [\mathcal{K}, A(\tau)]\,. \tag{2.1.27}$$

It can be shown that:

$$\partial_\tau \Psi_a^\dagger(\mathbf{x},\tau) = \int \mathrm{d}^3x'\, \Psi_b^\dagger(\mathbf{x}',\tau)K_{ba}(\mathbf{x}',\mathbf{x})\,, \tag{2.1.28a}$$

$$\partial_\tau \Psi_a(\mathbf{x},\tau) = -\int \mathrm{d}^3x'\, K_{ab}(\mathbf{x},\mathbf{x}')\Psi_b(\mathbf{x}',\tau)\,. \tag{2.1.28b}$$

Using these relations the energy current can be expressed as:

$$\boldsymbol{\mathcal{J}}_2(\tau) = \lim_{\tau'\to\tau^-} \frac{1}{2}[\partial_\tau - \partial_{\tau'} + 2\mu]\boldsymbol{\mathcal{J}}_1(\tau,\tau')\,. \tag{2.1.29}$$

Using this formula only the matrix elements of the current operator are needed, which do not include the impurity potential.

2.1.4 Chemical potential

The chemical potential is obtained by fixing the number density of electrons in the system:

$$n_e = \int_{-\infty}^{\infty} \mathrm{d}\varepsilon\, D(\varepsilon) f\left(\varepsilon - \mu\right) , \qquad D(\varepsilon) = \frac{1}{V}\sum_a \delta(\varepsilon - E_a) , \tag{2.1.30}$$

where $f(\varepsilon)$ is the Fermi-Dirac distribution and $D(\varepsilon)$ is the density of states. In semiconductor or semimetallic systems it is better to use the charge carrier density to fix the chemical potential[2]. This is defined as the number density of electrons minus the number density of holes:

$$n_c = \int_{0}^{\infty} \mathrm{d}\varepsilon \left[D(\varepsilon) f\left(\varepsilon - \mu\right) - D(-\varepsilon) f\left(\varepsilon + \mu\right)\right] . \tag{2.1.31}$$

2.2 Impurities

In this section we discuss the effects of impurities, and how the Green's function can be approximated when impurities are present. We will assume charged impurities, that are screened by the electron-electron interaction. The screening is calculated using the random phase approximation, and the scattering rate is calculated using the first-order Born approximation.

2.2.1 Dyson equation

The Hamiltonian with impurities is expressed as:

$$\mathbb{H}(\mathbf{p}, \mathbf{x}) = \mathbb{H}_0(\mathbf{p}, \mathbf{x}) + V(x) , \tag{2.2.1}$$

[2]The chemical potential will have the same value, but the charge carrier density has a more important meaning.

where $\mathbb{H}_0(\mathbf{p},\mathbf{x})$ is the Hamiltonian without impurities, $V(\mathbf{x}) = \sum_{j=1}^{N_i} u(\mathbf{x}-\mathbf{R}_j)$ is the sum of randomly distributed impurities with N_i being the number of impurities. We treat the impurities with the usual diagrammatic technique for impurity Green's functions (for details see Ref. [19]). In a magnetic field the translational invariance of the Hamiltonian is broken, so the Green's function is not diagonal in momentum space. Nevertheless, the diagrammatic technique is analogous with the one in [19], and the same diagrammatic rules can be used, with the only difference that each Green's function line has two independent momentums. After averaging over random impurities we get the following Dyson equation:

$$\mathbb{G}_{\mathbf{k}_b\mathbf{k}_a} = \mathbb{G}^{(0)}_{\mathbf{k}_b\mathbf{k}_a} + \frac{1}{V^2}\sum_{\mathbf{k}\mathbf{k}'} \mathbb{G}^{(0)}_{\mathbf{k}_b\mathbf{k}}\mathbf{\Sigma}_{\mathbf{k}\mathbf{k}'}\mathbb{G}_{\mathbf{k}'\mathbf{k}_a}\,, \tag{2.2.2}$$

where $\mathbb{G}^{(0)}_{\mathbf{k}_b\mathbf{k}_a}$ is the Green's function of the clean system and $\mathbf{\Sigma}_{\mathbf{k}\mathbf{k}'}$ is the self-energy. The diagram of the Dyson equation is shown in Fig. 2.1. The Dyson equation in the

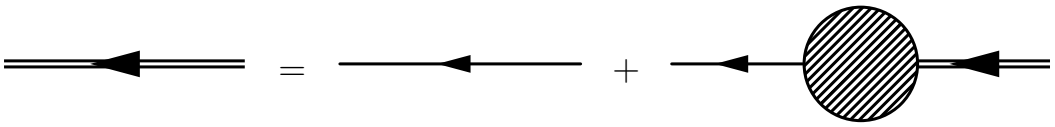

Figure 2.1: Feynman diagram of the Dyson equation in Eq. (2.2.2). The double arrow is the impurity Green's function, the single arrow is the impurity free Green's function and the filled circle is the self-energy.

eigenstate representation is expressed as:

$$G_{ba} = \delta_{ab}G^{(0)}_a + \sum_c G^{(0)}_b \Sigma_{bc} G_{ca}\,, \tag{2.2.3a}$$

$$\Sigma_{ba} = \frac{1}{V^2}\sum_{\mathbf{k},\mathbf{k}'} \boldsymbol{\phi}^\dagger_{b\mathbf{k}}\mathbf{\Sigma}_{\mathbf{k}\mathbf{k}'}\boldsymbol{\phi}_{a\mathbf{k}'}\,. \tag{2.2.3b}$$

If the self-energy is diagonal in the eigenstate representation, the impurity Green's function can be simply expressed as:

$$G_a(i\omega_m) = \frac{1}{i\omega_m + \mu - E_a - \Sigma_a(i\omega_m)}\,. \tag{2.2.4}$$

2.2.2 Self-energy and scattering rate

To calculate the self-energy we use the first-order Born approximation taking the Feynman diagram shown in Fig. 2.2 (for more details see Ref. [19]). This diagram can be expressed as:

$$\boldsymbol{\Sigma}^{B}_{\mathbf{k}\mathbf{k}'}(i\omega_m) = n_i \frac{1}{V} \sum_{\mathbf{q}} u^2_{\mathbf{q}} \mathbb{G}^{(0)}_{\mathbf{k}-\mathbf{q},\mathbf{k}'-\mathbf{q}}(i\omega_m)\,, \tag{2.2.5}$$

where n_i is the number density of the impurities and $u_{\mathbf{q}}$ is the Fourier transform of the effective impurity potential.

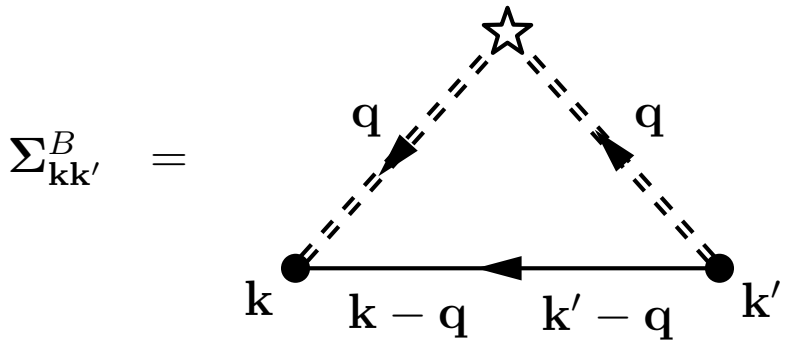

Figure 2.2: Feynman diagram for the first-order Born approximation of the self-energy (see Eq. (2.2.5)). The star is the impurity density and the double dashed line is the effective impurity potential.

In the eigenstate representation using Eqs. (2.2.3b) and (2.1.8):

$$\Sigma_{ab}(i\omega_m) = \frac{n_i}{V^3} \sum_{\mathbf{k},\mathbf{k}',\mathbf{q}} u^2_{\mathbf{q}} \boldsymbol{\phi}^{\dagger}_{a\mathbf{k}} \sum_{c} \frac{\boldsymbol{\phi}_{c,\mathbf{k}-\mathbf{q}} \boldsymbol{\phi}^{\dagger}_{c,\mathbf{k}'-\mathbf{q}}}{i\omega_m + \mu - E_c} \boldsymbol{\phi}_{b\mathbf{k}'} \tag{2.2.6}$$

By rearranging the summations this can be expressed as:

$$\Sigma_{ab}(i\omega_m) = \frac{n_i}{V} \sum_{\mathbf{q}} u^2_{\mathbf{q}} \sum_{c} \frac{F_{ac}(\mathbf{q}) F^{*}_{bc}(\mathbf{q})}{i\omega_m + \mu - E_c}\,, \tag{2.2.7a}$$

$$F_{ab}(\mathbf{q}) = \frac{1}{V} \sum_{\mathbf{k}} \boldsymbol{\phi}^{\dagger}_{a\mathbf{k}} \boldsymbol{\phi}_{b,\mathbf{k}-\mathbf{q}} = \int \mathrm{d}^3x\, \boldsymbol{\phi}^{\dagger}_{a}(\mathbf{x}) \boldsymbol{\phi}_{b}(\mathbf{x}) \mathrm{e}^{i\mathbf{q}\mathbf{x}}\,, \tag{2.2.7b}$$

where the convolution was transformed to a Fourier transform.

We will assume that the real part of the self energy is renormalized into the chemical potential and only use the scattering rate $\Gamma = -\operatorname{Im}\{\Sigma\}$. The analytic continuation of

the scattering rate is:

$$\Gamma_{ab}(\varepsilon) = \lim_{\delta \to 0^+} \Gamma_{ab}(\varepsilon + i\delta) \tag{2.2.8}$$

Henceforth we will focus on the diagonal elements of the scattering rate (later we will show that in the systems we study the off-diagonal elements are very small). The diagonal elements of the scattering rate after analytic continuation have different signs on the upper and lower half planes, with a branch cut on the real axis:

$$\Gamma_a(\varepsilon + i\delta) \propto \mathrm{sgn}(\delta)\,. \tag{2.2.9}$$

This property will be very important in the calculation of transport, which will be discussed in the next chapter. After performing the $\delta \to 0^+$ limit the scattering rate is:

$$\Gamma_a(\varepsilon) = n_i \sum_b \int \frac{\mathrm{d}^3 q}{2(2\pi)^2} u_{\mathbf{q}}^2 \delta\left(\varepsilon + \mu - E_b\right) \left|F_{ab}(\mathbf{q})\right|^2 . \tag{2.2.10}$$

With this, the retarded impurity Green's function becomes:

$$G_a^R(\varepsilon) = \frac{1}{\varepsilon + \mu - E_a + i\Gamma_a(\varepsilon)}\,. \tag{2.2.11}$$

2.2.3 Impurity potential screening

For the effective impurity potential $u_{\mathbf{q}}$ we use screened charged impurities. We start by taking the $v_{\mathbf{q}}$ Coulomb potential and the screening is calculated using the so called random phase approximation [18, 19] (RPA). In general the Green's function is not diagonal in the momentum space, so the RPA must be done using two momentums. Diagrammatically the RPA is expressed as in Fig. 2.3.

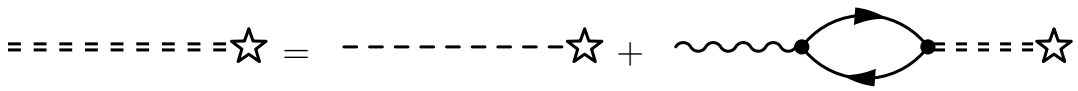

Figure 2.3: Feynman diagram of the RPA used to calculate the screening of the impurity potential. The double dashed lines are the effective impurity potentials, the single dashed lines are the bare impurity potentials and the wavy line represents the electron-electron interaction.

The equation of the Fig. 2.3 diagram is expressed using charged impurities in a

dielectric medium $v_{\mathbf{q}} = u_i/q^2$ (single dashed line) and the electron-electron interaction $w_{\mathbf{q}} = u_e/q^2$ (wavy line) the screened impurity potential is expressed implicitly as:

$$u_{\mathbf{qq'}}(i\omega_\lambda) = v_{\mathbf{q}}\delta_{\mathbf{qq'}} + \frac{1}{V}\sum_{\mathbf{q''}} w_{\mathbf{q}}\Pi^{(0)}_{\mathbf{qq''}}(i\omega_\lambda)u_{\mathbf{q''q'}}(i\omega_\lambda)\,, \tag{2.2.12}$$

where $\Pi^{(0)}$ is the bubble diagram for electrons. For simplicity we study the static and long-wave limit $i\omega_\lambda, \mathbf{q}, \mathbf{q'} \to 0$. In this limit we assume that the bubble diagram is diagonal and constant $\Pi^{(0)}_{\mathbf{qq'}}(i\omega_m) \approx \delta_{\mathbf{qq'}}\Pi^{(0)}_{\mathbf{00}}(0)$. With this the effective impurity potential will also be diagonal and simply expressed as:

$$u_{\mathbf{q}} = \frac{u_i}{q^2 - \frac{u_e}{V}\Pi^{(0)}_{\mathbf{00}}(0)} \equiv \frac{u_i}{q^2 + \kappa^2}\,. \tag{2.2.13}$$

Here κ is the screening wavenumber and it is obtained using the static and long-wave limit of the bubble diagram (see Fig. 2.4) as:

$$\kappa^2 = -\frac{u_e}{\beta V^3}\sum_{m,\mathbf{k},\mathbf{k'}} \mathrm{Tr}\left[\mathbb{G}^{(0)}_{\mathbf{kk'}}(i\omega_m)\mathbb{G}^{(0)}_{\mathbf{k'k}}(i\omega_m)\right]\,. \tag{2.2.14}$$

In the eigenstate representation this is:

$$\kappa^2 = -\frac{u_e}{\beta V}\sum_{m,a}\left[G^{(0)}_a(i\omega_m)\right]^2\,. \tag{2.2.15}$$

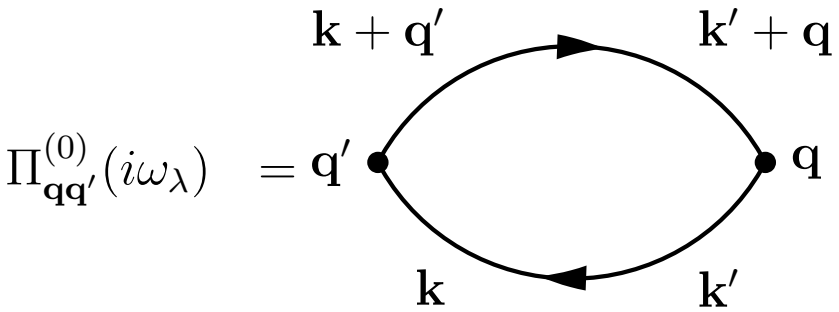

Figure 2.4: The bubble diagram used to calculate the screening wavenumber in Eq. (2.2.16).

The Matsubara summation can be evaluated using the residue of the second order

pole and the screening wavelength is simply expressed as:

$$\kappa^2 = -\frac{u_e}{V}\sum_a \frac{\partial f(E_a-\mu)}{\partial E_a}\,. \tag{2.2.16}$$

At zero temperature the derivative of the Fermi-Dirac distribution becomes a Dirac delta and the screening wavelength can be expressed using the density of states defined in Eq. (2.1.30) as:

$$\kappa^2 = u_e D(\mu)\,. \tag{2.2.17}$$

Chapter 3

Transport in magnetic fields

In this chapter we describe the formalism used to calculate the transport coefficients. The formalism is based on Luttinger's theory of thermoelectric transport [21] and the extension of this to magnetic fields, studied by Smrčka and Středa [22]. We extend the formalism to arbitrary multi-band systems and express the transport coefficients in the eigenstate representation. We show that the Mott's formula and Wiedemann-Franz law hold. We give expressions to calculate the transport coefficients in case of impurities, using the impurity Green's function and vertex correction.

3.1 Current operators under external fields

The total Hamiltonian of the $\mathcal{H}$ system under external fields can be written as [21, 22]:

$$\mathcal{H}_{\text{tot}} = \int \mathrm{d}^3x\, h(\mathbf{x})[1+\psi(\mathbf{x})] + \varrho_e(\mathbf{x})\phi(\mathbf{x})\,, \tag{3.1.1}$$

where ψ is a fictitious gravitational potential introduced as the dynamical counterpart of the temperature gradient, ϕ is the electric potential, h is the energy density and ϱ_e is the electric charge density. The kernel function in Eq. (2.1.17) of this Hamiltonian is:

$$H^{\text{tot}}_{ab}(\mathbf{x},\mathbf{x}') = H_{ab}(\mathbf{x},\mathbf{x}')\left[1+\frac{1}{2}\left(\psi(\mathbf{x})+\psi(\mathbf{x}')\right)\right] + \delta(\mathbf{x}-\mathbf{x}')\varrho_e(\mathbf{x})\phi(\mathbf{x})\,. \tag{3.1.2}$$

Using Eqs. (2.1.22a) and (2.1.22b) the single-particle current and energy current operators in Eq. (2.1.23) can be expressed as:

$$\mathbb{J}_1^{\text{tot}} = \mathbb{J}_1 + \frac{1}{2}\left[\mathbb{J}_1\psi + \psi\mathbb{J}_1\right] , \tag{3.1.3a}$$

$$\mathbb{J}_2^{\text{tot}} = \mathbb{J}_2 - \frac{e}{2}\left[\mathbb{J}_1\phi + \phi\mathbb{J}_1\right] + \frac{1}{2}\Big[\mathbb{J}_2\psi + \psi\mathbb{J}_2 + \mathbb{J}_1\psi\mathbb{H} + \mathbb{H}\psi\mathbb{J}_1\Big] , \tag{3.1.3b}$$

where $\mathbb{J}_1 = \boldsymbol{\nabla}_{\mathbf{p}}\mathbb{H}$, $\mathbb{J}_2 = \frac{1}{2}\left[\mathbb{J}_1\mathbb{H} + \mathbb{H}\mathbb{J}_1\right]$ and we kept only the first order terms in the external fields. This is equivalent to the currents obtained in Refs. [22] and [23].

3.2 Transport coefficients in magnetic fields

Phenomenologically the current density and energy current density can be expressed using the transport coefficients ($\mathbb{L}_{ij}$) and the driving forces as [18, 21, 22]:

$$\mathbf{j}_1 = -e^2\mathbb{L}_{11}\boldsymbol{\nabla}\phi + e\mathbb{L}_{12}\boldsymbol{\nabla}\psi , \tag{3.2.1a}$$

$$\mathbf{j}_2 = \quad e\ \mathbb{L}_{21}\boldsymbol{\nabla}\phi - \ \mathbb{L}_{22}\boldsymbol{\nabla}\psi , \tag{3.2.1b}$$

where we separated the elementary charge from the usual definitions and:

$$\mathbf{j}_1 = -e\frac{\left\langle \boldsymbol{\mathcal{J}}_1^{\text{tot}}\right\rangle_{\text{tot}}}{V} , \qquad \mathbf{j}_2 = \frac{\left\langle \boldsymbol{\mathcal{J}}_2^{\text{tot}}\right\rangle_{\text{tot}}}{V} , \tag{3.2.2}$$

where $\langle\rangle_{\text{tot}}$ is the thermal average using the total Hamiltonian.

For a uniform electric field the electric potential is $\phi = -\mathbf{xE}$. According to the arguments in Ref. [21, 22] the gradient of the gravitational potential is equivalent to the the temperature gradient $\boldsymbol{\nabla}\psi \equiv -T\boldsymbol{\nabla}\left(1/T\right)$. If this is also uniform then $\psi \equiv -T\mathbf{x}\boldsymbol{\nabla}\left(1/T\right)$.

Using Eqs. (3.1.3a), (3.1.3b) and (2.1.23) the thermal average of the many-body current operators can be expressed as:

$$\left\langle \boldsymbol{\mathcal{J}}_1^{\text{tot}}\right\rangle_{\text{tot}} \approx \langle \boldsymbol{\mathcal{J}}_1\rangle_{\text{tot}} + \left\langle \boldsymbol{\mathcal{J}}_1^{\psi}\right\rangle , \tag{3.2.3a}$$

$$\left\langle \boldsymbol{\mathcal{J}}_2^{\text{tot}}\right\rangle_{\text{tot}} \approx \langle \boldsymbol{\mathcal{J}}_2\rangle_{\text{tot}} + \left\langle \boldsymbol{\mathcal{J}}_1^{\phi}\right\rangle + \left\langle \boldsymbol{\mathcal{J}}_2^{\psi}\right\rangle . \tag{3.2.3b}$$

The $\langle\rangle$ is the thermal average using only the $\mathbb{H}$ Hamiltonian. In these formulas we only consider the potentials up to linear order. We divide the contributions to the transport

coefficients coming from the field independent and field dependent currents as:

$$\mathbb{L}_{ij} = \mathbb{K}_{ij} + \mathbb{M}_{ij}\,, \tag{3.2.4}$$

where $\mathbb{K}_{ij}$ comes from the field independent part of the current operators in Eq. (3.2.3). This will be calculated in Sec. 3.2.1 and we will see how this quantity is related to the current-current correlation. The $\mathbb{M}_{ij}$ quantities come from the field dependent part in the current operators in Eq. (3.2.3) that are only averaged using $\mathbb{H}$. These quantities will be discussed in Sec. 3.2.2

3.2.1 Current-current correlation function

The $\mathbb{K}_{ij}$ components coming from the $\langle \boldsymbol{\mathcal{J}}_i \rangle_{\text{tot}}$ terms can be calculated using the Kubo formula [18, 20] as:

$$K^{(ij)}_{\alpha\beta} = \lim_{\omega\to 0} \frac{i}{\omega} \lim_{\delta\to 0^+} \Pi^{(ij)}_{\alpha\beta}(i\omega_\lambda = \omega + i\delta)\,, \tag{3.2.5a}$$

$$\Pi^{(ij)}_{\alpha\beta}(i\omega_\lambda) = -\frac{1}{V}\int_0^\beta \mathrm{d}\tau\, \mathrm{e}^{i\omega_\lambda \tau} \left\langle \mathcal{J}^{(i)}_\alpha(\tau)\mathcal{J}^{(j)}_\beta(0)\right\rangle_0 . \tag{3.2.5b}$$

Using the many-body current operators with the formalism described in Eq. (2.1.29) the current-current correlation can be calculated as:

$$\Pi^{(ij)}_{\alpha\beta} = -\frac{1}{V}\int_0^\beta \mathrm{d}\tau\, \mathrm{e}^{i\omega_\lambda\tau} \lim_{\substack{\tau'\to\tau^- \\ \tau'''\to\tau''^- \\ \tau''\to 0^-}} \Delta_i(\partial_\tau,\partial_{\tau'})\Delta_j(\partial_{\tau''},\partial_{\tau'''}) \left\langle \mathcal{J}_\alpha(\tau,\tau')\mathcal{J}_\beta(\tau'',\tau''')\right\rangle_o , \tag{3.2.6}$$

where $\Delta_1(\partial_\tau,\partial_{\tau'}) := 1$ and $\Delta_2(\partial_\tau,\partial_{\tau'}) := \frac{1}{2}(\partial_\tau - \partial_{\tau'} + 2\mu)$. Using the (2.1.25) form of the many-body current operator, performing the thermal average over the field operators and transforming to the Matsubara frequency space we get:

$$\begin{aligned}\Pi^{(ij)}_{\alpha\beta}(i\omega_\lambda) = \frac{1}{V}\frac{1}{\beta}\sum_n \int \mathrm{d}^3x \int \mathrm{d}^3x'\, \Delta_i(i\omega_n, -i\omega_n - i\omega_\lambda)\Delta_j(i\omega_n + i\omega_\lambda, -i\omega_n)\times \\ \times \mathrm{Tr}\{\mathbb{J}_\alpha \mathbb{G}(\mathbf{x},\mathbf{x}', i\omega_n + i\omega_\lambda)\mathbb{J}_\beta \mathbb{G}(\mathbf{x}',\mathbf{x}, i\omega_n)\}\,,\end{aligned} \tag{3.2.7}$$

where $\mathbb{G}$ is the Green's function of the $\mathbb{H}$ Hamiltonian defined in Eq. (2.1.7). In the eigenstate basis ($\mathbb{H}\,|a\rangle = E_a\,|a\rangle$) this can be expressed as:

$$\Pi^{(ij)}_{\alpha\beta}(i\omega_\lambda) = -\frac{1}{V}\sum_{a,b} J^{(\alpha)}_{ab} J^{(\beta)}_{ba} C^{(ij)}_{ba}(i\omega_\lambda)\,, \tag{3.2.8a}$$

$$C^{(ij)}_{ba}(i\omega_\lambda) := -\frac{1}{\beta}\sum_n \left(i\omega_n + \mu + \frac{i\omega_\lambda}{2}\right)^{i+j-2} G_b(i\omega_n + i\omega_\lambda) G_a(i\omega_n)\,. \tag{3.2.8b}$$

The Matsubara summation can be transformed to line integrals (for details see Appendix A). Because of the $(i\omega_n + \mu + i\omega_\lambda/2)^{i+j-2}$ factor the (A.1.8) formula has to be modified a little. After analytic continuation ($i\omega_\lambda = \omega + 0^+$) the retarded current-current correlation function becomes:

$$C^{R(ij)}_{ba}(\omega) = \int_{-\infty}^{\infty} \frac{\mathrm{d}\varepsilon}{2\pi i} f(\varepsilon-\mu)\Bigg[\left(\varepsilon+\frac{\omega}{2}\right)^{i+j-2}\left(G^R_b(\varepsilon+\omega)G^R_a(\varepsilon) - G^R_b(\varepsilon+\omega)G^A_a(\varepsilon)\right) + \\ + \left(\varepsilon-\frac{\omega}{2}\right)^{i+j-2}\left(G^R_b(\varepsilon)G^A_a(\varepsilon-\omega) - G^A_b(\varepsilon)G^A_a(\varepsilon-\omega)\right)\Bigg], \tag{3.2.9}$$

where the retarded and advanced Green's functions are defined as[1]:

$$G^R_a(\varepsilon) = \frac{1}{\varepsilon - E_a + i\Gamma_a(\varepsilon)} \qquad G^A_a(\varepsilon) = \frac{1}{\varepsilon - E_a - i\Gamma_a(\varepsilon)} \tag{3.2.10}$$

We are interested in the $C^{(ij)}_{ba} := \lim_{\omega\to 0} C^{R(ij)}_{ab}(\omega)/\omega$ limit. Performing the limit on Eq. (3.2.9) we get:

$$C^{(ij)}_{ba} = \int_{-\infty}^{\infty} \frac{\mathrm{d}\varepsilon}{\pi} f(\varepsilon-\mu)\Bigg(\varepsilon^{i+j-2}\left[\partial_\varepsilon G^R_b(\varepsilon)\,\mathrm{Im}\,G^R_a(\varepsilon) - \partial_\varepsilon G^A_a(\varepsilon)\,\mathrm{Im}\,G^R_b(\varepsilon)\right] + \\ + \frac{i+j-2}{2}\varepsilon^{i+j-3}\left[G^R_b(\varepsilon)\,\mathrm{Im}\,G^R_a(\varepsilon) - G^A_a(\varepsilon)\,\mathrm{Im}\,G^R_b(\varepsilon)\right]\Bigg). \tag{3.2.11}$$

[1]For simplicity the the energy is shifted by the chemical potential from the usual definition.

We can divide this into real and imaginary parts as:

$$\operatorname{Im} C_{ba}^{(ij)} = -\int_{-\infty}^{\infty} \frac{\mathrm{d}\varepsilon}{\pi} \varepsilon^{i+j-2} \partial_\varepsilon f(\varepsilon-\mu)\ \operatorname{Im} G_b^R(\varepsilon) \operatorname{Im} G_a^R(\varepsilon)\,, \tag{3.2.12a}$$

$$\begin{aligned}\operatorname{Re} C_{ba}^{(ij)} = &\int_{-\infty}^{\infty} \frac{\mathrm{d}\varepsilon}{2\pi} f(\varepsilon-\mu) \Big[\partial_\varepsilon \left(\varepsilon^{i+j-2} \operatorname{Re} G_b^R(\varepsilon) \right) \operatorname{Im} G_a^R(\varepsilon) - a \leftrightarrow b \Big] + \\ &+ \int_{-\infty}^{\infty} \frac{\mathrm{d}\varepsilon}{2\pi} f(\varepsilon-\mu) \Big[\varepsilon^{i+j-2} \partial_\varepsilon \left(\operatorname{Re} G_b^R(\varepsilon) \right) \operatorname{Im} G_a^R(\varepsilon) - a \leftrightarrow b \Big]\,. \end{aligned} \tag{3.2.12b}$$

Substituting these in Eq. (3.2.5a) we get:

$$\operatorname{Re} K_{\alpha\beta}^{(ij)} = \frac{1}{V} \sum_{a,b} \operatorname{Im}\Big\{ J_{ab}^{(\alpha)} J_{ba}^{(\beta)} \Big\} \operatorname{Re} C_{ba}^{(ij)} + \operatorname{Re}\Big\{ J_{ab}^{(\alpha)} J_{ba}^{(\beta)} \Big\} \operatorname{Im} C_{ba}^{(ij)}\,, \tag{3.2.13a}$$

$$\operatorname{Im} K_{\alpha\beta}^{(ij)} = -\frac{1}{V} \sum_{a,b} \operatorname{Re}\Big\{ J_{ab}^{(\alpha)} J_{ba}^{(\beta)} \Big\} \operatorname{Re} C_{ba}^{(ij)} + \operatorname{Im}\Big\{ J_{ab}^{(\alpha)} J_{ba}^{(\beta)} \Big\} \operatorname{Im} C_{ba}^{(ij)}\,, \tag{3.2.13b}$$

Since the one-particle current operator is Hermitian the following relations hold:

$$\operatorname{Re}\Big\{ J_{ab}^{(\alpha)} J_{ba}^{(\beta)} \Big\} = \operatorname{Re}\Big\{ J_{ba}^{(\alpha)} J_{ab}^{(\beta)} \Big\}\,, \qquad \operatorname{Im}\Big\{ J_{ab}^{(\alpha)} J_{ba}^{(\beta)} \Big\} = -\operatorname{Im}\Big\{ J_{ba}^{(\alpha)} J_{ab}^{(\beta)} \Big\}\,. \tag{3.2.14}$$

Using Eq. (3.2.12) we can see that:

$$\operatorname{Re} C_{ba}^{(ij)} = -\operatorname{Re} C_{ab}^{(ij)}\,, \qquad \operatorname{Im} C_{ba}^{(ij)} = \operatorname{Im} C_{ab}^{(ij)}\,. \tag{3.2.15}$$

These relations guarantee that $\operatorname{Im}\{\mathbb{K}_{ij}\} = 0$. This way the components coming from the Kubo formula can be expressed as:

$$K_{\alpha\beta}^{(ij)} = \frac{1}{V} \sum_{a,b} \operatorname{Im}\Big\{ J_{ab}^{(\alpha)} J_{ba}^{(\beta)} \Big\} \operatorname{Re} C_{ba}^{(ij)} + \operatorname{Re}\Big\{ J_{ab}^{(\alpha)} J_{ba}^{(\beta)} \Big\} \operatorname{Im} C_{ba}^{(ij)}\,, \tag{3.2.16a}$$

$$\operatorname{Im} C_{ba}^{(ij)} = -\int_{-\infty}^{\infty} \frac{\mathrm{d}\varepsilon}{\pi} \varepsilon^{i+j-2} \partial_\varepsilon f(\varepsilon-\mu)\ \operatorname{Im} G_b^R(\varepsilon) \operatorname{Im} G_a^R(\varepsilon)\,, \tag{3.2.16b}$$

$$\operatorname{Re} C_{ba}^{(ij)} = \int_{-\infty}^{\infty} \frac{\mathrm{d}\varepsilon}{\pi} f(\varepsilon-\mu) \partial_\varepsilon \left(\varepsilon^{i+j-2} \operatorname{Re} G_b^R(\varepsilon) \right) \operatorname{Im} G_a^R(\varepsilon) +$$

$$+ \int_{-\infty}^{\infty} \frac{\mathrm{d}\varepsilon}{\pi} f(\varepsilon-\mu)\varepsilon^{i+j-2}\partial_\varepsilon \left(\operatorname{Re} G_b^R(\varepsilon)\right) \operatorname{Im} G_a^R(\varepsilon)\,. \tag{3.2.16c}$$

3.2.2 Magnetization and Energy magnetization

We move on with expressing the $\mathbb{M}_{ij}$ components in Eq. (3.2.4) coming from the field dependent part of the current operator. These are already linear in the external fields, so the thermal averaging is done only using the $\mathbb{H}$ Hamiltonian. Using the eigenstate representation we can write them as:

$$\mathbb{M}_{11} = 0\,, \tag{3.2.17a}$$

$$\mathbb{M}_{12} = -\frac{2}{V}\sum_a \int_{-\infty}^{\infty} \frac{\mathrm{d}\varepsilon}{2\pi} f(\varepsilon-\mu) \operatorname{Im}\{G_a^R(\varepsilon)\}\mathbb{M}_a = \mathbb{M}_{21}\,, \tag{3.2.17b}$$

$$\mathbb{M}_{22} = -\frac{4}{V}\sum_a \int_{-\infty}^{\infty} \frac{\mathrm{d}\varepsilon}{2\pi} \varepsilon f(\varepsilon-\mu) \operatorname{Im}\{G_a^R(\varepsilon)\}\mathbb{M}_a\,, \tag{3.2.17c}$$

where $M_{\alpha\beta}^{(a)} = \frac{1}{2}\langle a|\left[\mathbb{J}_\alpha x_\beta + x_\beta \mathbb{J}_\alpha\right]|a\rangle$. Using $\mathbb{J}_\alpha = i[\mathbb{H}, x_\alpha]$ this can be transformed to $M_{\alpha\beta}^{(a)} = \frac{1}{2}\langle a|\left[\mathbb{J}_\alpha x_\beta - \mathbb{J}_\beta x_\alpha\right]|a\rangle$. From this form we can see that $M_{\alpha\alpha}^{(ij)} = 0$.

3.2.3 Transport coefficients

Since every formula in Eqs. (3.2.16) and (3.2.17) is proportional to $f(\varepsilon-\mu)$ or $\partial_\varepsilon f(\varepsilon-\mu)$ it is always possible to express the finite temperature quantities with the zero temperature quantities as:

$$\mathbb{L}_{ij}(T,\mu) = -\int \mathrm{d}\varepsilon \frac{\mathrm{d}f(\varepsilon-\mu)}{\mathrm{d}\varepsilon} \mathbb{L}_{ij}(0,\varepsilon)\,, \tag{3.2.18}$$

Using Eq. (3.2.16) the diagonal elements of the transport coefficients can be expressed as:

$$L_{\alpha\alpha}^{11}(0,\varepsilon) = \frac{1}{\pi V}\sum_{a,b} \left|J_{ab}^{(\alpha)}\right|^2 \operatorname{Im} G_b^R(\varepsilon) \operatorname{Im} G_a^R(\varepsilon)\,, \tag{3.2.19a}$$

$$L_{\alpha\alpha}^{12}(0,\varepsilon) = \varepsilon L_{\alpha\alpha}^{11}(0,\epsilon)\,, \tag{3.2.19b}$$

$$L_{\alpha\alpha}^{22}(0,\varepsilon) = \varepsilon^2 L_{\alpha\alpha}^{11}(0,\epsilon)\,. \tag{3.2.19c}$$

For the off-diagonal components the calculation is more complex. We need to address both $\mathbb{K}$ and $\mathbb{M}$ contributions. It can be shown in a similar fashion as Ref. [22] that the components coming from $\mathbb{M}$ compensate for terms coming from $\mathbb{K}$ in a way that the off-diagonal components can be expressed similarly to the diagonal components. The conductivity is not affected by $\mathbb{M}$ and can be expressed using Eq. (3.2.16) as:

$$L^{11}_{\alpha\beta}(0,\varepsilon) = \frac{1}{\pi V}\sum_{a,b}\Bigg[\mathrm{Re}\Big\{J^{(\alpha)}_{ab}J^{(\beta)}_{ba}\Big\}\,\mathrm{Im}\,G^R_b(\varepsilon)\,\mathrm{Im}\,G^R_a(\varepsilon) + \\ + \mathrm{Im}\Big\{J^{(\alpha)}_{ab}J^{(\beta)}_{ba}\Big\}\int_{-\infty}^{\varepsilon}\mathrm{d}\xi\, 2\partial_\xi\,\mathrm{Re}\,G^R_b(\xi)\,\mathrm{Im}\,G^R_a(\xi)\Bigg]. \tag{3.2.20}$$

To calculate the other two transport coefficients we define the following functions:

$$A_0(\varepsilon) := \frac{1}{\pi V}\sum_{a,b}\mathrm{Re}\Big\{J^{(\alpha)}_{ab}J^{(\beta)}_{ba}\Big\}\,\mathrm{Im}\,G^R_b(\varepsilon)\,\mathrm{Im}\,G^R_a(\varepsilon)\,, \tag{3.2.21a}$$

$$A_1(\varepsilon) := \frac{2}{\pi V}\sum_{a,b}\mathrm{Im}\Big\{J^{(\alpha)}_{ab}J^{(\beta)}_{ba}\Big\}\partial_\varepsilon\,\mathrm{Re}\,G^R_b(\varepsilon)\,\mathrm{Im}\,G^R_a(\varepsilon)\,, \tag{3.2.21b}$$

$$A_2(\varepsilon) := \frac{1}{\pi V}\sum_{a,b}\mathrm{Im}\Big\{J^{(\alpha)}_{ab}J^{(\beta)}_{ba}\Big\}\,\mathrm{Re}\,G^R_b(\varepsilon)\,\mathrm{Im}\,G^R_a(\varepsilon)\,. \tag{3.2.21c}$$

With these definitions the transport coefficients calculated from Eq. (3.2.16) are:

$$K^{11}_{\alpha\beta}(0,\varepsilon) = A_0(\varepsilon) + \int_{-\infty}^{\varepsilon}\mathrm{d}\xi\, A_1(\varepsilon)\,, \tag{3.2.22a}$$

$$K^{12}_{\alpha\beta}(0,\varepsilon) = \varepsilon A_0(\varepsilon) + \int_{-\infty}^{\varepsilon}\mathrm{d}\xi\,\left[\xi A_1(\xi) + A_2(\xi)\right]\,, \tag{3.2.22b}$$

$$K^{22}_{\alpha\beta}(0,\varepsilon) = \varepsilon^2 A_0(\varepsilon) + \int_{-\infty}^{\varepsilon}\mathrm{d}\xi\,\left[\xi^2 A_1(\xi) + 2\xi A_2(\xi)\right]\,. \tag{3.2.22c}$$

After partial integrations:

$$K^{12}_{\alpha\beta}(0,\varepsilon) = \varepsilon K^{11}_{\alpha\beta}(0,\varepsilon) + \int_{-\infty}^{\varepsilon}\mathrm{d}\xi\,(\xi-\varepsilon)\,(A_1(\xi) - \partial_\xi A_2(\xi))\,, \tag{3.2.23a}$$

$$K^{12}_{\alpha\beta}(0,\varepsilon) = \varepsilon^2 K^{11}_{\alpha\beta}(0,\varepsilon) + \int_{-\infty}^{\varepsilon} \mathrm{d}\xi \, (\xi^2 - \varepsilon^2) \, (A_1(\xi) - \partial_\xi A_2(\xi)) \, . \tag{3.2.23b}$$

The next step is to evaluate $A(\xi) := (A_1(\xi) - \partial_\xi A_2(\xi))$. For this we go back to the general operators:

$$\begin{aligned} A &= \frac{1}{2i\pi V} \operatorname{Tr}\left[\mathbb{J}_\alpha \left(\partial_\xi \operatorname{Re} \mathbb{G}^R \right) \mathbb{J}_\beta \operatorname{Im} \mathbb{G}^R - \mathbb{J}_\alpha \operatorname{Re} \mathbb{G}^R \mathbb{J}_\beta \left(\partial_\xi \operatorname{Im} \mathbb{G}^R \right) - \alpha \leftrightarrow \beta \right] = \\ &= \frac{1}{4\pi V} \operatorname{Tr}\left[\left(\partial_\xi \mathbb{G}^R \right) \mathbb{J}_\alpha \mathbb{G}^R \mathbb{J}_\beta - \left(\partial_\xi \mathbb{G}^A \right) \mathbb{J}_\alpha \mathbb{G}^A \mathbb{J}_\beta - \alpha \leftrightarrow \beta \right] . \end{aligned} \tag{3.2.24}$$

Using the definition of the Green's function and current operator it can be shown that the following identity holds:

$$\mathbb{J}_\alpha = i \left[\left(\mathbb{G}^{R/A} \right)^{-1}, x_\alpha \right] , \tag{3.2.25}$$

and with this A can be transformed to:

$$A = -\frac{1}{2\pi V} \operatorname{Tr}\left[\left(\partial_\xi \operatorname{Im} \mathbb{G}^R \right) \mathbb{J}_\alpha x_\beta - \alpha \leftrightarrow \beta \right] . \tag{3.2.26}$$

After partial integration the terms containing A will be the same as the terms in $\mathbb{M}$, and the final expression for the transport coefficients is:

$$L^{11}_{\alpha\beta}(0,\varepsilon) = A_0(\varepsilon) + \int_{-\infty}^{\varepsilon} \mathrm{d}\xi \, A_1(\varepsilon) \, , \tag{3.2.27a}$$

$$L^{12}_{\alpha\beta}(0,\varepsilon) = \varepsilon L^{11}_{\alpha\beta}(0,\epsilon) \, , \tag{3.2.27b}$$

$$L^{22}_{\alpha\beta}(0,\varepsilon) = \varepsilon^2 L^{11}_{\alpha\beta}(0,\epsilon) \, . \tag{3.2.27c}$$

This means that all the necessary information is included in the zero temperature conductivity tensor as a function of chemical potential, and every other transport coefficient can be expressed with that.

The experimentally measurable quantities (conductivity ($\boldsymbol{\sigma}$), Seebeck ($\mathbb{S}$) and thermal conductivity ($\boldsymbol{\kappa}$) tensors) can be expressed using the transport coefficients as [18]:

$$\boldsymbol{\sigma} = e^2 \mathbf{L}_{11} \, , \tag{3.2.28a}$$

$$\mathbb{S} = -\frac{1}{eT}\mathbf{L}_{11}^{-1}(\mathbf{L}_{12} - \mu\mathbf{L}_{11})\,, \tag{3.2.28b}$$

$$\boldsymbol{\kappa} = \frac{1}{T}\left[\mathbf{L}_{22} - \mathbf{L}_{21}\mathbf{L}_{11}^{-1}\mathbf{L}_{12}\right]\,. \tag{3.2.28c}$$

Close to zero temperature ($T \to 0$) using the Sommerfeld expansion, we obtain:

$$\mathbb{L}_{11}(T,\mu) \approx \mathbb{L}_{11}(\mu) + \frac{\pi^2}{6}T^2\partial_\mu^2\mathbb{L}_{11}(\mu)\,, \tag{3.2.29a}$$

$$\mathbb{L}_{12}(T,\mu) \approx \mu\mathbb{L}_{11}(\mu) + \frac{\pi^2}{6}T^2\partial_\mu^2\left[\mu\mathbb{L}_{11}(\mu)\right]\,, \tag{3.2.29b}$$

$$\mathbb{L}_{22}(T,\mu) \approx \mu^2\mathbb{L}_{11}(\mu) + \frac{\pi^2}{6}T^2\partial_\mu^2\left[\mu^2\mathbb{L}_{11}(\mu)\right]\,. \tag{3.2.29c}$$

Using these expansions in Eq. (3.2.28) we get :

$$\boldsymbol{\sigma}(T,\mu) \approx e^2\mathbb{L}_{11}(\mu)\,, \tag{3.2.30a}$$

$$\mathbb{S}(T,\mu) \approx -\frac{\pi^2 T}{3e}\mathbb{L}_{11}^{-1}(\mu)\partial_\mu\mathbb{L}_{11}(\mu)\,, \tag{3.2.30b}$$

$$\boldsymbol{\kappa}(T,\mu) \approx \frac{\pi^2}{3}T\mathbb{L}_{11}(\mu)\,. \tag{3.2.30c}$$

As we can see the Mott's formula and the Wiedemann-Franz law hold even in a magnetic field.

3.3 Vertex correction

In the previous section we derived a formula for the transport coefficients in Eq. (3.2.27a). This formula assumes that the eigenstate representation and the Green's function of the whole Hamiltonian is known. In the case of impurities usually the clean system is solvable and we treat the impurities as perturbation. We assume that the Hamiltonian has the form:

$$\mathbb{H} = \mathbb{H}_0 + V(\mathbf{x})\,. \tag{3.3.1}$$

From now on the eigenstate basis will be defined using the eigenstates of the $\mathbb{H}_0$ Hamiltonian[2].

Here we only consider the first order approximation in the impurity density. After resummations as in Ref. [19] we get two terms. Diagrammatically this can be repre-

[2]For simplicity they will be denoted with the same index as before $\mathbb{H}_0\,|a\rangle = E_a\,|a\rangle$.

sented as in Fig. 3.1. The double lines in the diagrams represent the impurity Green's function (which is assumed to be diagonal in the $|a\rangle$ basis). The two contributions will be represented as $\mathbb{L}_{11} = \mathbb{L}_{11}^{(0)} + \mathbb{L}_{11}^{(1)}$.

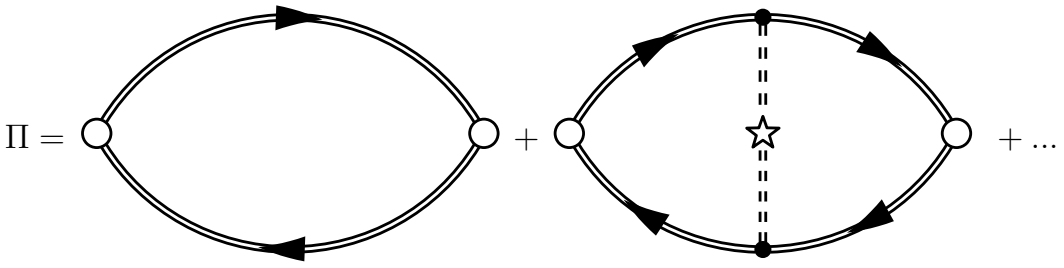

Figure 3.1: Feynman diagrams of the first order approximation of the correlation function. The double lines are the impurity Green's function, the double dashed lines are the effective impurity potentials and the star is the impurity density.

The first diagram ($\mathbb{L}_{11}^{(0)}$) gives exactly the same contribution as in Eq. (3.2.27a), but now the expression is in the eigenstate basis of only $\mathbb{H}_0$ and the Green's functions are the impurity Green's functions (2.2.11).

The second diagram has four Green's functions, and in the momentum representation can be expressed as:

$$\Pi_{\alpha\beta}^{(1)}(i\omega_\lambda) = \frac{1}{V^6} \sum_{\substack{\mathbf{k},\mathbf{k}' \\ \mathbf{k}'',\mathbf{k}''' \\ \mathbf{q}}} \frac{1}{\beta} \sum_n n_i |u_{\mathbf{q}}|^2 \times$$
$$\times \operatorname{Tr}\Big\{ \mathbb{J}_{\mathbf{kk}}^{(\alpha)} \mathbb{G}_{\mathbf{kk}'''}(i\omega_n) \mathbb{G}_{\mathbf{k}'''-\mathbf{qk}''}(i\omega_n) \mathbb{J}_{\mathbf{k}''\mathbf{k}''}^{(\beta)} \mathbb{G}_{\mathbf{k}''\mathbf{k}'-\mathbf{q}}(i\omega_n + i\omega_\lambda) \mathbb{G}_{\mathbf{k}'\mathbf{k}}(i\omega_n + i\omega_\lambda) \Big\} . \tag{3.3.2}$$

In the eigenstate basis this becomes:

$$\Pi_{\alpha\beta}^{(1)}(i\omega_\lambda) = -\frac{1}{V} \sum_{a,b,c,d} V_{ab}^{dc} J_{ad}^{(\alpha)} J_{cb}^{(\beta)} C_{ab}^{dc}(i\omega_\lambda) , \tag{3.3.3a}$$

$$C_{ab}^{dc}(i\omega_\lambda) := -\frac{1}{\beta} \sum_n G_a(i\omega_n + i\omega_\lambda) G_b(i\omega_n + i\omega_\lambda) G_c(i\omega_n) G_d(i\omega_n) , \tag{3.3.3b}$$

$$V_{ab}^{dc} := \frac{1}{V^3} \sum_{\substack{\mathbf{k},\mathbf{k}' \\ \mathbf{q}}} n_i |u_{\mathbf{q}}|^2 \boldsymbol{\phi}_{d\mathbf{k}'}^\dagger \boldsymbol{\phi}_{c\mathbf{k}'-\mathbf{q}} \boldsymbol{\phi}_{b\mathbf{k}-\mathbf{q}}^\dagger \boldsymbol{\phi}_{a\mathbf{k}} . \tag{3.3.3c}$$

Using Eq. (A.1.11) in Appendix A the Matsubara summation can be transformed

into an integral. After performing the zero frequency limit:

$$C_{ab}^{dc} = \int_{-\infty}^{\infty} \frac{\mathrm{d}\varepsilon}{2\pi i} f'(\varepsilon-\mu)\left[g_{abcd}^{AR}(\varepsilon,\varepsilon) - g_{abcd}^{AA}(\varepsilon,\varepsilon)\right] + \\ + f(\varepsilon-\mu)\partial_\omega \left[g_{abcd}^{RR}(\varepsilon,\varepsilon+\omega) - g_{abcd}^{AA}(\varepsilon,\varepsilon+\omega)\right]\big|_{\omega=0} , \tag{3.3.4}$$

where $g_{abcd}^{XX'}(\varepsilon,\varepsilon') := G_a^X(\varepsilon)G_b^X(\varepsilon)G_c^{X'}(\varepsilon')G_d^{X'}(\varepsilon')$. Using this, the vertex correction of the conductivity can be expressed as:

$$L_{\alpha\beta}^{11(1)} = -\frac{i}{\pi V}\sum_{a,b,c,d} V_{ab}^{dc} J_{ad}^{(\alpha)} J_{cb}^{(\beta)} C_{ab}^{dc} , \tag{3.3.5a}$$

$$V_{ab}^{dc} = \frac{1}{V}\sum_{\mathbf{q}} n_i |u_{\mathbf{q}}|^2 F_{ab}^*(\mathbf{q}) F_{dc}(\mathbf{q}) , \tag{3.3.5b}$$

where we used the F functions defined in Eq. (2.2.7b). To get the first order approximation in C_{ab}^{dc} it is enough to take the $\Gamma \to 0$ limit, since V_{ab}^{dc} is already proportional to the impurity density.

Chapter 4

Conductivity in low magnetic fields

In this chapter we show how the conductivity can be calculated microscopically at low fields. The results shown here are published in Ref. [122]. In the previous chapter we showed that the conductivity is enough to express all the transport coefficients, so in this section we only discuss the conductivity tensor. First we show the expression for the zero magnetic field and then the linear order in the magnetic field. In both cases we are interested in the low scattering rate limit, and only keep the lowest order terms in the scattering rate.

4.1 Conductivity at zero magnetic field

In the absence of the magnetic field, a periodic Hamiltonian will be diagonal in the quasi momentum described by the (2.1.3) Bloch Hamiltonian. The eigenvalues and eigenvectors of this are denoted as $\mathbb{H}_{\mathbf{k}} |a, \mathbf{k}\rangle = E_{a\mathbf{k}} |a, \mathbf{k}\rangle$. For simplicity from now on $\mathbb{H}_{\mathbf{k}} \equiv \mathbb{H}$, $E_{a\mathbf{k}} \equiv E_a$, $|a, \mathbf{k}\rangle \equiv |a\rangle$, and $\partial_{k_\mu} \equiv \partial_\mu$. The current operators can be expressed using the generalized Hellmann-Feynman theorem [127]:

$$J^{(\mu)}_{ab} = \langle a|\mathbb{J}_\mu|b\rangle = \langle a|\partial_\mu \mathbb{H}|b\rangle = \delta_{a,b}\partial_\mu E_a + (E_b - E_a)\langle a|\partial_\mu b\rangle \ . \tag{4.1.1}$$

As explained in the previous chapter the conductivity can be calculated through the retarded current-current correlation function as:

$$\sigma_{\mu\nu} = \lim_{\omega\to 0} \frac{ie^2}{\omega} \Pi^R_{\mu\nu}(\omega) \,, \tag{4.1.2}$$

Using Eq. (3.2.16) the Matsubara current-current correlation function in zero magnetic

field is expressed as:

$$\sigma^{(0)}_{\mu\nu} = \frac{e^2}{V}\sum_{\mathbf{k},a,b} \mathrm{Im}\Big\{ J^{(\mu)}_{ab} J^{(\nu)}_{ba} \Big\} \,\mathrm{Re}\, C_{ba} + \mathrm{Re}\Big\{ J^{(\mu)}_{ab} J^{(\nu)}_{ba} \Big\} \,\mathrm{Im}\, C_{ba}\,, \tag{4.1.3a}$$

$$\mathrm{Im}\, C_{ba} = -\int_{-\infty}^{\infty} \frac{\mathrm{d}\varepsilon}{\pi} \partial_\varepsilon f(\varepsilon-\mu)\ \ \mathrm{Im}\, G^R_b(\varepsilon)\,\mathrm{Im}\, G^R_a(\varepsilon)\,, \tag{4.1.3b}$$

$$\mathrm{Re}\, C_{ba} = 2\int_{-\infty}^{\infty} \frac{\mathrm{d}\varepsilon}{\pi} f(\varepsilon-\mu)\partial_\varepsilon \big(\mathrm{Re}\, G^R_b(\varepsilon)\big)\,\mathrm{Im}\, G^R_a(\varepsilon)\,. \tag{4.1.3c}$$

Since we are interested in the low scattering rate limit, we assume that the Green's function can be expressed as:

$$G^R_a(\varepsilon) = \frac{1}{\varepsilon - E_a + i\Gamma}\,, \tag{4.1.4}$$

where the scattering rate Γ is constant, and $\Gamma \to 0$. With this assumption the integrals in Eqs. (4.1.3b) and (4.1.3c) can be evaluated (for details see Appendix A):

$$\mathrm{Im}\, C_{ba} = -\delta_{ab}\frac{f'(E_a-\mu)}{2\Gamma} + \mathcal{O}\big(\Gamma^1\big)\,, \tag{4.1.5a}$$

$$\mathrm{Re}\, C_{ba} = \frac{2f(E_a-\mu)}{(E_a-E_b)^2} + \mathcal{O}\big(\Gamma^1\big)\,. \tag{4.1.5b}$$

Taking the products of two current operator matrix elements (4.1.1) we get:

$$J^{(\mu)}_{a,b} J^{(\nu)}_{b,a} = \delta_{a,b}\partial_\mu E_a \partial_\nu E_a + (E_b - E_a)^2 \left\langle \partial_\mu a \,|b\rangle\langle b|\, \partial_\nu a \right\rangle \tag{4.1.6}$$

Substituting everything back in Eq. (4.1.3) we get two contributions $\sigma^{(0)}_{\mu\nu} = \sigma^N_{\mu\nu} + \sigma^A_{\mu\nu}$:

$$\sigma^N_{\mu\nu} = -\frac{e^2\tau}{V}\sum_{\mathbf{k},a} \partial_\mu E_a \partial_\nu E_a f'(E_a-\mu)\,, \tag{4.1.7a}$$

$$\sigma^A_{\mu\nu} = -\frac{e^2}{V}\sum_{\mathbf{k},a} \Omega^a_{\mu\nu} f(E_a-\mu)\,, \tag{4.1.7b}$$

where $\Gamma = \hbar/2\tau$ and $\Omega^a_{\mu\nu}$ is the the Berry curvature [3, 8]:

$$\Omega^a_{\mu\nu} = i\big[\,\langle \partial_x a|\partial_y a\rangle - \langle \partial_y a|\partial_x a\rangle\,\big]\,. \tag{4.1.8}$$

At zero magnetic field we recover the usual Boltzmann result $\sigma^N_{\mu\nu}$ [18, 19] and the anomalous conductivity $\sigma^A_{\mu\nu}$ connected to the Berry curvature [8, 28]. Because of the symmetry properties of the Berry curvature, the anomalous contribution only appears in the off-diagonal conductivity, giving rise to the anomalous Hall effect.

4.2 Linear order of the magnetic field

In this section we will express the conductivity up to linear order of the magnetic field. The uniform magnetic field points in the z direction, and we are interested in the Hall conductivity σ_{xy} and longitudinal conductivity σ_{zz}. For the calculation of the current-current correlation we base our calculation on the microscopic theory of Hall conductivity developed by Fukuyama [30, 31]. Here the magnetic field is treated as a perturbation similarly to the electric field. In the first order of the magnetic field the current-current correlation function is (for details on how these formulas are derived see Appendix B):

$$\Pi^{(1)}_{xy}(i\omega_\lambda) = -\frac{ieB}{\beta V}\sum_{n,\mathbf{k}} \mathrm{Tr}[\mathbb{J}_x\mathbb{G}_+\mathbb{J}_y\mathbb{G}\mathbb{J}_x\mathbb{G}\mathbb{J}_y\mathbb{G} - \mathbb{J}_x\mathbb{G}_+\mathbb{J}_y\mathbb{G}_+\mathbb{J}_x\mathbb{G}_+\mathbb{J}_y\mathbb{G}]\,, \tag{4.2.1a}$$

$$\Pi^{(1)}_{zz}(i\omega_\lambda) = -\frac{ieB}{\beta V}\sum_{n,\mathbf{k}} \mathrm{Tr}[\mathbb{J}_z\mathbb{G}_+\mathbb{J}_z\mathbb{G}\mathbb{J}_x\mathbb{G}\mathbb{J}_y\mathbb{G} - \mathbb{J}_z\mathbb{G}_+\mathbb{J}_y\mathbb{G}_+\mathbb{J}_x\mathbb{G}_+\mathbb{J}_z\mathbb{G}]\,. \tag{4.2.1b}$$

where $\mathbb{G} \equiv \mathbb{G}(\mathbf{k}, i\varepsilon_n)$ and $\mathbb{G}_+ \equiv \mathbb{G}(\mathbf{k}, i\varepsilon_n + i\omega_\lambda)$.

4.2.1 Hall conductivity

We start with discussing the Hall conductivity. Using Eq. (4.2.1a) in the eigenstate basis the Hall conductivity can be expressed as:

$$\sigma^{(1)}_{xy} = -B\frac{e^3}{V}\sum_{\mathbf{k}}\sum_{a,b,c,d} J^{(x)}_{da}J^{(y)}_{ab}J^{(x)}_{bc}J^{(y)}_{cd}C_{abcd}\,, \tag{4.2.2a}$$

$$C_{abcd} = -\lim_{\omega\to 0}\frac{1}{\beta\omega}\sum_n G^+_a G_d(G_bG_c - G^+_bG^+_c)\,, \tag{4.2.2b}$$

where the $i\omega_\lambda = \omega + i\eta$ substitution was made and the $\eta \to 0$ limit was taken in C_{abcd}. Using the Eq. (4.1.1) form of the current operator we will have five different type of terms in Eq. (4.2.2a) based on the number of Kronecker deltas. The terms containing

three Kronecker deltas will vanish after summation so we only have to consider the other four type of terms $\sigma_{xy}^{(1)} = \sigma_{xy}^{O} + \sigma_{xy}^{I} + \sigma_{xy}^{II} + \sigma_{xy}^{IV}$, where the indices represent the number of Kronecker deltas. After evaluating the sums over the Kronecker deltas and renaming indices we get:

$$\sigma_{xy}^{IV} = -B\frac{e^3}{V}\sum_{\mathbf{k},a}(\partial_x E_a)^2(\partial_y E_a)^2 C_{aaaa}\,, \tag{4.2.3a}$$

$$\begin{aligned}\sigma_{xy}^{II} = -B\frac{e^3}{V}\sum_{\mathbf{k},a,b}(E_a - E_b)^2\times \\ \times\Big\{\partial_x E_a\partial_x E_b\,\langle\partial_y a|b\rangle\,\langle b|\partial_y a\rangle\,C_{abba} + \partial_y E_a\partial_y E_b\,\langle\partial_x a|b\rangle\,\langle b|\partial_x a\rangle\,C_{aabb} + \\ + \partial_x E_a\partial_y E_a\Big[\,\langle\partial_y a|b\rangle\,\langle b|\partial_x a\rangle\,(C_{aaab} + C_{abaa}) + \langle\partial_x a|b\rangle\,\langle b|\partial_y a\rangle\,(C_{aaba} + C_{baaa})\Big]\Big\}\,,\end{aligned} \tag{4.2.3b}$$

$$\begin{aligned}\sigma_{xy}^{I} = -B\frac{e^3}{V}\sum_{\mathbf{k},a,b,c}(E_a - E_b)(E_b - E_c)(E_c - E_a)\times \\ \times\Big\{\partial_y E_a\,\langle a|\partial_x c\rangle\,\langle b|\partial_x a\rangle\,\langle c|\partial_y b\rangle\,(C_{aacb} + C_{cbaa}) - \\ - \partial_x E_a\,\langle c|\partial_y a\rangle\,\langle a|\partial_y b\rangle\,\langle b|\partial_x c\rangle\,(C_{abca} + C_{caab})\Big\}\,,\end{aligned} \tag{4.2.3c}$$

$$\begin{aligned}\sigma_{xy}^{O} = -B\frac{e^3}{V}\sum_{\mathbf{k},a,b,c,d}(E_a - E_d)(E_b - E_a)(E_c - E_b)(E_d - E_c)\times \\ \times\,\langle d|\partial_x a\rangle\,\langle a|\partial_y b\rangle\,\langle b|\partial_x c\rangle\,\langle c|\partial_y d\rangle\,C_{abcd}\,.\end{aligned} \tag{4.2.3d}$$

The next step is to evaluate the Matsubara summations. The details of these are discussed in Appendix A. We are interested in the low impurity case so we assume that the scattering rate is constant $\Gamma_a(\varepsilon, \mathbf{k}) \equiv \Gamma$ and small, and we neglect terms of $\mathcal{O}(\Gamma^0)$. It can be shown that $\sigma_{xy}^{I} = \mathcal{O}(\Gamma^0)$. Keeping only the terms $\mathcal{O}(\Gamma^{-2})$ and $\mathcal{O}(\Gamma^{-1})$, only σ_{IV}, σ_{II}, and σ_{O} remain:

$$\sigma_{xy}^{IV} = -\frac{Be^3}{4\Gamma^2 V}\sum_{\mathbf{k},a}(\partial_x E_a)^2(\partial_y E_a)^2 f_a''\,, \tag{4.2.4a}$$

$$\sigma_{xy}^{II} = -\frac{3Be^3}{4\Gamma^2 V}\sum_{\mathbf{k},a}\partial_x E_a\partial_y E_a f_a'\left(\Theta_{xy}^a + \Theta_{yx}^a\right) + \frac{Be^3}{2\Gamma V}\sum_{\mathbf{k},a}\partial_x E_a\partial_y E_a f_a'\Omega_{xy}^a -$$

$$- \frac{Be^3}{4\Gamma V} \sum_{\mathbf{k},a} \partial_x E_a \partial_y E_a f_a'' i \left(\Theta_{xy}^a - \Theta_{yx}^a\right) , \tag{4.2.4b}$$

$$\sigma_{xy}^O = - \frac{Be^3}{2\Gamma V} \sum_{\mathbf{k},a} f_a' i \left(\Theta_{xy}^a - \Theta_{yx}^a\right) \left(\Theta_{xy}^a + \Theta_{yx}^a\right) , \tag{4.2.4c}$$

where $f_a = (\exp\{\beta(E_a - \mu)\} + 1)^{-1}$ is the Fermi-Dirac distribution, Ω_{xy}^a is the Berry curvature defined in Eq. (4.1.8), and:

$$\Theta_{xy}^a = \sum_b (E_a - E_b) \langle \partial_x a | b \rangle \langle b | \partial_y a \rangle . \tag{4.2.5}$$

The quantity Θ_{xy}^a can be transformed to:

$$\Theta_{xy}^a = \langle \partial_x a | \partial_y H - \partial_y E_a | a \rangle . \tag{4.2.6}$$

Then, using $\partial_x \partial_y \mathbb{H} = 0$ and the derivative of $\langle a | \partial_y \mathbb{H} | a \rangle = \partial_y E_a$ we can show the following (similarly to Ref. [38]):

$$\Theta_{xy}^a + \Theta_{yx}^a = \partial_x \partial_y E_a . \tag{4.2.7}$$

The imaginary part of Θ_{xy}^a is the orbital magnetic moment [5, 8]:

$$M_{xy}^a = \frac{1}{2i} \left(\Theta_{xy}^a - \Theta_{xy}^a\right) = \mathrm{Im}\{ \langle \partial_x a | (E_a - H) | \partial_y a \rangle \} . \tag{4.2.8}$$

Using partial integrations and separating terms proportional to $1/\Gamma^2$ and $1/\Gamma$ the magnetic field dependent part of the Hall conductivity becomes ($\sigma_{xy}^{(1)} = \sigma_{xy}^B + \sigma_{xy}^Q$)

$$\sigma_{xy}^B = \frac{Be^3\tau^2}{\hbar^4 V} \sum_{\mathbf{k},a} f_a' \left\{ \frac{1}{2} \Big[\left(\partial_x E_a\right)^2 \partial_y^2 E_a + \left(\partial_y E_a\right)^2 \partial_x^2 E_a \Big] - \partial_x E_a \partial_x \partial_y E_a \partial_y E_a \right\} , \tag{4.2.9a}$$

$$\sigma_{xy}^Q = \frac{Be^3\tau}{\hbar^3 V} \sum_{\mathbf{k},a} f_a' \left\{ \partial_x E_a \partial_y E_a \Omega_{xy}^a + \partial_x \partial_y E_a M_{xy}^a - \frac{1}{2} \Big[\partial_x E_a \partial_y M_{xy}^a + \partial_y E_a \partial_x M_{xy}^a \Big] \right\} , \tag{4.2.9b}$$

where $\Gamma = \hbar/2\tau$. In this final form only the partial derivatives of the energy and gauge invariant quantities such as the Berry curvature and the orbital magnetic moment appear. The σ_{xy}^B term is the same as the result of the semiclassical Boltzmann transport theory with relaxation time approximation [31]. The σ_{xy}^Q term is the quantum

correction that contains the Berry curvature and orbital magnetic moment.

4.2.2 Longitudinal conductivity

We continue with the longitudinal conductivity. Using Eq. (4.2.1b) in the eigenstate basis the longitudinal conductivity can be expressed as:

$$\sigma_{zz}^{(1)} = -B\frac{e^3}{V}\sum_{\substack{\mathbf{k}\\a,b\\c,d}} v_{da}^z v_{ab}^z \left(J_{bc}^{(x)} J_{cd}^{(y)} D_{abcd} - J_{bc}^{(y)} J_{cd}^{(x)} \tilde{D}_{abcd} \right) , \tag{4.2.10a}$$

$$D_{abcd} = -\lim_{\omega\to 0}\frac{1}{\beta\omega}\sum_n G_a^+ G_b G_c G_d \,, \tag{4.2.10b}$$

$$\tilde{D}_{abcd} = -\lim_{\omega\to 0}\frac{1}{\beta\omega}\sum_n G_a G_b^+ G_c^+ G_d^+ \,. \tag{4.2.10c}$$

After summation over the Kronecker deltas we get:

$$\sigma_{zz}^{IV} = -B\frac{e^3}{V}\sum_{\mathbf{k},a}(\partial_z E_a)^2 \partial_x E_a \partial_y E_a (D_{aaaa} - \tilde{D}_{aaaa}) \,, \tag{4.2.11a}$$

$$\begin{aligned}\sigma_{zz}^{II} = -B\frac{e^3}{V}\sum_{\mathbf{k},a,b}(E_a - E_b)^2 \times \\ \times \Big[\partial_z E_a \partial_x E_b \langle \partial_z a|b\rangle \langle b|\partial_y a\rangle D_{abba} + \partial_z E_a \partial_y E_b \langle \partial_x a|b\rangle \langle b|\partial_z a\rangle D_{aabb} + \\ + \partial_x E_a \partial_y E_a \langle \partial_z a|b\rangle \langle b|\partial_z a\rangle D_{baaa} + \partial_z E_a \partial_z E_a \langle \partial_x a|b\rangle \langle b|\partial_y a\rangle D_{aaba} + \\ + \partial_x E_a \partial_z E_a \langle \partial_y a|b\rangle \langle b|\partial_z a\rangle D_{aaab} + \partial_y E_a \partial_z E_a \langle \partial_z a|b\rangle \langle b|\partial_x a\rangle D_{abaa} - \\ - (x \leftrightarrow y, D \leftrightarrow \tilde{D}) \Big] \,,\end{aligned} \tag{4.2.11b}$$

$$\begin{aligned}\sigma_{zz}^{I} = -B\frac{e^3}{V}\sum_{\mathbf{k},a,b,c}(E_a - E_b)(E_b - E_c)(E_c - E_a) \times \\ \times \Big[\partial_y E_a \langle a|\partial_z c\rangle \langle b|\partial_x a\rangle \langle c|\partial_z b\rangle D_{cbaa} - \partial_x E_a \langle a|\partial_y b\rangle \langle b|\partial_z c\rangle \langle c|\partial_z a\rangle D_{caab} + \\ + \partial_z E_a \langle a|\partial_x c\rangle \langle b|\partial_z a\rangle \langle c|\partial_y b\rangle D_{aacb} - \partial_z E_a \langle a|\partial_z b\rangle \langle b|\partial_x c\rangle \langle c|\partial_y a\rangle D_{abca} - \\ - (x \leftrightarrow y, D \leftrightarrow \tilde{D}) \Big] \,,\end{aligned} \tag{4.2.11c}$$

$$\begin{aligned}\sigma_{zz}^{O} = -B\frac{e^3}{V}\sum_{\mathbf{k},a,b,c,d}(E_a - E_d)(E_b - E_a)(E_c - E_b)(E_d - E_c) \times \\ \times \Big[\langle d|\partial_z a\rangle \langle a|\partial_z b\rangle \langle b|\partial_x c\rangle \langle c|\partial_y d\rangle D_{abcd} - (x \leftrightarrow y, D \leftrightarrow \tilde{D}) \Big] \,.\end{aligned} \tag{4.2.11d}$$

The Matsubara summation is evaluated the same way as for the Hall conductivity (for details see Appendix A) and we get:

$$\sigma_{zz}^{IV} = -B\frac{e^3}{4\Gamma^2 V}\sum_{\mathbf{k},a}(\partial_z E_a)^2\partial_x E_a\partial_y E_a f_a'' \,, \tag{4.2.12a}$$

$$\begin{aligned}\sigma_{zz}^{II} =& -B\frac{e^3}{4\Gamma^2 V}\sum_{\mathbf{k},a}\partial_z E_a\big[\partial_x E_a\partial_y\partial_z E_a + \partial_y E_a\partial_z\partial_x E_a + \partial_z E_a\partial_x\partial_y E_a\big] - \\ &- B\frac{e^3}{2\Gamma V}\sum_{\mathbf{k},a}\partial_z E_a\Big\{f_a'\boldsymbol{\nabla}E_a\cdot\boldsymbol{\Omega}^a + f_a''\boldsymbol{\nabla}E_a\cdot\mathbf{M}^a + \\ &\quad + if_a'\sum_b\left[(\partial_x E_b\,\langle\partial_y a|b\rangle\,\langle b|\partial_z a\rangle - z\leftrightarrow y) - x\leftrightarrow y\right]\Big\}\,,\end{aligned} \tag{4.2.12b}$$

$$\begin{aligned}\sigma_{zz}^{I} =& -B\frac{ie^3}{2\Gamma V}\sum_{\mathbf{k},a}f_a'\partial_z E_a\Bigg\{\partial_z\partial_x E_a\,\langle a|\partial_y a\rangle - \partial_y\partial_z E_a\,\langle a|\partial_x a\rangle - \\ &- \sum_b\left[(\partial_x E_b\,\langle\partial_y a|b\rangle\,\langle b|\partial_z a\rangle - z\leftrightarrow y) - x\leftrightarrow y\right] + \\ &+ \left[\Big(\langle\partial_y a|\partial_x H|\partial_z a\rangle - y\leftrightarrow z\Big) - x\leftrightarrow y\right]\Bigg\}\,,\end{aligned} \tag{4.2.12c}$$

$$\sigma_{zz}^{O} = -B\frac{e^3}{2\Gamma V}\sum_{\mathbf{k},a}f_a'\big[\partial_z\partial_x E_a M_x^a - \partial_y\partial_z E_a M_y^a\big]\,. \tag{4.2.12d}$$

Using partial integrations a lot of these terms can be canceled. One of the less trivial partial integrations done in Eq. (4.2.12b) is of the form:

$$\begin{aligned}\sum_{\mathbf{k},a}\partial_z E_a f_a''\boldsymbol{\nabla}E_a\cdot\mathbf{M}^a = -\sum_{\mathbf{k},a}\Big[&\partial_z E_a f_a''\partial_z E_a M_z^a + 2f_a'\partial_z(\partial_z E_a M_z^a) + \\ &+ f_a'\partial_x(\partial_z E_a M_x^a) + f_a'\partial_y(\partial_z E_a M_y^a)\Big]\,.\end{aligned} \tag{4.2.13}$$

Using equations like $\partial_x\partial_z[(E_a - H)\,|a\rangle] = 0$ this can be transformed and used to cancel some terms in Eq. (4.2.12). After several transformations the longitudinal conductivity can also be expressed as $\sigma_{zz}^{(1)} = \sigma_{zz}^B + \sigma_{zz}^Q$ with terms proportional to τ^2 and τ:

$$\sigma_{zz}^B = 0\,, \tag{4.2.14a}$$

$$\sigma_{zz}^Q = -\frac{Be^3\tau}{\hbar^3 V}\sum_{\mathbf{k},a}f_a'\Big[\partial_z E_a\,(2\boldsymbol{\nabla}E_a\cdot\boldsymbol{\Omega}^a - \partial_z E_a\Omega_z^a) + \partial_z E_a\partial_z M_z^a - \partial_z^2 E_a M_z^a\Big]\,, \tag{4.2.14b}$$

where $\Omega^a_\mu = \frac{1}{2}\varepsilon_{\mu\nu\eta}\Omega^a_{\nu\eta}$ and $M^a_\mu = \frac{1}{2}\varepsilon_{\mu\nu\eta}M^a_{\nu\eta}$.

After the partial integrations the Boltzmann contribution σ^B_{zz} vanishes as expected from the Boltzmann theory. Similarly to the Hall-conductivity, in the case of the longitudinal conductivity we also have a quantum contribution σ^Q_{zz} expressed with the Berry curvature and orbital magnetic moment.

If the system is time reversal symmetric $E_a(\mathbf{k}) = E_a(-\mathbf{k})$, $\partial_\mu E_a(\mathbf{k}) = -\partial_\mu E_a(-\mathbf{k})$, $\Omega^a_\mu(\mathbf{k}) = -\Omega^a_\mu(-\mathbf{k})$ and $M^a_\mu(\mathbf{k}) = -M^a_\mu(-\mathbf{k})$. These relations guarantee that both $\sigma^Q_{xy} = 0$ and $\sigma^Q_{zz} = 0$. Thus, in order to see the quantum contributions we need to break time reversal symmetry.

The expressions of the Berry curvature (4.1.8) and orbital magnetic moment (4.2.8), are hard to use in these forms. These quantities can be expressed in an easier to evaluate formula where the derivatives of eigenstates do not appear. Using Eq. (4.1.1) and the completeness of eigenstates:

$$\Omega^a_{\mu\nu} = i\sum_{b\neq a}\frac{\langle a|\partial_\mu H|b\rangle\ \langle b|\partial_\nu H|a\rangle}{(E_a - E_b)^2} - \mu \leftrightarrow \nu\,, \tag{4.2.15a}$$

$$M^a_{\mu\nu} = \frac{1}{2i}\sum_{b\neq a}\frac{\langle a|\partial_\mu H|b\rangle\ \langle b|\partial_\nu H|a\rangle}{E_a - E_b} - \mu \leftrightarrow \nu\,. \tag{4.2.15b}$$

A simple example for the calculation of the magnetoconductivity using Eqs. (4.2.9) and (4.2.14) is the calculation for the nearly free electron model:

$$H = \frac{\hbar^2 k^2}{2m}\,, \qquad\qquad E = \frac{\hbar^2 k^2}{2m}\,. \tag{4.2.16}$$

The different components of the magnetoconductivity are:

$$\sigma^B_{xy} = -\frac{Be^3\tau^2}{m^2}n_e\,, \qquad \sigma^Q_{xy} = 0\,, \qquad \sigma^B_{zz} = 0\,, \qquad \sigma^Q_{zz} = 0\,, \tag{4.2.17}$$

where $n_e = \frac{1}{V}\sum_{\mathbf{k}} f$ is the number density of electrons. This result is the same as the classical result [2].

4.3 Tilted Weyl node

In this section we study the magnetoconductivity of a tilted Weyl node. We start with a general two-level system with the following Hamiltonian:

$$H = \mathbf{h}(\mathbf{k}) \cdot \boldsymbol{\sigma} + h_0(\mathbf{k})\sigma_0 \,, \qquad E_\pm = h_0 \pm h \,, \tag{4.3.1}$$

where σ_α are the Pauli matrices. Using Eq. (4.2.15) for the Berry curvature and orbital magnetic moment we get:

$$\Omega^\pm_{\mu\nu} = \mp\frac{1}{2}\frac{\mathbf{h}\cdot(\partial_\mu\mathbf{h}\times\partial_\nu\mathbf{h})}{h^3} \,, \qquad M^\pm_{\mu\nu} = \frac{1}{2}\frac{\mathbf{h}\cdot(\partial_\mu\mathbf{h}\times\partial_\nu\mathbf{h})}{h^2} \,. \tag{4.3.2}$$

First, we discuss a simple example for a two-level system, a single Weyl node described by the Weyl Hamiltonian:

$$\mathbf{h} = v\hbar\mathbf{k} \,, \qquad h_0 = 0 \,, \qquad E_\pm = \pm v\hbar k \,. \tag{4.3.3}$$

The Berry curvature and orbital magnetic moment using Eq. (4.3.2) becomes:

$$\boldsymbol{\Omega}^\pm = \mp\frac{1}{2}\frac{\mathbf{k}}{k^3} \,, \qquad \mathbf{M}^\pm = \frac{1}{2}\frac{\mathbf{k}}{k^2} \,. \tag{4.3.4}$$

The different components of the magnetoconductivity calculated from Eqs. (4.2.9) and (4.2.14) at zero temperature are:

$$\sigma^B_{xy} = -\frac{v\mu B e^3\tau^2}{6\pi^2\hbar^3} \,, \qquad \sigma^Q_{xy} = 0 \,, \qquad \sigma^B_{zz} = 0 \,, \qquad \sigma^Q_{zz} = 0 \,. \tag{4.3.5}$$

Even though the Berry curvature and orbital magnetic moment are not vanishing, after integration the quantum contributions vanish because of the mirror symmetries of the system.

In order to get a finite quantum contribution we introduce a small tilting ($t < 1$) in the k_z direction:

$$\mathbf{h} = v\hbar\mathbf{k} \,, \qquad h_0 = v\hbar t k_z \,, \qquad E_\pm = v\hbar(tk_z \pm k) \,. \tag{4.3.6}$$

The dispersion relation with different tiltings is shown in Fig. 4.1. The Berry curvature and orbital magnetic moment is unchanged, but the tilting breaks the mirror symmetry in the dispersion relation, and the components of the zero temperature magnetocon-

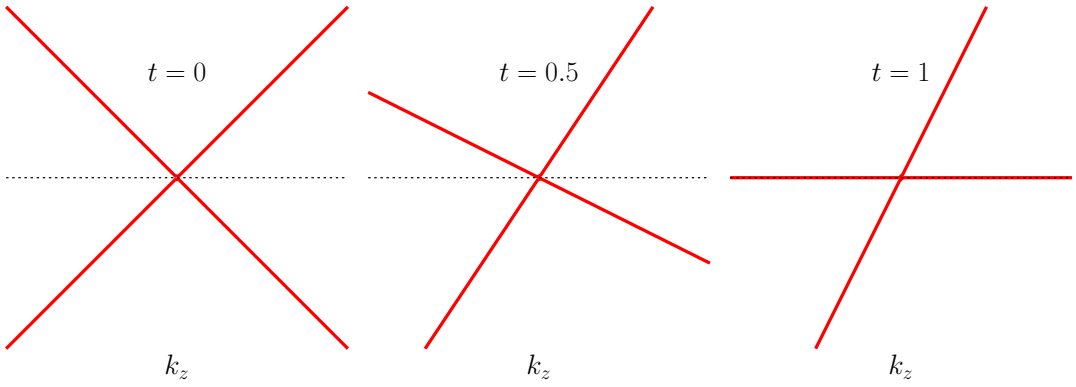

Figure 4.1: Schematic dispersion relation in the k_z direction of a tilted Weyl node with tilting t.

ductivity calculated from Eqs. (4.2.9) and (4.2.14) become:

$$\sigma_{xy}^{B} = \sigma_h \frac{3\tanh^{-1}(t) - 3t}{t^3}\,, \qquad \sigma_h = -\frac{v\mu B e^3 \tau^2}{6\pi^2\hbar^3}\,, \tag{4.3.7a}$$

$$\sigma_{zz}^{Q} = \sigma_l t\,, \qquad \sigma_l = -\frac{vBe^3\tau}{4\pi^2\hbar^2}\,, \tag{4.3.7b}$$

where σ_h is the Hall conductivity of the not tilted Weyl node in Eq. (4.3.5). The rest

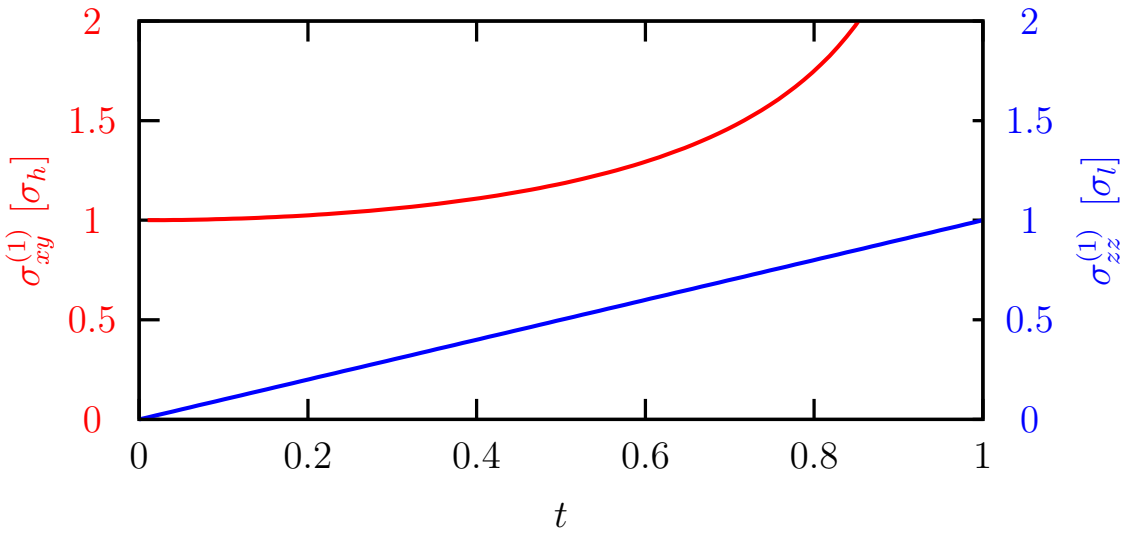

Figure 4.2: The Hall conductivity (4.3.7a) and longitudinal magnetoconductivity (4.3.7b) of a tilted Weyl node with tilting t. $\sigma_h = -\frac{v\mu Be^3\tau^2}{6\pi^2\hbar^3}$ is the Hall conductivity at $t = 0$ and $\sigma_l = -\frac{vBe^3\tau}{4\pi^2\hbar^2}$.

of the components are still zero. The magnetoconductivity as a function of the tilting parameter is shown in Fig. 4.2.

As a consequence of the tilting a linear longitudinal magnetoconductivity appears. This effect was studied using the semiclassical Boltzmann transport theory in Refs. [106] and [107]. These studies do not take into account the effect of the orbital magnetic moment. In order to compare our results we separated the longitudinal magnetoconductivity in Eq. (4.3.7b) to the term coming from the Berry curvature and the term coming from the orbital magnetic moment:

$$\sigma_{zz}^{Q(\mathrm{berry})} = \sigma_l \frac{-3t + 5t^3 + 3t^5 + 3(t^2-1)^2 \tanh^{-1}(t)}{3t^4}\,, \tag{4.3.8a}$$

$$\sigma_{zz}^{Q(\mathrm{mag})} = \sigma_l \frac{3t - 5t^3 - 3(t^2-1)^2 \tanh^{-1}(t)}{3t^4}\,. \tag{4.3.8b}$$

These separated components can be seen in Fig. 4.3. The result containing only the Berry curvature coincides with the result gotten in the semiclassical Boltzmann theory [106, 107]. But as we can see on the figure the terms containing the orbital magnetic moment significantly modify the result. The qualitative behavior of the result is not affected, but the quantitative value changes.

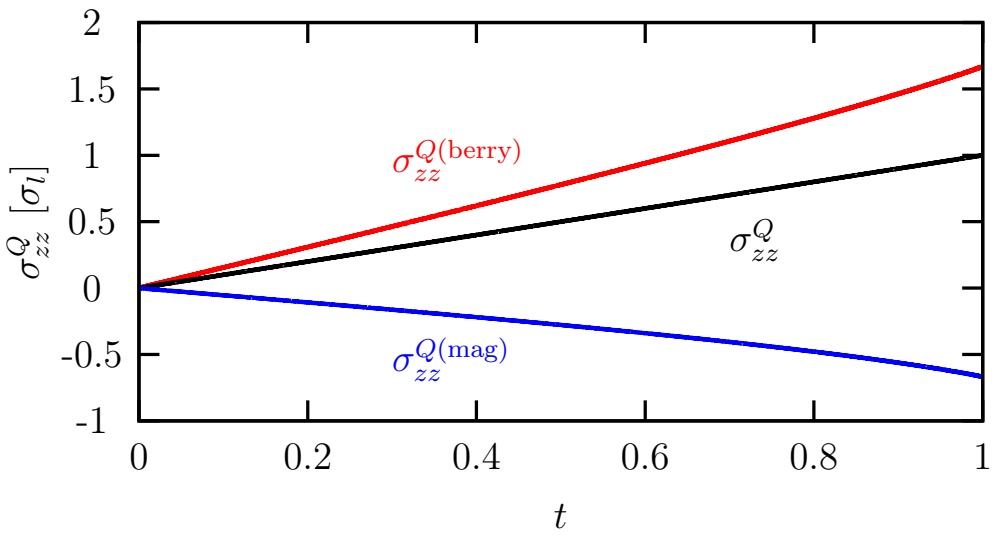

Figure 4.3: The longitudinal magnetoconductivity (4.3.7b) of a tilted Weyl node with tilting t. The red and blue line show the contribution of the Berry curvature and the orbital magnetic moment separately as in Eq. (4.3.8). $\sigma_l = -\frac{vBe^3\tau}{4\pi^2\hbar^2}$.

In real materials Weyl nodes come in pairs with opposite tilting and opposite chirality, and the Hamiltonian of the second Weyl node is expressed as [106, 107, 128]:

$$\mathbf{h} = -v\hbar\mathbf{k}\,, \qquad h_0 = -v\hbar t k_z\,, \qquad E_\pm = -v\hbar(tk_z \pm k)\,. \tag{4.3.9}$$

Because of the sign change of both the tilting and the chirality the linear longitudinal conductivity persists even in the case of a pair of Weyl nodes. The total conductivity of two Weyl nodes separated into $\sigma_{zz}^{2W} = \sigma_{zz}^{2W(\mathrm{berry})} + \sigma_{zz}^{2W(\mathrm{mag})}$ can be expressed as:

$$\sigma_{zz}^{2W(\mathrm{berry})} = 4\sigma_l \tanh^{-1}(t)\,, \tag{4.3.10a}$$

$$\sigma_{zz}^{2W(\mathrm{mag})} = \sigma_l \frac{-4t - 2(t^2-2)\tanh^{-1}(t)}{t^2}\,. \tag{4.3.10b}$$

The longitudinal conductivity of the two Weyl nodes is shown in Fig. 4.4. As we can see the qualitative behavior for small tiltings does not change when two Weyl nodes are present.

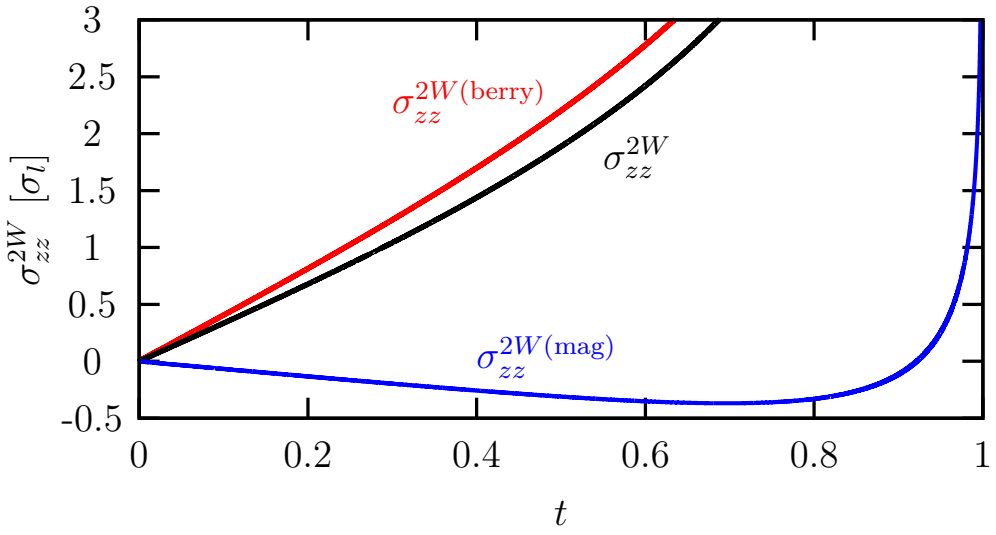

Figure 4.4: The longitudinal magnetoconductivity (4.3.7b) of a pair of tilted Weyl nodes with tilting t. The red and blue line show the contribution of the Berry curvature and the orbital magnetic moment separately as in Eq. (4.3.10). $\sigma_l = -\frac{vBe^3\tau}{4\pi^2\hbar^2}$.

This type of linear longitudinal magnetoconductivity has very unusual properties. The sign of the conductivity changes with the magnetic field, which can be used ex-

perimentally to distinguish this component from $\sigma_{zz}^{(0)}$ and $\sigma_{zz}^{(2)}$. It produces a negative magnetoresistance[1] and gives an alternate mechanism to the chiral anomaly that produces a negative magnetoresistance. The chiral anomaly is also an effect that happens when the magnetic field and electric field is parallel, but the longitudinal magnetoconductivity in that case is quadratic in the magnetic field, and happens without any tilting in the Weyl node. The symmetry properties in the magnetic field can be used to separate these two effects experimentally.

In order to estimate the magnitude of the linear longitudinal magnetoconductivity we can compare it to the conductivity at zero magnetic field and zero tilting calculated from Eq. (4.1.7):

$$\sigma_{zz}^{(0)} = \frac{4\pi}{3}\frac{e^2}{h}\frac{\mu^2\tau}{h^2 v}\,. \tag{4.3.11}$$

Since both quantities are proportional to the relaxation time, the ratio of σ_l to $\sigma_{zz}^{(0)}$ becomes a τ independent number:

$$\delta = \frac{\sigma_l}{\sigma_{zz}^{(0)}} = \frac{3}{2}\frac{\hbar v^2 eB}{\mu^2}\,. \tag{4.3.12}$$

Assuming realistic parameters such as $v = 10 \times 10^6\,\mathrm{m\,s^{-1}}$, $\mu = 200\,\mathrm{meV}$, and $B = 1\,\mathrm{T}$ the ratio becomes $\delta \approx 0.025$. The effect is small, but not negligible and it can be enhanced with a smaller chemical potential.

4.4 Summary

In this chapter we studied the magnetoconductivity at low magnetic fields. We discussed the conductivity up to linear order of the magnetic field using linear response theory. We evaluated the microscopic formula developed by Fukuyama [30, 31] in a general manner for small scattering rates (Eqs. (4.2.9) and (4.2.14)). These expressions were not derived before from a microscopic theory and are one of the main results of this chapter.

In the two lowest orders of the scattering rate we got terms of order $\mathcal{O}(\Gamma^{-2})$ ($\sigma_{\mu\nu}^{B}$) and $\mathcal{O}(\Gamma^{-1})$ ($\sigma_{\mu\nu}^{Q}$). In the $\sigma_{\mu\nu}^{B}$ term we recover the magnetoconductivity described by the semiclassical Boltzmann transport theory without anomalous velocity [31]. The

[1] Or positive magnetoresistance, for opposite sign of the magnetic field.

$\sigma^{Q}_{\mu\nu}$ term is a quantum correction expressed in terms of the Berry curvature $\sigma^{Q(\mathrm{berry})}_{\mu\nu}$ and orbital magnetic moment $\sigma^{Q(\mathrm{mag})}_{\mu\nu}$. The $\sigma^{Q(\mathrm{berry})}_{\mu\nu}$ part was previously derived using the anomalous velocity in the Boltzmann theory [13, 106, 107]. The additional $\sigma^{Q(\mathrm{mag})}_{\mu\nu}$ term is not present in these theories. In our calculation these terms appear naturally without assuming an anomalous velocity.

The $\sigma^{Q}_{\mu\nu}$ quantity can only be nonzero if time reversal symmetry is broken. This is consistent with the Onsager relations, where these type of terms are forbidden. An interesting symmetry property of the Hall conductivity is that the quantum contribution is symmetric for the $x \leftrightarrow y$ change, while the Boltzmann contribution is antisymmetric.

Finally, we studied a tilted Weyl node using the above formalism. This system was discussed with the semiclassical Boltzmann theory [106, 107]. Our microscopic treatment is new in the literature. We showed that in a tilted Weyl node a finite linear longitudinal magnetoconductivity σ^{Q}_{zz} is present which is proportional to the tilting. This term was also found using the Boltzmann transport theory [106, 107], but only the effects of the Berry curvature were discussed. Our main result is that we showed that the orbital magnetic moment affects the magnetoconductivity and gives significant quantitative corrections.

A finite tilting is present in many Weyl semimetals [129–132], making this effect relevant experimentally. In real materials the Weyl nodes come in pairs with opposite chirality, but they also tilt in opposite direction. As we showed this ensures that the effect of linear longitudinal magnetoconductivity persists even with two Weyl nodes. As we discussed the effect is small, but not negligible. The effect is enhanced for smaller charge carrier densities, larger tiltings, or larger magnetic fields. The conductivity changes sign with the magnetic field, making it possible to distinguish it from the zero field conductivity.

Chapter 5

Relativistic electron gas

In this chapter we study the magnetotransport of a massive three-dimensional relativistic electron gas, which can be used as a simple model for Dirac materials. The results of this chapter were published in Refs. [123] and [124]. First, the model is described in detail, and solved exactly in a magnetic field. Then, we calculate the chemical potential, the screening wavenumber, and the scattering rate with the formalism described in Chapter 2. Finally, using these and the formalism of Chapter 3 we study the magnetoconductivity and magnetothermopower.

5.1 Model

As a simple model for Dirac materials we use the Dirac Hamiltonian [44] with effective speed of light (v) and effective mass (Δ):

$$\mathbb{H}_D := \gamma^0 \left(v \boldsymbol{\gamma} \mathbf{p} + \Delta \right) , \tag{5.1.1}$$

where γ^μ are the Dirac matrices. Experimentally realistic parameters for the effective parameters are:

$$v = 10^6 \mathrm{m\,s^{-1}} \text{ [64, 66, 67, 69, 70]} \qquad \Delta = 10 - 100 \mathrm{meV} \text{ [55, 60, 78, 81]} . \tag{5.1.2}$$

From now on v is defined into the unit of energy and is omitted from the following formulas for simplicity. With the Dirac matrices taken in the Dirac representation the

Dirac Hamiltonian is:

$$\mathbb{H} = \begin{pmatrix} \Delta & 0 & p_z & p_x - ip_y \\ 0 & \Delta & p_x + ip_y & -p_z \\ p_z & p_x - ip_y & -\Delta & 0 \\ p_x + ip_y & -p_z & 0 & -\Delta \end{pmatrix} . \tag{5.1.3}$$

As described in Sec. 2.1.2 the Hamiltonian in a magnetic field becomes:

$$\mathbb{H} = \begin{pmatrix} \Delta & 0 & p_z & \frac{\sqrt{2}}{\ell_B} a \\ 0 & \Delta & \frac{\sqrt{2}}{\ell_B} a^\dagger & -p_z \\ p_z & \frac{\sqrt{2}}{\ell_B} a & -\Delta & 0 \\ \frac{\sqrt{2}}{\ell_B} a^\dagger & -p_z & 0 & -\Delta \end{pmatrix} . \tag{5.1.4}$$

Using the eigenstates $|n\rangle$ of the $a^\dagger a$ operator ($a^\dagger a\,|n\rangle = n\,|n\rangle$) the eigenvalue problem can be solved and the Landau levels are given by:

$$E_{n\lambda s}(p_z) = \lambda\sqrt{2neB + \Delta^2 + p_z^2}\,, \tag{5.1.5}$$

where $n = 0, 1, 2, \ldots$ is the Landau index, $\lambda = \pm 1$ represents the band index and $s = \pm 1$ represents the two-fold degeneracy (for $n \neq 0$ levels). These Landau levels are shown on Fig. 5.1. In the case of $\Delta = 0$ the $n = 0$ Landau level is completely linear and gapless, while in the $\Delta \neq 0$ case there is a gap of 2Δ.

The eigenstates in the magnetic field are [119]:

$$|n, \lambda, s\rangle = \begin{pmatrix} u_{n,\lambda,s} & |n-1\rangle \\ -s u_{n,\lambda,-s} & |n\rangle \\ s\lambda u_{n,-\lambda,s} & |n-1\rangle \\ -\lambda u_{n,-\lambda,-s} & |n\rangle \end{pmatrix} \qquad |0, \lambda\rangle = \begin{pmatrix} 0 & \\ -\tilde{s} u_{n,\lambda,-\tilde{s}} & |0\rangle \\ 0 & \\ -\lambda u_{n,-\lambda,-\tilde{s}} & |0\rangle \end{pmatrix} \tag{5.1.6}$$

where $n > 0$, $\tilde{s} = -\mathrm{sgn}(p_z)$, and the $|n\rangle$ states are given in Eq. (2.1.14). The $u_{n\lambda s}$ functions are given by:

$$u_{n\lambda s} = \frac{1}{2}\sqrt{\left(1 + \frac{s p_z}{\sqrt{E_n^2 - \Delta^2}}\right)\left(1 + \lambda\frac{\Delta}{E_n}\right)}\,, \tag{5.1.7}$$

with $E_n \equiv E_{n11}(p_z)$. The quantum numbers describing these states are $\mathbf{n} \equiv (n, \lambda, s, p_z, p_y)$.

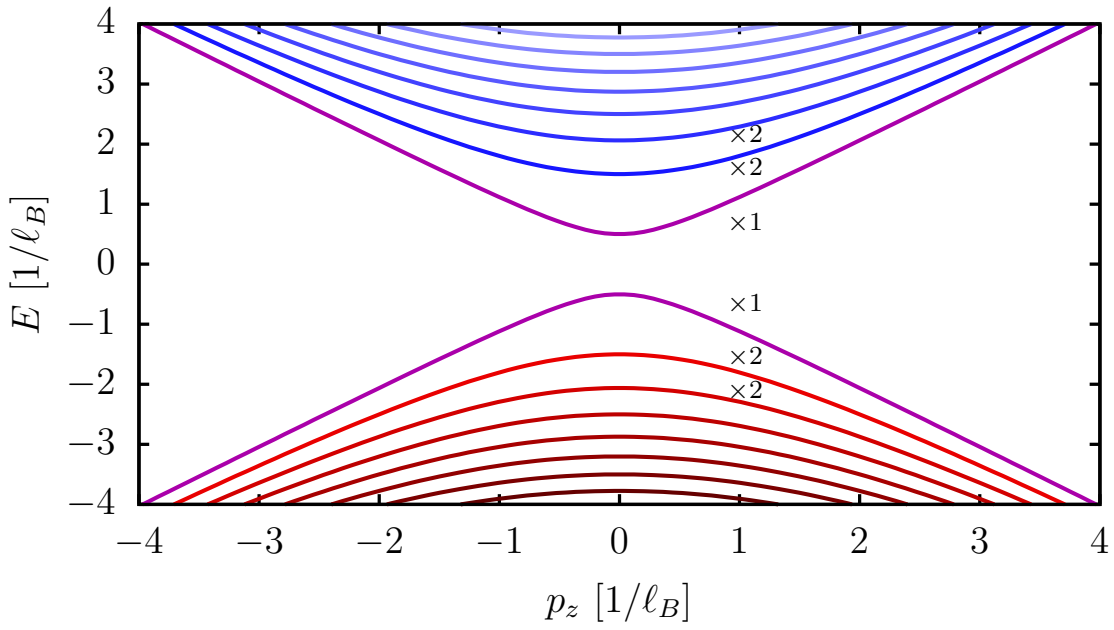

Figure 5.1: Landau levels (5.1.5) of the Dirac Hamiltonian. The degeneracy of each level is 2 except the $n = 0$ levels. $\Delta = 0.5/\ell_B$ and $\ell_B = \sqrt{\hbar/eB}$ are used.

The wave functions will be denoted as:

$$\boldsymbol{\phi}_{\mathbf{n}} = \boldsymbol{\psi}_{n\lambda s}(x; p_y, p_z)\frac{1}{L}\mathrm{e}^{ip_y y}\mathrm{e}^{ip_z z} := \langle x|\mathbf{n}\rangle \ , \tag{5.1.8}$$

where we separated the part depending on x which is not a plane wave.

The dispersion relation only depends on n, λ and p_z. Each Landau level is $L^2/2\pi\ell_B^2$-fold degenerate in p_y (L is the length of the system) and twofold degenerate in s (for $n \neq 0$). The $n = 0$ Landau level is not degenerate in s and must be treated with caution.

The current operator using Eq. (2.1.24) is:

$$\mathbb{J}_\alpha = \gamma^0\gamma^\alpha = \begin{pmatrix} 0 & \sigma^\alpha \\ \sigma^\alpha & 0 \end{pmatrix} . \tag{5.1.9}$$

Using the Eq. (5.1.6) eigenstates, the matrix elements of the current operator becomes:

$$J^{(x)}_{\mathbf{n}\mathbf{n}'} = \ \delta_{p_y p_y'}\delta_{p_z p_z'}\delta_{n,n'-1}U^{n'\lambda's'}_{n\lambda s} + (\mathbf{n} \leftrightarrow \mathbf{n}') \, , \tag{5.1.10a}$$

$$J^{(y)}_{\mathbf{n}\mathbf{n}'} = i\delta_{p_y p'_y}\delta_{p_z p'_z}\delta_{n,n'-1}U^{n'\lambda's'}_{n\lambda s} - (\mathbf{n} \leftrightarrow \mathbf{n}')\,, \tag{5.1.10b}$$

$$J^{(z)}_{\mathbf{n}\mathbf{n}'} = \delta_{p_y p'_y}\delta_{p_z p'_z}\delta_{n,n'}\tilde{U}^{n'\lambda's'}_{n\lambda s} + (\mathbf{n} \leftrightarrow \mathbf{n}')\,, \tag{5.1.10c}$$

$$U^{n'\lambda's'}_{n\lambda s} := -\lambda u_{n,-\lambda,-s}u_{n',\lambda',s'} - ss'\lambda' u_{n,\lambda,-s}u_{n',-\lambda',s'}\,. \tag{5.1.10d}$$

$$\tilde{U}^{n'\lambda's'}_{n\lambda s} := s'\lambda' u_{n,\lambda,s}u_{n',-\lambda',s'} - s\lambda' u_{n,\lambda,-s}u_{n',-\lambda',-s'}\,. \tag{5.1.10e}$$

5.1.1 Chemical potential

We calculate the chemical potential fixing the charge carrier density as explained in Sec. 2.1.4. As a realistic charge carrier density, we use $n_c = 10^{18}\mathrm{cm}^{-3}$ [69, 81]. The density of states is calculated as:

$$D(\varepsilon) = \frac{1}{2\pi^2\ell_B^2}\sum_{n=0}^{\left\lfloor\left(\varepsilon^2-\Delta^2\right)\frac{\ell_B^2}{2}\right\rfloor}(2-\delta_{n0})\frac{|\varepsilon|}{\sqrt{\varepsilon^2-\Delta^2-\frac{2n}{\ell_B^2}}}\,. \tag{5.1.11}$$

In the case of $\Delta = 0$ this is the same as the result obtained in Ref. [133]. The density of states is shown in Fig. 5.2.

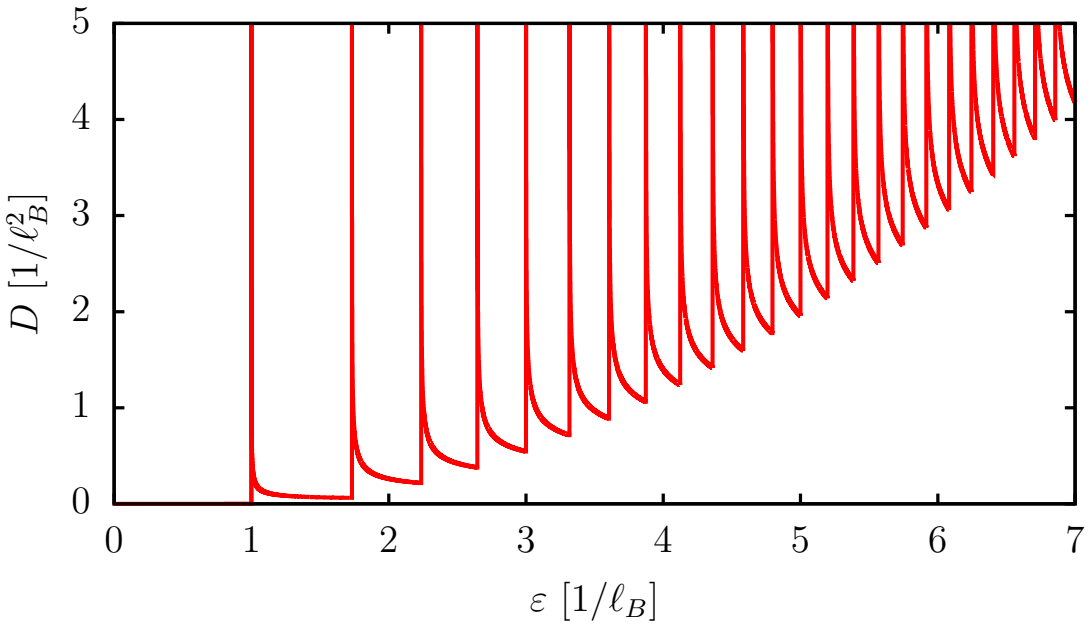

Figure 5.2: Density of states calculated from Eq. (5.1.11). The mass term is chosen as $\ell_B\Delta = 1$.

Substituting the density of states in Eq. (2.1.31) we obtain the expression for the

charge carrier density. At zero temperature after integration:

$$n_c = \frac{1}{2\pi^2 \ell_B^2} \sum_{n=0}^{\left\lfloor \frac{(\mu^2-\Delta^2)\ell_B^2}{2} \right\rfloor} (2-\delta_{n0}) \sqrt{\mu^2 - \Delta^2 - \frac{2n}{\ell_B^2}}\,. \tag{5.1.12}$$

This is consistent with the $\Delta = 0$ result in Ref. [114].

In the high magnetic field limit ($\ell_B \to 0$) only the lowest Landau level contributes and the chemical potential can be expressed as:

$$\mu \sim \sqrt{\Delta_B^2 + \Delta^2} \qquad\qquad \Delta_B := 2\pi^2 n_c \ell_B^2 \propto \frac{1}{B}\,. \tag{5.1.13}$$

As we can see at high magnetic fields $\mu \to \Delta$, and for $\Delta = 0$ $\mu \propto 1/B$ as in Refs. [43, 114]. The high field[1] behavior for different mass terms can be seen in Fig. 5.3.

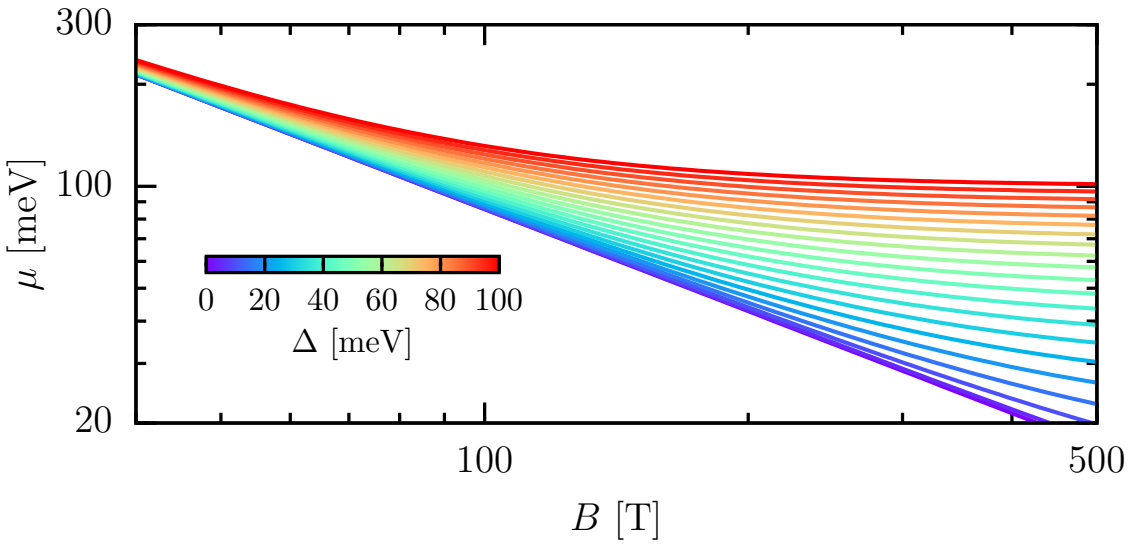

Figure 5.3: Asymptotic behavior of the chemical potential at high magnetic fields and zero temperature using Eq. (5.1.13). The carrier density is fixed at $n_c = 10^{18}\text{cm}^{-3}$.

In the low magnetic field limit ($\ell_B \to \infty$) the summation can be substituted with

[1] In the figures of this chapter we present the results up to very high magnetic fields, that experimentally are not realizable. We do so in order to be able to show the effects of the mass term, because in the case of $n_c = 10^{18}\text{cm}^{-3}$ the magnetic field needs to be very large for this. In order to have the effects observable at lower magnetic fields, materials with a lower charge carrier density are needed.

an integral and we obtain:

$$n_c = \frac{(\mu^2 - \Delta^2)^{\frac{3}{2}}}{3\pi^2}, \tag{5.1.14}$$

which reproduces the zero magnetic field result. For intermediate fields at finite temperature the chemical potential can be calculated numerically using the density of states (5.1.11) in Eq. (2.1.31) and the result can be seen in Fig. 5.4. For the high and

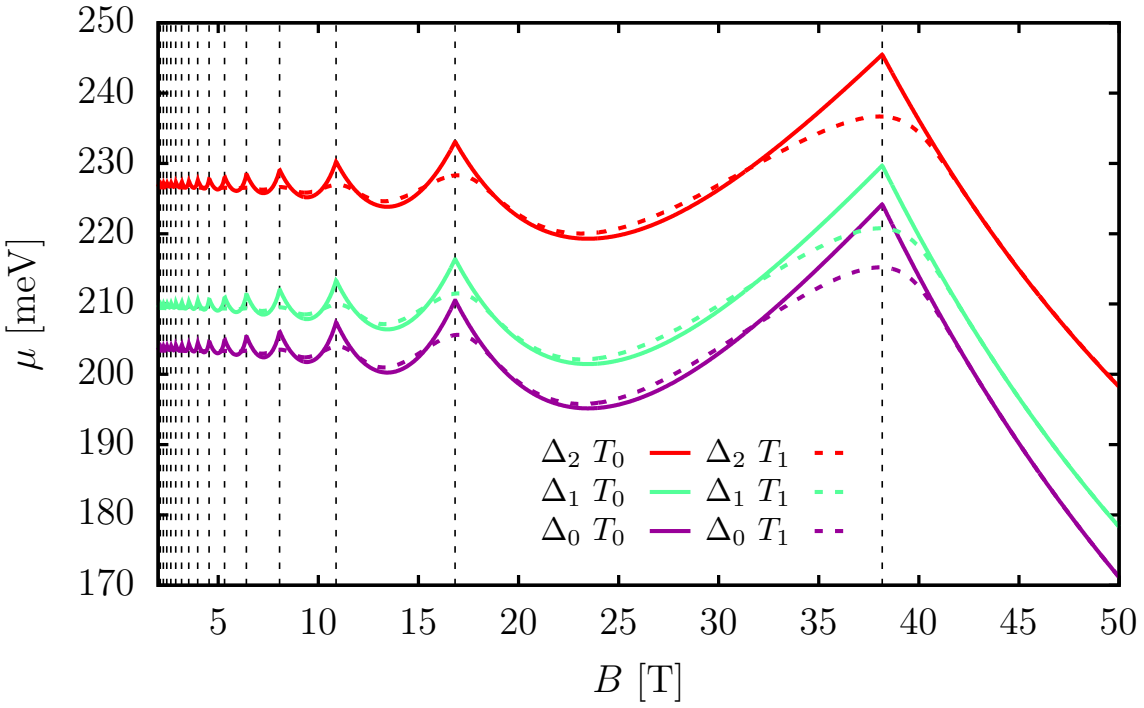

Figure 5.4: Magnetic field dependence of the chemical potential for three mass terms $\Delta_0 = 0$, $\Delta_1 = 50\,\text{meV}$ and $\Delta_2 = 100\,\text{meV}$ and for two temperatures $T_0 = 0\,\text{K}$ and $T_1 = 50\,\text{K}$. The carrier density is fixed at $n_c = 10^{18}\text{cm}^{-3}$. The vertical lines show the magnetic fields where the chemical potential crosses a Landau level as calculated from Eq. (5.1.15).

low magnetic field limits we see the behavior explained using Eq. (5.1.12). In the case of finite temperature we see some deviation but the qualitative behavior remains the same. Between the two limits we see oscillations caused by the singularities present in the density of states. At zero temperature the oscillations are more prominent with sharp changes in the chemical potential. Finite temperature smoothens the curves and at high temperatures the oscillations almost completely disappear.

An oscillation occurs when the chemical potential crosses a Landau level. At zero temperature the magnetic fields where the oscillations occur can be calculated from

the condition of $(\mu^2 - \Delta^2)\ell_B^2/2 \in \mathbb{N}$. Solving Eq. (5.1.12) with this condition yields:

$$eB_m = \left(\frac{\sqrt{2}\pi^2 n_c}{A(m)}\right)^{\frac{2}{3}}, \; A(m) := \sum_{n=0}^{m}(2-\delta_{n0})\sqrt{m-n}\,, \tag{5.1.15}$$

where $m \in \mathbb{N}$ denotes the m^{th} Landau level that crosses the chemical potential. We can see from the formula and the numerical results as well that the peaks occur at the same magnetic fields independently of Δ. We define the quantum limit as the magnetic field where at zero temperature only the lowest Landau level is occupied. From the above formula the criteria for this is $\ell_B^2(\sqrt{2}\pi^2 n_c)^{2/3} < 1$. For $n_c = 10^{18}\text{cm}^{-3}$ [69, 81] the quantum limit is reached above $B \approx 40\,\text{T}$.

Another critical magnetic field which is important is where the mass term becomes relevant in Eq. (5.1.13). This happens when $\Delta_B = \Delta$. In the two limiting cases where $\Delta_B \ll \Delta$ and $\Delta_B \gg \Delta$ we expect two very distinct behaviors. And we will see in the following sections that this is indeed the case. For $\Delta = 10 - 100\text{meV}$ [55, 60] the mass term becomes relevant above $B = 850 - 170\text{T}$.

5.2 Impurity Green's function

In this section we express the impurity Green's function. We start with calculating the screened impurity potential, and use this to calculate the scattering rate. With the scattering rate the impurity Green's function can be calculated from the Dyson equation as:

$$G_{\mathbf{n}}(i\omega_m) = \frac{1}{i\omega_m + \mu - E_{\mathbf{n}} + i\Gamma_{\mathbf{n}}(i\omega_m)}\,. \tag{5.2.1}$$

5.2.1 Screening

As explained in Sec. 2.2.3, in the long wavelength limit ($\mathbf{q} \to 0$) the screened impurity potential can be expressed as:

$$u_{\mathbf{q}} = \frac{u_i}{q^2 + \kappa^2}\,, \tag{5.2.2}$$

where the screening wavenumber using Eq. (2.2.16) is calculated as:

$$\kappa^2 = -\frac{u_e}{2\pi\ell_B^2}\int_{-\infty}^{\infty}\frac{\mathrm{d}p_z}{2\pi}\sum_{\substack{n=0\\ \lambda=\pm1}}^{\infty}(2-\delta_{n0})\frac{\partial f(\lambda E_n - \mu)}{\partial \lambda E_n}\,. \tag{5.2.3}$$

The screening wavenumber as a function of the magnetic field at different temperatures and for different mass terms is shown in Fig. 5.5.

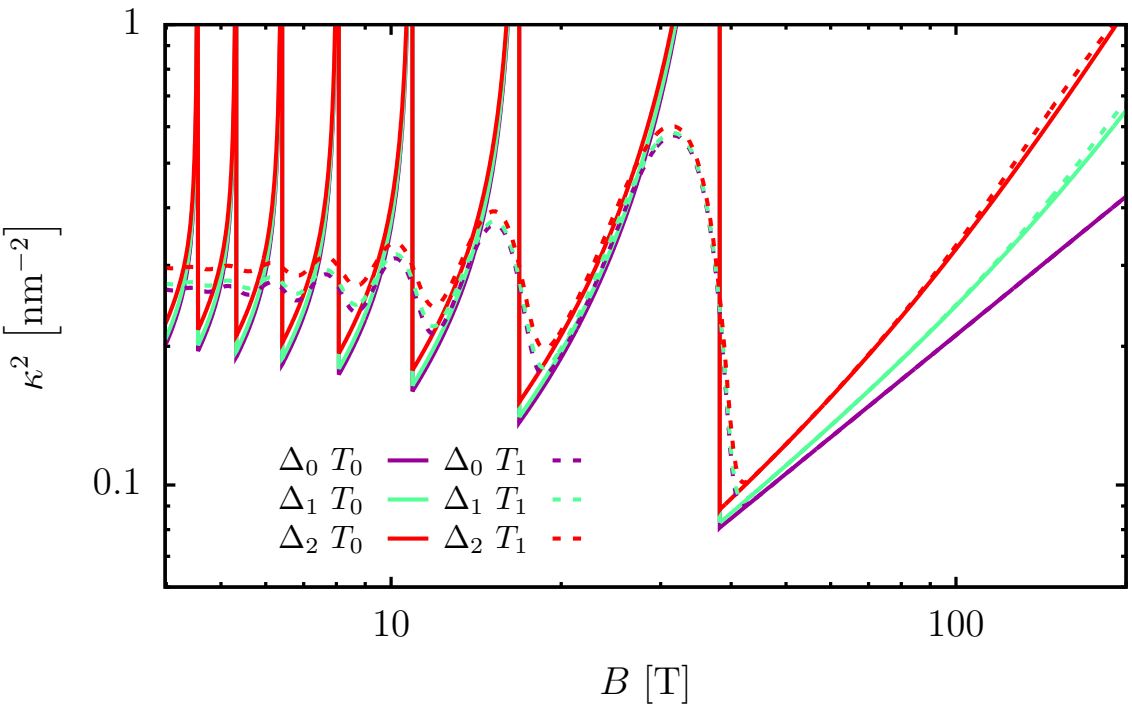

Figure 5.5: Magnetic field dependence of the screening wavenumber for several cases using the same parameters as in Fig. 5.4.

At zero temperature using Eqs. (2.2.17) and (5.1.11) the screening wavenumber is:

$$\kappa^2 = \frac{u_e}{2\pi^2\ell_B^2} \sum_{n=0}^{\left\lfloor \frac{(\mu^2-\Delta^2)\ell_B^2}{2} \right\rfloor} (2-\delta_{n0}) \frac{|\mu|}{\sqrt{\mu^2-\Delta^2-\frac{2n}{\ell_B^2}}} \,. \tag{5.2.4}$$

For high magnetic fields ($\ell_B \to 0$) only the zeroth Landau level contributes to the screening. Using the high magnetic field dependence of μ (5.1.13), we obtain:

$$\kappa^2 \sim \frac{u_e}{2\pi^2\ell_B^2} \frac{\sqrt{\Delta_B^2+\Delta^2}}{\Delta_B} \propto \begin{cases} B & \Delta_B \gg \Delta \\ B^2 & \Delta_B \ll \Delta \end{cases} . \tag{5.2.5}$$

The screening wavenumber at high magnetic fields for different mass terms is shown in Fig. 5.6. For $\Delta = 0$ we recover the $\kappa^2 \propto B$ result used in Ref. [43].

In the zero magnetic field limit similarly to Eq. (5.1.14) the sum can be substituted

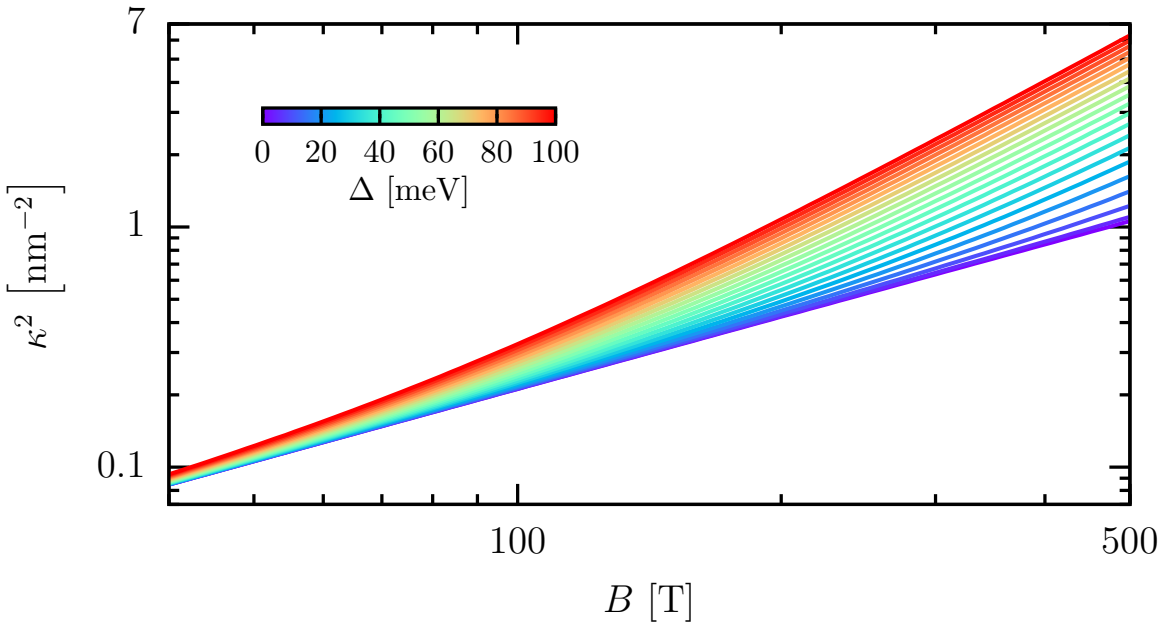

Figure 5.6: Screening wavenumber in the quantum limit (5.2.5) as a function of the magnetic field using different mass terms. The parameters used are: $n_c = 10^{18}\mathrm{cm}^{-3}$ and $v = 10^6 \mathrm{m\,s}^{-1}$.

with an integral and the screening wavenumber goes to a constant:

$$\kappa^2 = \frac{u_e}{\pi^2}\mu\sqrt{\mu^2 - \Delta^2} = \frac{u_e}{\pi^2}\sqrt{(3\pi^2 n_c)^{\frac{4}{3}} + (3\pi^2 n_c)^{\frac{2}{3}}\,\Delta^2}\,. \tag{5.2.6}$$

5.2.2 Scattering rate

To calculate the scattering rate we use the first-Born approximation described in Sec. 2.2.2. Using Eq. (2.2.10) the scattering rate can be calculated as:

$$\Gamma_{\mathbf{n}}(\varepsilon) = n_i \sum_{\mathbf{n}'} \int \frac{\mathrm{d}^3 q}{2(2\pi)^2} u_{\mathbf{q}}^2 \delta\left(\varepsilon + \mu - E_{\mathbf{n}'}\right) \left|F_{\mathbf{n}}^{\mathbf{n}'}(\mathbf{q})\right|^2 , \tag{5.2.7}$$

$$F_{\mathbf{n}}^{\mathbf{n}'}(\mathbf{q}) = \int \mathrm{d}^3 x\, \boldsymbol{\phi}_{\mathbf{n}}^\dagger(\mathbf{x}) \boldsymbol{\phi}_{\mathbf{n}'}(\mathbf{x}) \mathrm{e}^{i\mathbf{q}\mathbf{x}}\,. \tag{5.2.8}$$

Using the eigenstates from Eq. (5.1.8) this becomes (with explicitly writing the different quantum indices):

$$\Gamma_{n\lambda s}(\varepsilon, p_z) = n_i \sum_{n'\lambda' s'} \int \frac{\mathrm{d}^3 q}{2(2\pi)^2} u_{\mathbf{q}}^2 \delta\left(\varepsilon + \mu - \lambda' E_{n'}(p_z - q_z)\right) \left|F_{n\lambda s}^{n'\lambda' s'}(\mathbf{q}, p_z)\right|^2 , \tag{5.2.9}$$

$$F_{n\lambda s}^{n'\lambda' s'}(\mathbf{q}, p_z) = \int \mathrm{d}x\, \boldsymbol{\psi}^{\dagger}_{n\lambda s}(x; 0, p_z)\boldsymbol{\psi}_{n'\lambda' s'}(x, -q_y, p_z - q_z)\mathrm{e}^{iq_x x}\,, \tag{5.2.10}$$

where p_y was eliminated using variable substitution in x. This way, the scattering rate is completely independent of p_y, as expected. Using the following property of the Dirac delta function:

$$\int f(x)\delta(g(x))\,\mathrm{d}x = \sum_{x_o \in g^{-1}(0)} \left.\frac{f(x)}{|\partial_x g(x)|}\right|_{x=x_o}\,, \tag{5.2.11}$$

the integration of q_z can be evaluated and we get:

$$\Gamma_{n\lambda s}(\varepsilon, p_z) = n_i \sum_{\ell=0}^{\left\lfloor \ell_B^2 \frac{(\varepsilon+\mu)^2-\Delta^2}{2} \right\rfloor} \sum_{\substack{\alpha=\pm 1 \\ t=\pm 1}} \int \frac{\mathrm{d}q_x\,\mathrm{d}q_y}{2(2\pi)^2} u^2_{\mathbf{q}_{\ell\alpha}} \left| \frac{\varepsilon+\mu}{\sqrt{(\varepsilon+\mu)^2 - \frac{2\ell}{\ell_B^2} - \Delta^2}} \right| \left| F_{n\lambda s}^{\ell\gamma_o t}(\mathbf{q}_{\ell\alpha}, p_z) \right|^2\,,$$

$$\mathbf{q}_{\ell\pm} := (q_x, q_y, q_{\ell\pm})\,, \qquad q_{\ell\pm} := p_z \pm \sqrt{(\varepsilon+\mu)^2 - \frac{2\ell}{\ell_B} - \Delta^2}\,. \tag{5.2.12}$$

where $\gamma_o = \mathrm{sgn}(\varepsilon + \mu)$ and the summation over t is only done for $l \neq 0$.

Using this formula we calculated the scattering rate as a function of the magnetic field for several mass terms. The results of this are shown in Fig. 5.7. For the numerical calculations $u_e = e^2/\varepsilon_0$ is used. The Fourier transformation in Eq (5.2.13) is calculated using the fractional Fourier transform [134]. The $\mathcal{Q}_x$ integral is done using the Simpson's rule on the result of the fractional Fourier transform and finally the $\mathcal{Q}_y$ integral is done through Gaussian quadrature.

As shown in Fig. 5.7, at low fields we get SdH oscillations. The effect of the mass term is only relevant at high magnetic fields. As a function of the magnetic field the scattering rate first has an increasing background (with SdH oscillations) then after reaching the quantum limit it starts to decrease.

To get the expression of the scattering rate we assumed that the scattering rate is diagonal in the Landau level representation. This assumption is not trivial and is not proven analytically. We evaluated the formula for several non-diagonal elements numerically and we found that the difference between diagonal and non-diagonal elements is several orders of magnitude smaller in the used magnetic field ranges, thus the diagonality is a valid assumption.

In order to study the asymptotic behavior of the scattering rate analytically it is useful to introduce dimensionless quantities. Using $\ell_B = \sqrt{\hbar/eB}$ the dimensionless

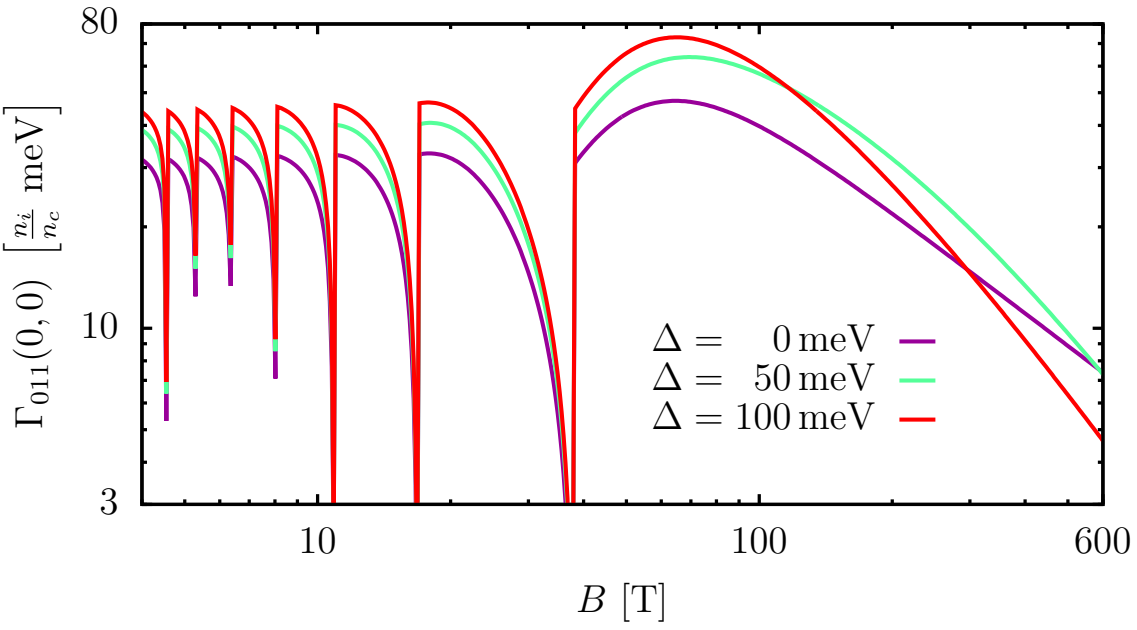

Figure 5.7: Scattering rate calculated from Eq. (5.2.13) with indices $n = 0$ and $\lambda = 1$ as a function of magnetic field at zero temperature. The scattering rate is calculated at $\mathcal{P}_z = 0$ and $\mathcal{E} = 0$. The screening wavenumber is calculated using Eq. (5.2.3). The density of charge carriers is $n_c = 10^{18}\text{cm}^{-3}$.

quantities are $(\boldsymbol{\mathcal{P}}, \boldsymbol{\mathcal{Q}}, \mathcal{E}, \mathcal{M}, \mathcal{D}, x) := \ell_B(\mathbf{p}, \mathbf{q}, \varepsilon, \mu, \Delta, \mathcal{X})$. Using Eq. (5.2.12) for the scattering rate we obtain:

$$\Gamma_{n\lambda s}(\mathcal{E}, \mathcal{P}_z) = n_i \ell_B^2 \sum_{\ell=0}^{\left\lfloor \frac{(\mathcal{E}+\mathcal{M})^2-\mathcal{D}^2}{2} \right\rfloor} \sum_{\substack{\alpha=\pm 1 \\ t=\pm 1}} \int \frac{\mathrm{d}\mathcal{Q}_x\, \mathrm{d}\mathcal{Q}_y}{2(2\pi)^2} u^2_{\mathcal{Q}_{\ell\alpha}} \left| \frac{\mathcal{E}+\mathcal{M}}{\sqrt{(\mathcal{E}+\mathcal{M})^2 - 2\ell - \mathcal{D}^2}} \right| \left| F^{\ell\gamma_o t}_{n\lambda s}(\mathcal{Q}_{\ell\alpha}, \mathcal{P}_z) \right|^2,$$

$$F^{\ell\gamma t}_{n\lambda s}(\mathcal{Q}, \mathcal{P}_z) := \int \mathrm{d}\mathcal{X}\, \boldsymbol{\phi}^\dagger_{n\lambda s}(\mathcal{X}; 0, \mathcal{P}_z) \boldsymbol{\phi}_{\ell\gamma t}(\mathcal{X}; \mathcal{Q}_y, \mathcal{P}_z - \mathcal{Q}_z) \mathrm{e}^{i\mathcal{Q}_x \mathcal{X}}\,,$$

$$\mathcal{Q}_{\ell\pm} := (\mathcal{Q}_x, \mathcal{Q}_y, \mathcal{Q}_{\ell\pm})\,, \qquad \mathcal{Q}_{\ell\pm} := \mathcal{P}_z \pm \sqrt{(\mathcal{E}+\mathcal{M})^2 - 2\ell - \mathcal{D}^2}\,. \tag{5.2.13}$$

In this formula the magnetic field dependence of the scattering rate comes from the explicit $1/\ell_B^2$ factor, the effective impurity potential $\left(u_{\mathbf{Q}} = \frac{u_i}{Q^2 + \ell_B^2 \kappa^2}\right)$, and the parameters[2] $\mathcal{M}$ and $\mathcal{D}$.

[2]We have to keep in mind that μ and Δ are not integration variables but parameters thus $\mathcal{M}$ and $\mathcal{D}$ are functions of B.

In later sections we will see that at low temperatures the important part of the scattering rate is at $\mathcal{E} = 0$. Using the (5.2.5) screening, the (5.2.13) scattering rate in the quantum limit becomes ($\Gamma_{n\lambda s} \equiv \Gamma_{n\lambda s}(0, \mathcal{P}_z)$):

$$\Gamma_{n\lambda s} = n_i u_i^2 \ell_B^2 \sum_{\alpha=\pm} \int \frac{\mathrm{d}\mathcal{Q}_x \, \mathrm{d}\mathcal{Q}_y}{2(2\pi)^2} \frac{\frac{\sqrt{\mathcal{D}_B^2+\mathcal{D}^2}}{\mathcal{D}_B} \left| F_{n\lambda s}^{0\gamma_0 \tilde{t}}(\boldsymbol{\mathcal{Q}}_{0\alpha}, \mathcal{P}_z) \right|^2}{\left(\boldsymbol{\mathcal{Q}}_{0\alpha}^2 + \frac{u_e}{2\pi^2} \frac{\sqrt{\mathcal{D}_B^2+\mathcal{D}^2}}{\mathcal{D}_B} \right)^2}, \tag{5.2.14}$$

where from the summation over ℓ only the the zeroth Landau level plays a role.

In the ultra quantum limit ($\ell_B \to 0$) this can be expressed as:

$$\Gamma_{n\lambda s} = n_i u_i^2 \ell_B^2 \begin{cases} I_{n\lambda s} & \Delta_B \gg \Delta \\ \frac{\Delta_B}{\Delta} J_{n\lambda s} & \Delta_B \ll \Delta \end{cases}, \tag{5.2.15a}$$

$$I_{n\lambda s} := \sum_{\alpha=\pm 1} \int \frac{\mathrm{d}\mathcal{Q}_x \, \mathrm{d}\mathcal{Q}_y}{2(2\pi)^2} \frac{\left| F_{n\lambda s}^{0\gamma_o \tilde{t}}(\boldsymbol{\mathcal{Q}}_{0\alpha}, 0) \right|^2}{\left(\boldsymbol{\mathcal{Q}}_{0\alpha}^2 + \frac{u_e}{2\pi^2} \right)^2}, \tag{5.2.15b}$$

$$J_{n\lambda s} := \sum_{\alpha=\pm 1} \int \mathrm{d}\mathcal{Q}_x \, \mathrm{d}\mathcal{Q}_y \frac{\pi^2}{2u_e^2} \left| F_{n\lambda s}^{0\gamma_o \tilde{t}}(\boldsymbol{\mathcal{Q}}_{0\alpha}, 0) \right|^2. \tag{5.2.15c}$$

The magnetic field dependence is:

$$\Gamma_{n\lambda s} \propto \begin{cases} B^{-1} & \Delta_B \gg \Delta \\ B^{-2} & \Delta_B \ll \Delta \end{cases}. \tag{5.2.16}$$

This asymptotic behavior is also visible in the numerical results in Fig. 5.7.

The scattering rate in the quantum limit calculated numerically from Eq. (5.2.14) can be seen in Fig. 5.8. As we can see the scattering rate depends strongly on the Landau index. At lower fields the mass term only affects the quantitative value of the scattering rate, but the magnetic field dependence is unaffected. At high fields we can see the dependencies described in Eq. (5.2.16). For higher Landau levels a higher magnetic field is needed to get the asymptotic behavior.

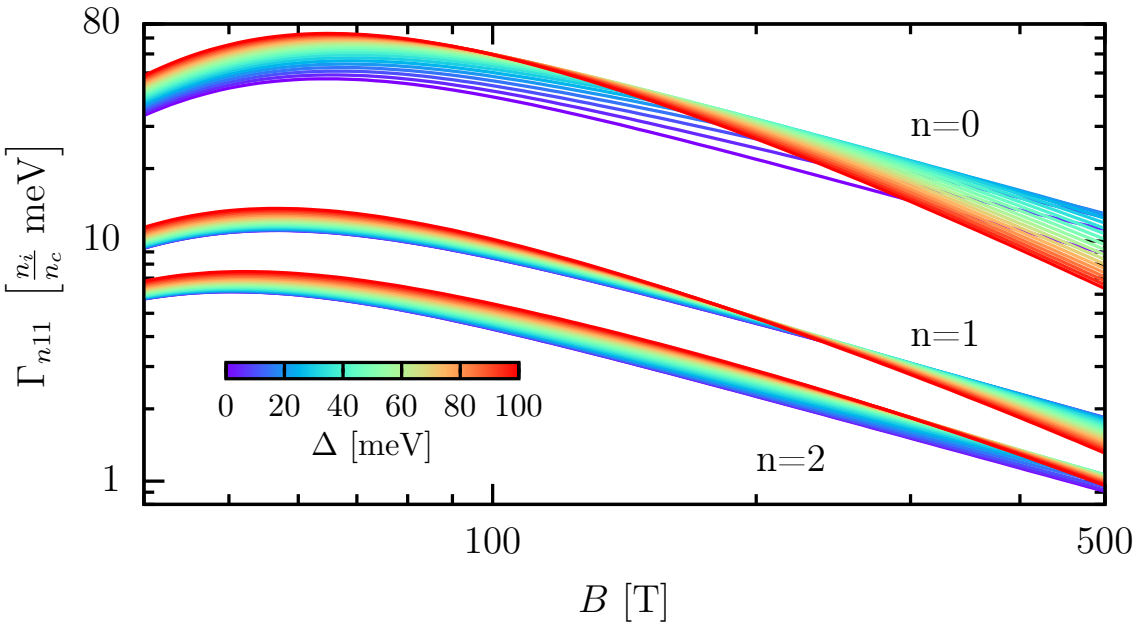

Figure 5.8: Scattering rate of the $n = 0, 1, 2$ Landau levels in the quantum limit (5.2.14) as a function of the magnetic field using different mass terms. The scattering rate is calculated at $\mathcal{P}_z = 0$ and $\mathcal{E} = 0$. The parameters used are: $n_c = 10^{18}\text{cm}^{-3}$ and $v = 10^6\text{m}\,\text{s}^{-1}$.

5.3 Magnetoconductivity

In this section we calculate the magnetoconductivity using the equations explained in Sec. 3.2. We study the components perpendicular to the magnetic field (σ_{xx} and σ_{xy}).

5.3.1 Hall conductivity σ_{xy}

We start with calculating the Hall conductivity. Using Eq. (3.2.27a) only the second part is needed since the product of matrix elements of the current operators in Eq. (5.1.10) are purely imaginary. Furthermore, we only use the lowest order approximation in the impurities and take the clean limit (similarly to the case of the Weyl Hamiltonian in Refs. [43] and [114]):

$$L_{xy}^{11}(\mu) = \frac{1}{\pi V}\sum_{\mathbf{n},\mathbf{n}'} \text{Im}\left\{J^{(x)}_{\mathbf{n}\mathbf{n}'} J^{(y)}_{\mathbf{n}'\mathbf{n}}\right\} \int_{-\infty}^{\mu} \text{d}\xi\, 2\partial_\xi \,\text{Re}\, G^R_{\mathbf{n}'}(\xi)\,\text{Im}\, G^R_{\mathbf{n}}(\xi)\,. \tag{5.3.1}$$

With no impurities the imaginary part of the Green's function will be a Dirac delta $\operatorname{Im} G^R_{\mathbf{n}}(\xi) = -\pi\delta(\xi - E_{\mathbf{n}})$. With this the integral in Eq. (5.3.1) can be evaluated:

$$L^{11}_{xy}(\mu) = -\frac{1}{2\pi^2}\sum_{n=0}^{\infty}\sum_{\substack{\lambda,\lambda'=\pm1\\ s,s'=\pm1}}\int \mathrm{d}p_z \left(U^{n+1\lambda' s'}_{n\lambda s}\right)^2 \frac{f(\lambda E_n - \mu) - f(\lambda' E_{n+1} - \mu)}{(\lambda E_n - \lambda' E_{n+1})^2}\,, \quad (5.3.2)$$

where the summation over s is taken only for $n \neq 0$.

This formula can be simplified by using the properties of the Fermi-Dirac distribution ($f(-\varepsilon - \mu) = 1 - f(\varepsilon + \mu)$), the definition of $U^{n'\lambda' s'}_{n\lambda s}$ in Eq. (5.1.10d) and the explicit form of E_n. After the summations over the λ, λ', s, s' indices, we can show that the formula becomes:

$$L^{11}_{xy}(\mu) = -\frac{1}{4\pi^2}\sum_{n=0}^{\infty}\int \mathrm{d}p_z\,(1+2n)\big[f(E_n-\mu)-f(E_n+\mu)-f(E_{n+1}-\mu)+f(E_{n+1}+\mu)\big]\,. \quad (5.3.3)$$

After rearranging the summation over n we get:

$$L^{11}_{xy}(\mu) = -\frac{1}{4\pi^2}\sum_{n=0}^{\infty}\int \mathrm{d}p_z\,(2-\delta_{n0})\left[f(E_n-\mu)-f(E_n+\mu)\right]\,. \quad (5.3.4)$$

This formula is proportional to the charge carries density and the Hall conductivity can be expressed as:

$$\sigma_{xy} = -\frac{en_c}{B}\,. \quad (5.3.5)$$

To check the validity of Eq. (5.3.5) the Hall conductivity is calculated numerically from Eq. (5.3.2). The numerical results at different mass terms can be seen in Fig. 5.9 (the results are only shown at one finite temperature, but at different temperatures we get exactly the same result). As we can see the Hall conductivity does not depend on the mass term nor the temperature (in the case of no impurities) and it exactly satisfies Eq. (5.3.5). Since the charge carrier density is constant the Hall conductivity is exactly inversely proportional to the magnetic field.

In the quantum limit, we can express the Hall conductivity using the chemical potential (5.1.13) as:

$$\sigma_{xy} = -\frac{e^2}{2\pi^2}\sqrt{\mu^2 - \Delta^2}\,. \quad (5.3.6)$$

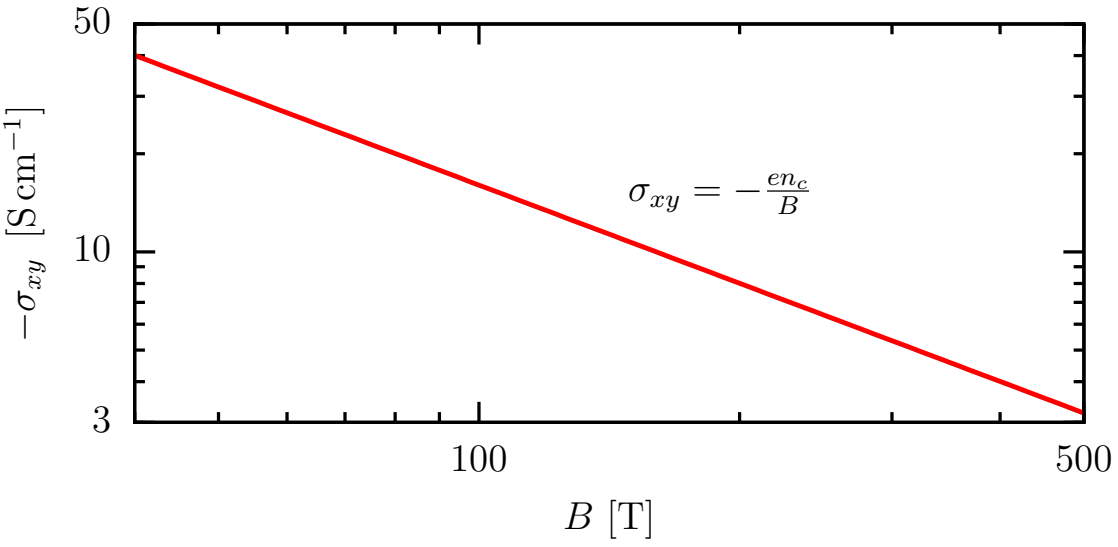

Figure 5.9: Hall conductivity σ_{xy} calculated from Eq. (5.3.2) as a function of magnetic field at $T = 30\,\mathrm{K}$. The density of charge carriers is $n_c = 10^{18}\mathrm{cm}^{-3}$.

5.3.2 Conductivity σ_{xx}

We continue with calculating the diagonal component of the conductivity. In this case the impurities are necessary to give a non-zero result. As explained in Sec. 3.3 the lowest order approximation of the conductivity with respect to the impurities has two terms:

$$L_{xx}^{11} = L_{xx}^{11(0)} + L_{xx}^{11(1)}\,, \tag{5.3.7}$$

where $L_{xx}^{11(1)}$ is the vertex correction.

We start with calculating the first term using Eq. (3.2.19a):

$$L_{xx}^{11(0)}(\mu) = \frac{1}{\pi V}\sum_{\mathbf{n},\mathbf{n}'}\left|J_{\mathbf{n}\mathbf{n}'}^{(x)}\right|^2 \operatorname{Im} G_{\mathbf{n}'}^{R}(\mu)\operatorname{Im} G_{\mathbf{n}}^{R}(\mu)\,, \tag{5.3.8}$$

where the impurity Green's function is taken from Eq. (5.2.1) and the matrix elements of the current operator are taken from Eq. (5.1.10). With the dimensionless units defined in Sec. 5.2.2 we obtain:

$$L_{xx}^{11(0)}(\mu) = \frac{1}{4\pi^3\ell_B}\sum_{n=0}^{\infty}\sum_{\substack{\lambda,\lambda'=\pm1\\ s=\pm1,s'=\pm1}}\int \mathrm{d}\mathcal{P}_z\left(U_{n\lambda s}^{n+1\lambda' s'}\right)^2 \operatorname{Im} G_{n\lambda s}^{R}(\mathcal{M})\operatorname{Im} G_{n+1\lambda' s'}^{R}(\mathcal{M})\,. \tag{5.3.9}$$

The imaginary part of the Green's function is expressed as:

$$\mathrm{Im}\big\{G^R_{\mathbf{n}}(\mathcal{M})\big\} = -\frac{\ell_B\Gamma_{\mathbf{n}}(\mathcal{M},\mathcal{P}_z)}{(E_{\mathbf{n}}-\mathcal{M})^2+(\ell_B\Gamma_{\mathbf{n}}(\mathcal{M},\mathcal{P}_z))^2}\,. \tag{5.3.10}$$

In the quantum limit the scattering rate is small (if the impurity density is small enough) and the imaginary parts of the Green's function can be approximated as:

$$\mathrm{Im}\big\{G^R_{0\lambda s}(\mathcal{M})\big\} \approx -\pi\delta(E_{0\lambda\tilde{s}}-\mathcal{M})\,, \qquad \mathrm{Im}\big\{G^R_{n+1\lambda s}(\mathcal{M})\big\} \approx -\frac{\ell_B\Gamma_{n+1\lambda s}(\mathcal{M},\mathcal{P}_z)}{(E_{n+1\lambda s}-\mathcal{M})^2}\,. \tag{5.3.11}$$

In the lowest order of the impurity density we have to keep only the $n=0$ term which leads to:

$$L^{11(0)}_{xx} = \frac{1}{4\pi^2}\sum_{\substack{\lambda,\lambda'=\pm1\\ s'=\pm1}}\int \mathrm{d}\mathcal{P}_z\left(U^{1\lambda' s'}_{0\lambda\tilde{s}}(\mathcal{P}_z,\mathcal{D})\right)^2\delta(E_{0\lambda\tilde{s}}-\mathcal{M})\frac{\Gamma_{1\lambda' s'}(\mathcal{M},\mathcal{P}_z)}{(E_{1\lambda' s'}-\mathcal{M})^2}\,, \tag{5.3.12}$$

where $\tilde{s}=-\mathrm{sgn}(\mathcal{P}_z)$. After performing the $\mathcal{P}_z$ integral and using the Eq. (5.1.13) form of the chemical potential at high fields (assuming $\mu>0$) we obtain:

$$L^{11(0)}_{xx} = \frac{1}{4\pi^2}\sum_{\substack{\lambda'=\pm1\\ s'=\pm1\\ \xi=\pm1}}\left(U^{1\lambda' s'}_{01\tilde{s}}(\xi\mathcal{D}_B,\mathcal{D})\right)^2\frac{\sqrt{\mathcal{D}_B^2+\mathcal{D}^2}}{\mathcal{D}_B}\frac{\Gamma_{1\lambda' s'}\left(\sqrt{\mathcal{D}_B^2+\mathcal{D}^2},\xi\mathcal{D}_B\right)}{\left(\lambda'\sqrt{2+\mathcal{D}_B^2+\mathcal{D}^2}-\sqrt{\mathcal{D}_B^2+\mathcal{D}^2}\right)^2}\,. \tag{5.3.13}$$

In the very high field limit we can use Eq. (5.2.16) for the scattering rate:

$$L^{11(0)}_{xx} = \begin{cases} n_i u_i^2\ell_B^2 I & \Delta_B\gg\Delta \\ n_i u_i^2\ell_B^2 J & \Delta_B\ll\Delta \end{cases} \propto \frac{1}{B}\,, \tag{5.3.14}$$

where:

$$I := \sum_{\substack{\lambda'=\pm1\\ s'=\pm1,\xi=\pm1}}\frac{1}{8\pi^2}\left(U^{1\lambda' s'}_{01-\xi}(0,0)\right)^2 I_{1\lambda' s'}\,, \tag{5.3.15a}$$

$$J := \sum_{\substack{\lambda'=\pm1\\ s'=\pm1,\xi=\pm1}}\frac{1}{8\pi^2}\left(U^{1\lambda' s'}_{01-\xi}(0,0)\right)^2 J_{1\lambda' s'}\,. \tag{5.3.15b}$$

The conductivity ($\sigma^0_{xx} = e^2 L^{11(0)}_{xx}$) in the quantum limit calculated numerically using Eq. (5.3.13) can be seen in Fig. 5.10.

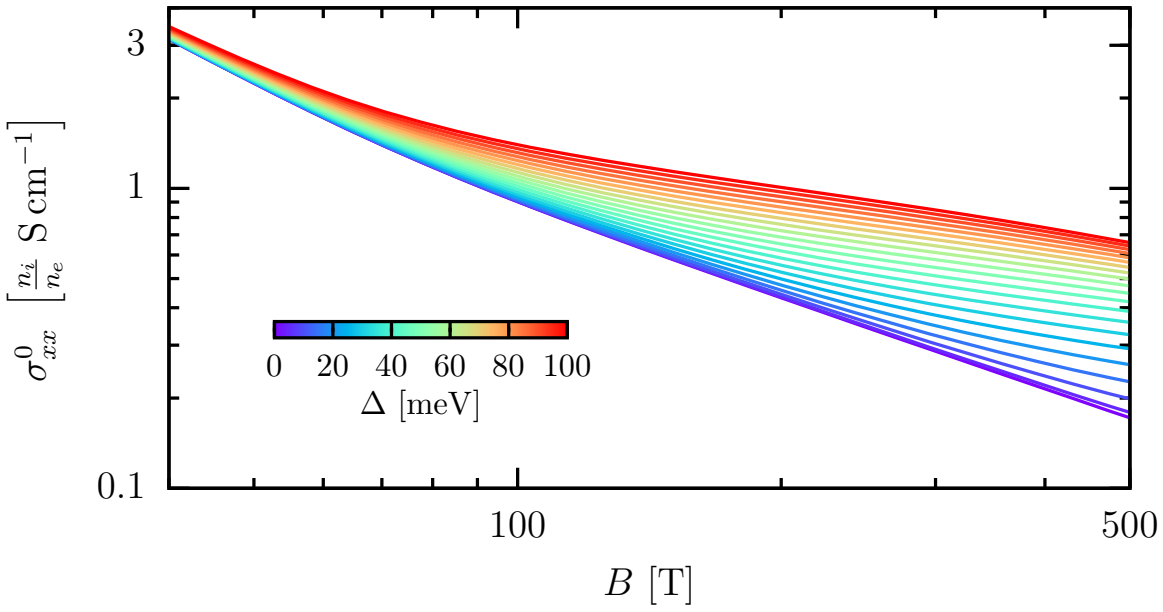

Figure 5.10: The conductivity without the vertex correction in the quantum limit (5.3.13) as a function of the magnetic field using different mass terms. The parameters used are: $n_c = 10^{18}\mathrm{cm}^{-3}$ and $v = 10^6\mathrm{m\,s}^{-1}$.

As we can see in the high field limit we recover the asymptotic behavior described in Eq. (5.3.14), and at lower fields the effect of the mass term becomes less relevant. The real asymptotic behavior is only reached at very high fields. In the intermediate region where the curves with different mass term start to diverge from each other the decrease is weaker than B^{-1}. As a consequence in the high field limit the quantitative value of the conductivity is larger for larger values of the mass term.

At lower magnetic fields we need to evaluate Eq. (5.3.9) numerically. First, we do a phenomenological study, where we take the scattering rate phenomenologically in order to clarify its effects on σ_{xx}. We assume the scattering rate to be independent of Landau levels and other variables except the magnetic field. The impurity density is chosen in a way that the ratio of σ_{xx} to σ_{xy} in our results is similar to the experimental results [69]. The obtained results of σ_{xx} for different mass terms are shown in Fig. 5.11.

When we assume that the scattering rate has the same magnetic-field dependence as the high magnetic field limit dependence described in Sec. 5.2.2 (i.e., $\Gamma \propto B^{-1}$ for

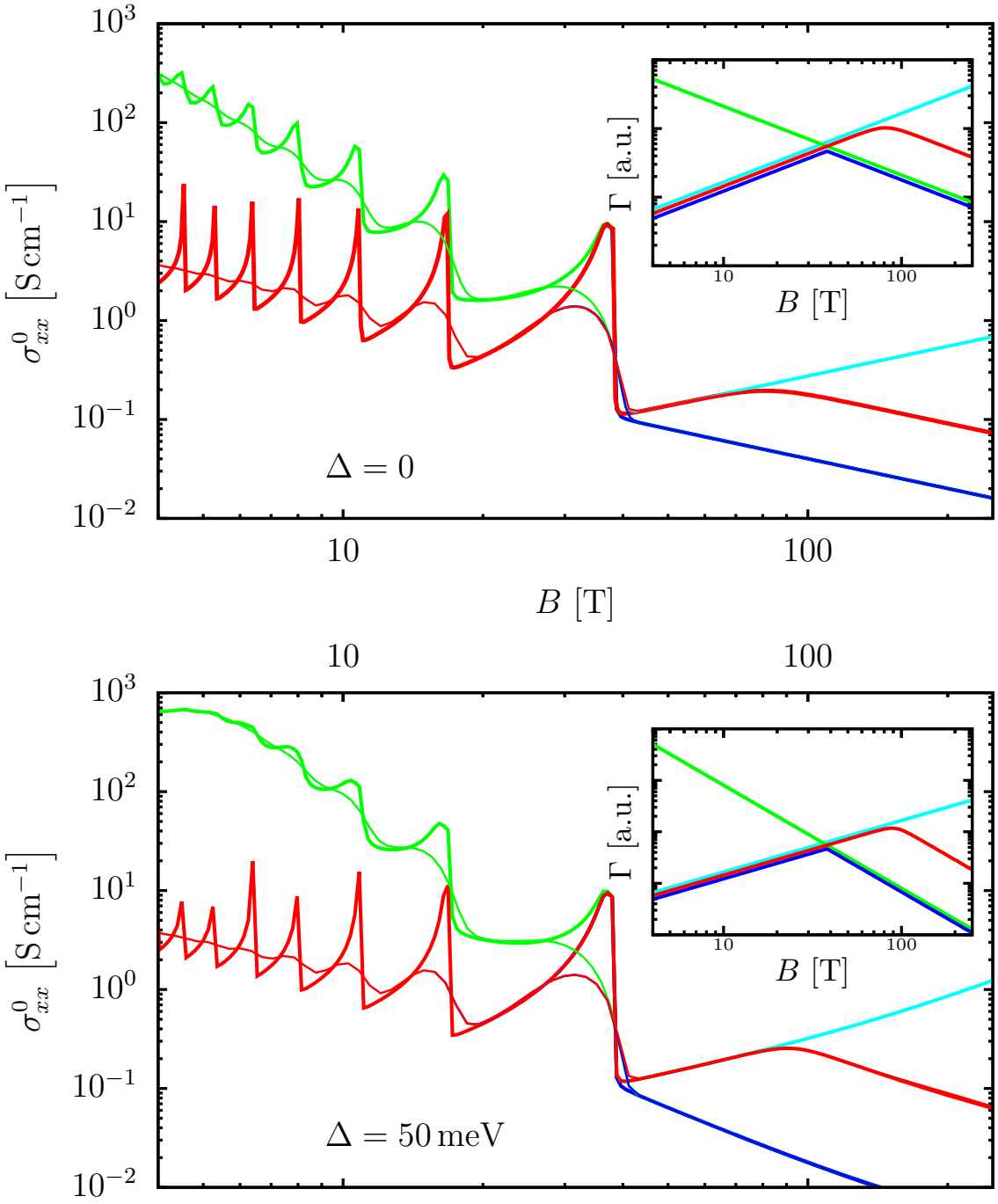

Figure 5.11: Transverse diagonal conductivity σ_{xx} calculated from Eq. (5.3.9) as a function of magnetic field at different temperatures. $\Delta = 0$ (top plot) and $\Delta = 50\,\mathrm{meV}$ (bottom plot). The scattering rate is chosen phenomenologically based on the numerical results in Fig. 5.7. The inset shows the scattering rates used (no Landau level dependence is assumed). The thick lines show results at $T = 0\,\mathrm{K}$ and the thin lines show $T = 50\,\mathrm{K}$. The density of charge carriers is $n_c = 10^{18}\mathrm{cm}^{-3}$.

$\Delta = 0$ and $\Gamma \propto B^{-2}$ for $\Delta \neq 0$, green lines in the insets of Fig. 5.11), the analytic behaviors in high magnetic fields are reproduced[3]. However, in the low field region, we get a much faster decrease than B^{-1}. This scattering rate is the same as used by Abrikosov [43].

On the other hand, if we assume $\Gamma \propto B$ (cyan lines in Fig. 5.11), we obtain $\sigma_{xx} \propto B^{-1}$ in the low field region. However, in this case, the analytic behaviors in high magnetic fields are not reproduced.

As shown in Fig. 5.7 in Sec. 5.2.2, the numerically obtained scattering rate first increases in the low field region, and then decreases as $\Gamma \propto B^{-1}$ for $\Delta = 0$ and $\Gamma \propto B^{-2}$ for $\Delta \neq 0$ in the high field region. Therefore, we connect these dependencies phenomenologically as shown with blue and red curves in Fig. 5.11. In these cases, we obtain a $\sigma_{xx} \propto B^{-1}$ background with SdH oscillations superimposed in all the magnetic field region. As shown in Fig. 5.7, there is no significant difference between Γ_0 for $\Delta = 0$ and Γ_0 for $\Delta \neq 0$ in the low field region. The conductivity also behaves similarly, and the two cases behave differently only in the quantum limit where only the lowest Landau level is important.

The temperature dependence is negligible at high fields as we can see in Fig. 5.11. After changing to dimensionless units the relevant parameter will be the dimensionless temperature $\mathcal{T} := \ell_B T$. So the criteria for low temperatures is:

$$\frac{k_B T}{v\sqrt{\hbar e B}} \ll 1\,, \tag{5.3.16}$$

which shows that the temperature range where the low temperature approximation can be used increases with increasing magnetic fields. For $B = 1\,\mathrm{T}$ the criteria is $T \ll 300\,\mathrm{K}$. At lower magnetic fields the finite temperature smoothens the SdH oscillations.

A more precise numerical result can be achieved using the scattering rate calculated from Eq. (5.2.13). However, the exact numerical integration of Γ is a very heavy calculation. Therefore, we assume that the scattering rate is independent of momentum and energy ($\mathcal{P}_z = 0$ and $\mathcal{E} = 0$) and only the Landau level dependence and magnetic field dependence are kept. For the strength of the interactions we assume $u_e = u_i = e^2/\varepsilon_0\varepsilon_r$ considering different relative permittivities. The results for both the massless and massive cases are shown in Fig. 5.12.

In the high magnetic field region, we recover the magnetic field dependencies dis-

[3]Note that the green lines in the main figures of Fig. 5.11 overlap with blue lines in the high field region.

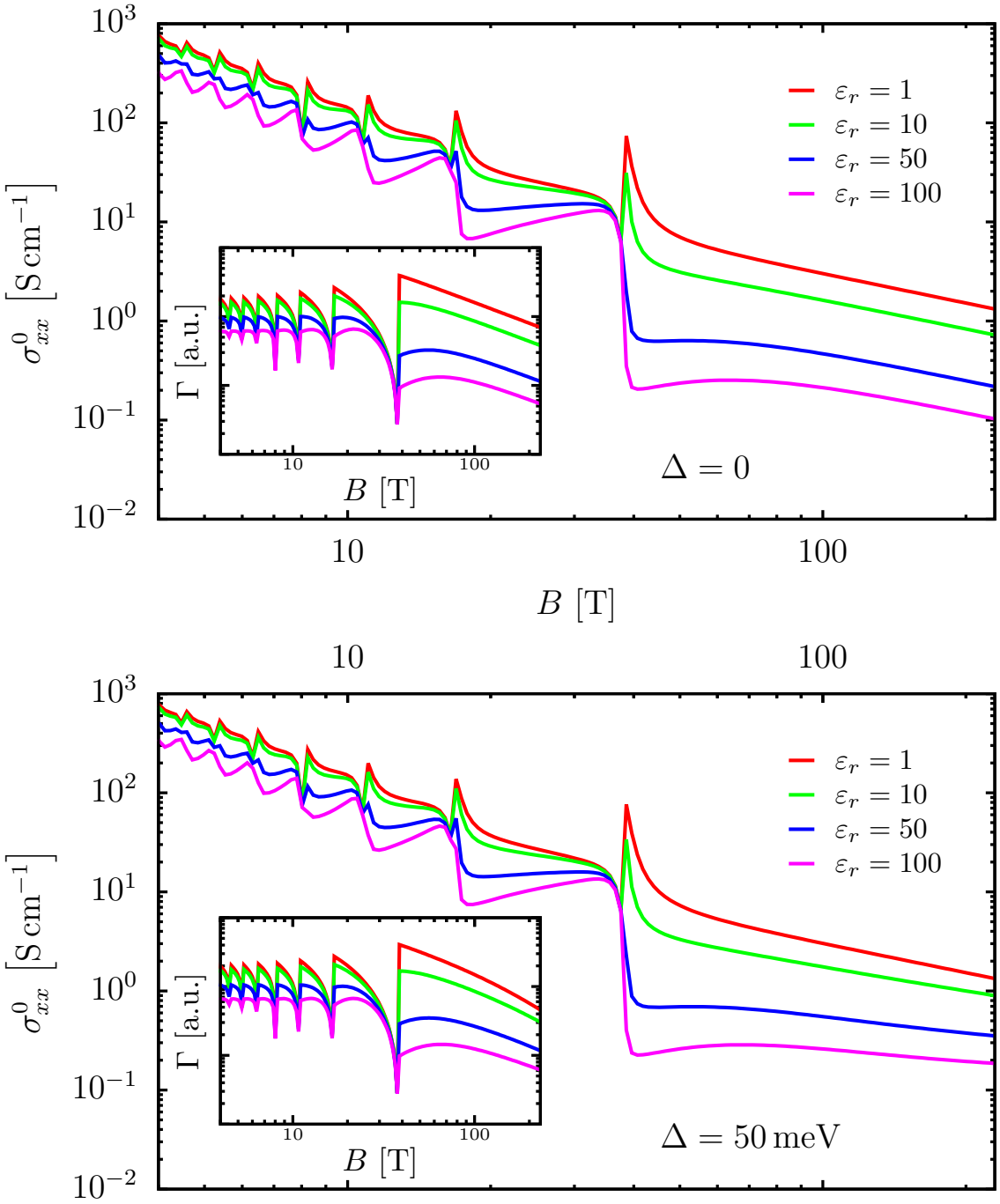

Figure 5.12: Transverse diagonal conductivity σ_{xx} calculated from Eq. (5.3.9) as a function of magnetic field at zero temperature. $\Delta = 0$ (top plot) and $\Delta = 50\,\text{meV}$ (bottom plot). The scattering rate is calculated using Eq. (5.2.13) using screening wavenumbers calculated through Eq. (5.2.3). The inset figure shows the scattering rates used (n=1 Landau level). The density of charge carriers is $n_c = 10^{18}\text{cm}^{-3}$.

cussed above. In the low field region, $\sigma_{xx} \propto B^{-5/3}$ and the effect of the first Landau level appears as a very strong jump similarly to what was found in Ref. [114]. We see that changing the relative permittivity changes the height of this jump. In the inset, we also show Γ_1, since this determines mainly the conductivity in high fields. In this system higher scattering rate means higher conductivity (contrary to normal system where the opposite is true). This means that if we increase the density of impurities the conductivity is also increased.

5.3.3 Vertex correction

Now we move on with the calculation of the vertex correction, $L_{xx}^{11(1)}$. As explained in Sec. 3.3 in the lowest order approximation this can be calculated as:

$$L_{xx}^{11(1)} = -\frac{i}{\pi V} \sum_{\mathbf{n},\mathbf{n}',\mathbf{m},\mathbf{m}'} V_{\mathbf{nm}}^{\mathbf{n}'\mathbf{m}'} J_{\mathbf{nn}'}^{(x)} J_{\mathbf{m}'\mathbf{m}}^{(x)} C_{\mathbf{nm}}^{\mathbf{n}'\mathbf{m}'}\,, \tag{5.3.17a}$$

$$V_{\mathbf{nm}}^{\mathbf{n}'\mathbf{m}'} = \frac{1}{V} \sum_{\mathbf{q}} n_i |u_{\mathbf{q}}|^2 F_{\mathbf{nm}}^{*}(\mathbf{q}) F_{\mathbf{n}'\mathbf{m}'}(\mathbf{q})\,, \tag{5.3.17b}$$

where for the quantum numbers we use: $\mathbf{n} \equiv (n, \lambda, s, p_z, p_y)$, $\mathbf{n}' \equiv (n', \lambda', s', p_z, p_y)$, $\mathbf{m} \equiv (m, \gamma, t, p_z', p_y')$ and $\mathbf{m}' \equiv (m', \gamma', t', p_z', p_y')$. The part with the impurity potential is very similar to the scattering rate:

$$\begin{aligned} V_{n\lambda s;m\gamma t}^{n'\lambda' s';m'\gamma' t'}(\mathcal{P}_y, \mathcal{P}_y', \mathcal{P}_z, \mathcal{P}_z') = \\ = \frac{n_i}{\ell_B^3} \int \frac{\mathrm{d}^3\mathcal{Q}}{(2\pi)^3} u_{\mathcal{Q}}^2 \delta_{\mathcal{P}_y - \mathcal{Q}_y, \mathcal{P}_y'} \delta_{\mathcal{P}_z - \mathcal{Q}_z, \mathcal{P}_z'} F_{n'\lambda' s'}^{m'\gamma' t'}(\boldsymbol{\mathcal{Q}}, \mathcal{P}_z) F_{n\lambda s}^{m\gamma t *}(\boldsymbol{\mathcal{Q}}, \mathcal{P}_z)\,, \end{aligned} \tag{5.3.18}$$

where F is defined in Eq. (5.2.13). It can be shown that V is real. The matrix elements of the current operator are also real. This way, for the real part of the vertex correction only the imaginary part of C is needed. This can be expressed as:

$$\begin{aligned} \operatorname{Im} C_{\mathbf{nm}}^{\mathbf{n}'\mathbf{m}'} = \frac{[(E_{\mathbf{n}} - \mu)\Gamma_{\mathbf{m}} + (E_{\mathbf{m}} - \mu)\Gamma_{\mathbf{n}}][(E_{\mathbf{m}'} - \mu)\Gamma_{\mathbf{n}'} + (E_{\mathbf{n}'} - \mu)\Gamma_{\mathbf{m}'}]}{\Gamma_{\mathbf{n}}\Gamma_{\mathbf{m}}\Gamma_{\mathbf{m}'}\Gamma_{\mathbf{n}'}} \times \\ \times \operatorname{Im} G_{\mathbf{n}}^R \operatorname{Im} G_{\mathbf{m}}^R \operatorname{Im} G_{\mathbf{m}'}^R \operatorname{Im} G_{\mathbf{n}'}^R\,, \end{aligned} \tag{5.3.19}$$

where the Green's functions and scattering rates are evaluated at the chemical potential ($\Gamma_{\mathbf{n}} \equiv \Gamma_{\mathbf{n}}(\mu, p_z)$ and $G_{\mathbf{n}}^R \equiv G_{\mathbf{n}}^R(\mu)$).

In the lowest order approximation in the impurity density we can again use Eq.

(5.3.11) for the imaginary part of the Green's function. Using the matrix elements of the current operator keeping only the lowest Landau indexes (higher indexes will have little contribution at high fields), we obtain:

$$L_{xx}^{11(1)} = \frac{2\pi\ell_B^4}{V} \sum_{\substack{\lambda,\lambda',\gamma,\gamma' \\ s',t \\ \mathcal{P}_z,\mathcal{P}_z',\mathcal{P}_y,\mathcal{P}_y'}} V_{0\lambda\tilde{s};1\gamma t}^{1\lambda' s';0\gamma'\tilde{t}'}(\mathcal{P}_y,\mathcal{P}_y',\mathcal{P}_z,\mathcal{P}_z') U_{0\lambda\tilde{s}}^{1\lambda' s'}(\mathcal{P}_z) U_{0\gamma'\tilde{t}'}^{1\gamma t}(\mathcal{P}_z') \times \\ \times \frac{\delta(E_{0\gamma'\tilde{t}'}(\mathcal{P}_z') - \mathcal{M})}{E_{1\gamma t}(\mathcal{P}_z') - \mathcal{M}} \frac{\delta(E_{0\lambda\tilde{s}}(\mathcal{P}_z) - \mathcal{M})}{E_{1\lambda' s'}(\mathcal{P}_z) - \mathcal{M}}, \tag{5.3.20}$$

where we use the fact that V is real and the symmetry properties in the quantum numbers. Using the Kronecker deltas in V and evaluating all momentum integrals except $\mathcal{Q}_x$ and $\mathcal{Q}_y$, we obtain:

$$L_{xx}^{11(1)} = \frac{n_i u_i^2 \ell_B^2}{4\pi^2} \sum_{\substack{\lambda',\gamma=\pm1 \\ s',t=\pm1 \\ \xi,\eta=\pm1}} \frac{U_{01\tilde{s}}^{1\lambda' s'}(\xi\mathcal{D}_B,\mathcal{D}) U_{01\tilde{t}'}^{1\gamma t}(\eta\mathcal{D}_B,\mathcal{D}) \frac{\sqrt{\mathcal{D}_B^2+\mathcal{D}^2}}{\mathcal{D}_B} \Theta_{01\tilde{s};1\gamma t}^{1\lambda' s';01\tilde{t}'}((\xi+\eta)\mathcal{D}_B,\xi\mathcal{D}_B)}{\left(\lambda'\sqrt{2+\mathcal{D}_B^2+\mathcal{D}^2}-\sqrt{\mathcal{D}_B^2+\mathcal{D}^2}\right)\left(\gamma\sqrt{2+\mathcal{D}_B^2+\mathcal{D}^2}-\sqrt{\mathcal{D}_B^2+\mathcal{D}^2}\right)}, \tag{5.3.21a}$$

$$\Theta_{n\lambda s;m\gamma t}^{n'\lambda' s';m'\gamma' t'}(\mathcal{Q}_z,\mathcal{P}_z) := \int \frac{\mathrm{d}\mathcal{Q}_x\,\mathrm{d}\mathcal{Q}_y}{(2\pi)^2} \frac{\frac{\sqrt{\mathcal{D}_B^2+\mathcal{D}^2}}{\mathcal{D}_B} F_{n'\lambda' s'}^{m'\gamma' t'}(\boldsymbol{\mathcal{Q}},\mathcal{P}_z) F_{n\lambda s}^{m\gamma t*}(\boldsymbol{\mathcal{Q}},\mathcal{P}_z)}{\left(\boldsymbol{\mathcal{Q}}^2 + \frac{u_e}{2\pi^2}\frac{\sqrt{\mathcal{D}_B^2+\mathcal{D}^2}}{\mathcal{D}_B}\right)^2}. \tag{5.3.21b}$$

The structure of the vertex correction is very similar to that of $L_{xx}^{11(0)}$, but the origin of each term is different. Similarly to how we calculated the limit of the scattering rate and $L_{xx}^{11(0)}$ we can evaluate the high field limit of the vertex correction. Since the structure is similar we get the same asymptotic behavior as in Eq. (5.3.14) but the proportionality constants will be different:

$$L_{xx}^{11(1)} = \begin{cases} n_i u_i^2 \ell_B^2 \tilde{I} & \Delta_B \gg \Delta \\ n_i u_i^2 \ell_B^2 \tilde{J} & \Delta_B \ll \Delta \end{cases} \propto \frac{1}{B}, \tag{5.3.22}$$

where:

$$\tilde{I} := \frac{1}{8\pi^2} \sum_{\substack{\lambda',\gamma=\pm1 \\ s',t=\pm1 \\ \xi,\eta=\pm1}} \frac{U^{1\lambda' s'}_{01\tilde{s}}(0,0) U^{1\gamma t}_{01\tilde{t}'}(0,0)}{\lambda'\gamma} \int \frac{\mathrm{d}\mathcal{Q}_x \mathrm{d}\mathcal{Q}_y}{(2\pi)^2} \frac{F^{01\tilde{t}'}_{1\lambda' s'}(\mathcal{Q}_x,\mathcal{Q}_y,\mathcal{Q}_z{=}0,0) F^{1\gamma t *}_{01\tilde{s}}(\mathcal{Q}_x,\mathcal{Q}_y,\mathcal{Q}_z{=}0,0)}{\left(\mathcal{Q}_x^2+\mathcal{Q}_y^2+\frac{u_e}{2\pi^2}\right)^2}, \tag{5.3.23a}$$

$$\tilde{J} := \frac{1}{8\pi^2} \sum_{\substack{\lambda',\gamma=\pm1 \\ s',t=\pm1 \\ \xi,\eta=\pm1}} \frac{U^{1\lambda' s'}_{01\tilde{s}}(0,0) U^{1\gamma t}_{01\tilde{t}'}(0,0)}{\lambda'\gamma} \int \frac{\mathrm{d}\mathcal{Q}_x \mathrm{d}\mathcal{Q}_y}{(2\pi)^2} \frac{F^{01\tilde{t}'}_{1\lambda' s'}(\mathcal{Q}_x,\mathcal{Q}_y,\mathcal{Q}_z{=}0,0) F^{1\gamma t *}_{01\tilde{s}}(\mathcal{Q}_x,\mathcal{Q}_y,\mathcal{Q}_z{=}0,0)}{\left(\frac{u_e}{2\pi^2}\right)^2}. \tag{5.3.23b}$$

The vertex correction contribution was numerically calculated from Eq. (5.3.21). The results can be seen on Fig. 5.13.

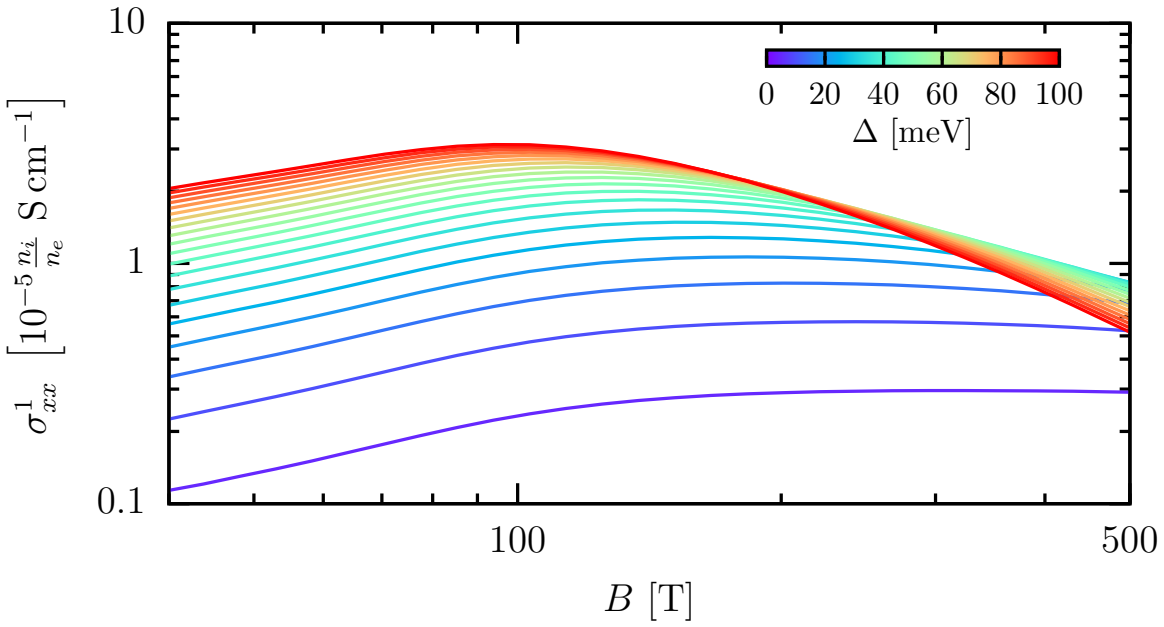

Figure 5.13: The vertex correction of the conductivity in the quantum limit (5.3.21) as a function of the magnetic field using different mass terms. The parameters used are: $n_c = 10^{18}\mathrm{cm}^{-3}$ and $v = 10^6 \mathrm{m\,s}^{-1}$.

At high fields we do not recover the asymptotic behavior described in Eq. (5.3.22), but instead we get a more rapid decrease. This is because in the analytic formula we assumed that $\tilde{I}$ and $\tilde{J}$ are non-zero. From the numerics we can see that they are numerically zero. This gives an extra decrease when $\mathcal{D}_B,\ \mathcal{D} \to 0$. From the numerical results we can see that the vertex correction is several orders of magnitude smaller than

σ^0_{xx}. This is because in the summation over indices in Eq. (5.3.21) Θ is close to zero when the matrix elements of the current operators give finite values. Furthermore, the vertex correction at $\Delta = 0$ is numerically zero (it is not visible on the figure). When $\mathcal{D} \gg 0$ the vertex correction becomes more relevant, but at reasonable values of the mass term it is negligible. In the following sections we will neglect the vertex correction, since it has a very small contribution to the overall conductivity.

5.3.4 Magnetoresistance

Using the previous results for the magnetoconductivity we show the results for the magnetoresistivity. The resistivity is calculated as:

$$\varrho_{xx} = \frac{\sigma_{xx}}{\sigma_{xx}^2 + \sigma_{xy}^2}\,, \qquad \varrho_{xy} = \frac{\sigma_{xy}}{\sigma_{xx}^2 + \sigma_{xy}^2}\,. \tag{5.3.24}$$

In the previous results we have seen that $\sigma_{xy} \gg \sigma_{xx}$. Because of this the Hall resistance using Eq. (5.3.5) can be simply expressed as:

$$\varrho_{xy} = -\frac{B}{en_c} = BR_H\,. \tag{5.3.25}$$

This is the usual Hall resistance.

In the case of ϱ_{xx} we need to consider σ_{xx}. First, we discuss the magnetoresistance in the quantum limit. Using Eq. (5.3.24) on the high field magnetoconductivity (5.3.14) the magnetoresistance becomes proportional to the magnetic field. The magnetoresistance in the quantum limit calculated numerically is shown in Fig. 5.14.

After the high field limit, we study the magnetoresistance calculated from the phenomenological scattering rate represented by the red line in the insets of Fig. 5.11. In this case, the obtained σ_{xx} is proportional to B^{-1} with SdH oscillations. The magnetoresistance calculated in Eq. (5.3.24) becomes $\rho_{xx} \propto B$ since both σ_{xx} and σ_{xy} are proportional to B^{-1}. This is shown with the red lines in Fig. 5.15. For the case of finite Δ, the lower field region (oscillating region) behaves similarly to the massless case as explained previously. The main difference is at high fields as seen previously in the high field limit.

Finally, we show the magnetoresistances calculated using the numerically calculated scattering rates (corresponding to the case with $\varepsilon_r = 1$ of Fig. 5.12). The results are shown with blue lines in Fig. 5.15. In the high field region, they behave similarly to

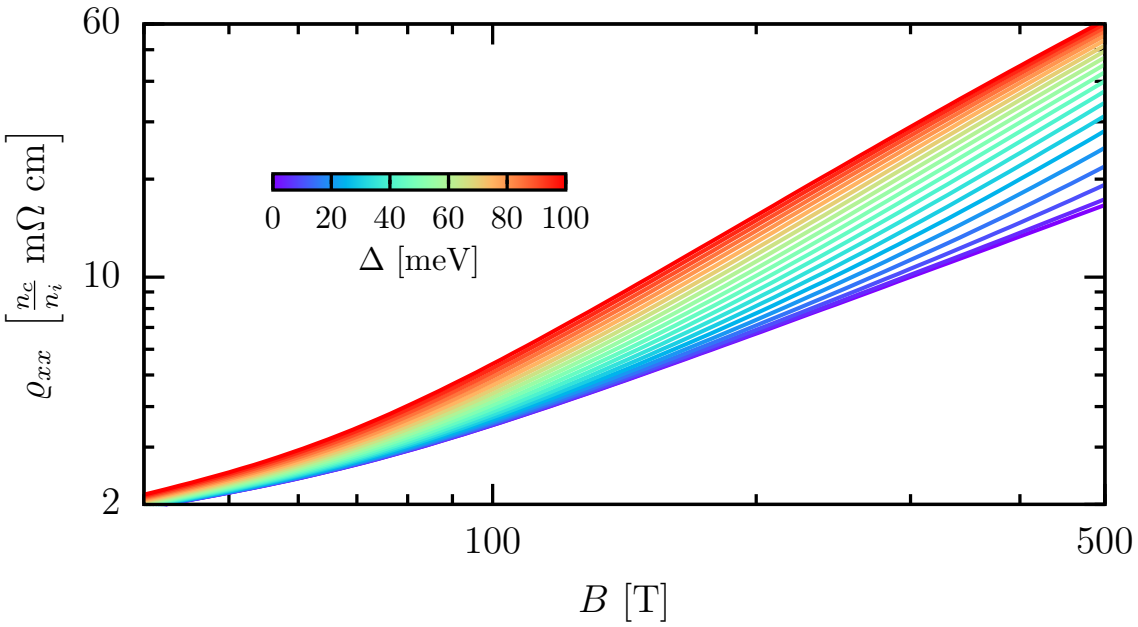

Figure 5.14: Magnetoresistance ϱ_{xx} calculated from Eqs. (5.3.24) and (5.3.13) as a function of magnetic field. The density of charge carriers is $n_c = 10^{18}\text{cm}^{-3}$.

those calculated using the phenomenological scattering rates. However, the low field behavior shows a sublinear increase, since the B dependence of the conductivity is no longer B^{-1} as shown in Fig. 5.12.

5.4 Magnetothermopower

Finally, we study the Seebeck tensor using Eq. (3.2.30b). For this, we need the resistivity tensor and the derivative of the conductivity with respect to the chemical potential. The independent elements of the Seebeck tensor are:

$$S_{xx} = -T\frac{\pi^2}{3e}\frac{\sigma_{xx}\partial_\mu\sigma_{xx} + \sigma_{xy}\partial_\mu\sigma_{xy}}{\sigma_{xx}^2 + \sigma_{xy}^2}\,, \qquad S_{xy} = -T\frac{\pi^2}{3e}\frac{\sigma_{xx}\partial_\mu\sigma_{xy} - \sigma_{xy}\partial_\mu\sigma_{xx}}{\sigma_{xx}^2 + \sigma_{xy}^2}\,. \tag{5.4.1}$$

The result for the Seebeck (S_{xx}) and Nernst (S_{xy}) coefficients depends strongly on the Hall angle ($\tan\vartheta_H = \sigma_{xy}/\sigma_{xx}$), which is mainly determined by the ratio of charge carrier density and the impurity density. Based on experimental results for the Hall angle [95] we will assume $\sigma_{xy} > \sigma_{xx}$. This is in good agreement with the assumption that the impurity density is not too high. For simplicity we will now assume that

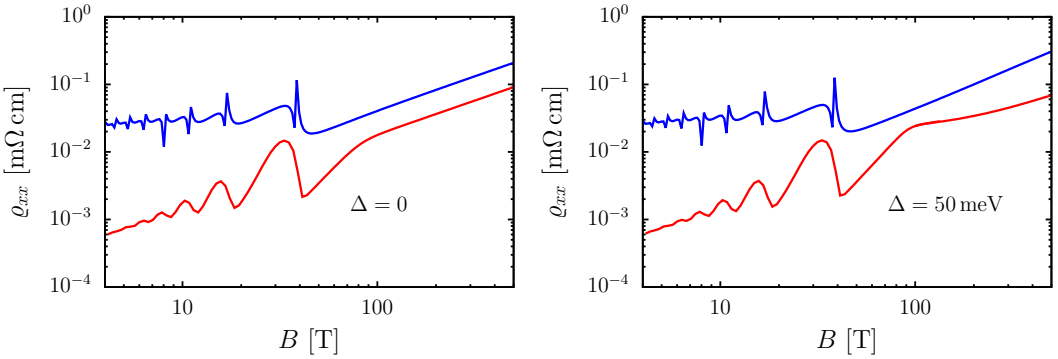

Figure 5.15: Magnetoresistance ϱ_{xx} calculated from Eq. (5.3.24) as a function of magnetic field. $\Delta = 0$ (left panel) and $\Delta = 50\,\mathrm{meV}$ (right panel). The resistivity calculated from the phenomenological result (red line) and the resistivity calculated microscopically using the first Born approximation with $\varepsilon_r = 1$ (blue). The density of charge carriers is $n_c = 10^{18}\mathrm{cm}^{-3}$.

$\tan\vartheta_H \gg 1$. In this case the elements of the Seebeck tensor are:

$$S_{xx} = -T\frac{\pi^2}{3e}\frac{\partial_\mu \sigma_{xy}}{\sigma_{xy}}\,, \qquad S_{xy} = -T\frac{\pi^2}{3e}\frac{\sigma_{xx}\partial_\mu\sigma_{xy} - \sigma_{xy}\partial_\mu\sigma_{xx}}{\sigma_{xy}^2}\,. \tag{5.4.2}$$

In the quantum limit the derivative of the Hall conductivity (5.3.6) with respect to the chemical potential is:

$$\partial_\mu \sigma_{xy} = -\frac{e^2}{2\pi^2}\frac{\sqrt{\Delta_B^2 + \Delta^2}}{\Delta_B}\,. \tag{5.4.3}$$

With this the Seebeck coefficient can be expressed analytically as:

$$S_{xx} = -T\frac{\pi^2}{3e}\frac{\sqrt{\Delta_B^2+\Delta^2}}{\Delta_B^2} \propto \begin{cases} B & \Delta_B \gg \Delta \\ B^2 & \Delta_B \ll \Delta \end{cases}\,. \tag{5.4.4}$$

For the massless case we recover the linear non-saturating result obtained experimentally and theoretically in Refs. [117] and [83]. For the massive case we get a significantly different behavior since the Seebeck coefficient is proportional to the square of the magnetic field. As we can see this result does not depend on the impurity density as long as the impurities can be neglected in the calculation of the Hall-conductivity. The Seebeck coefficient (5.4.4) using different mass terms can be seen in Fig. 5.16.

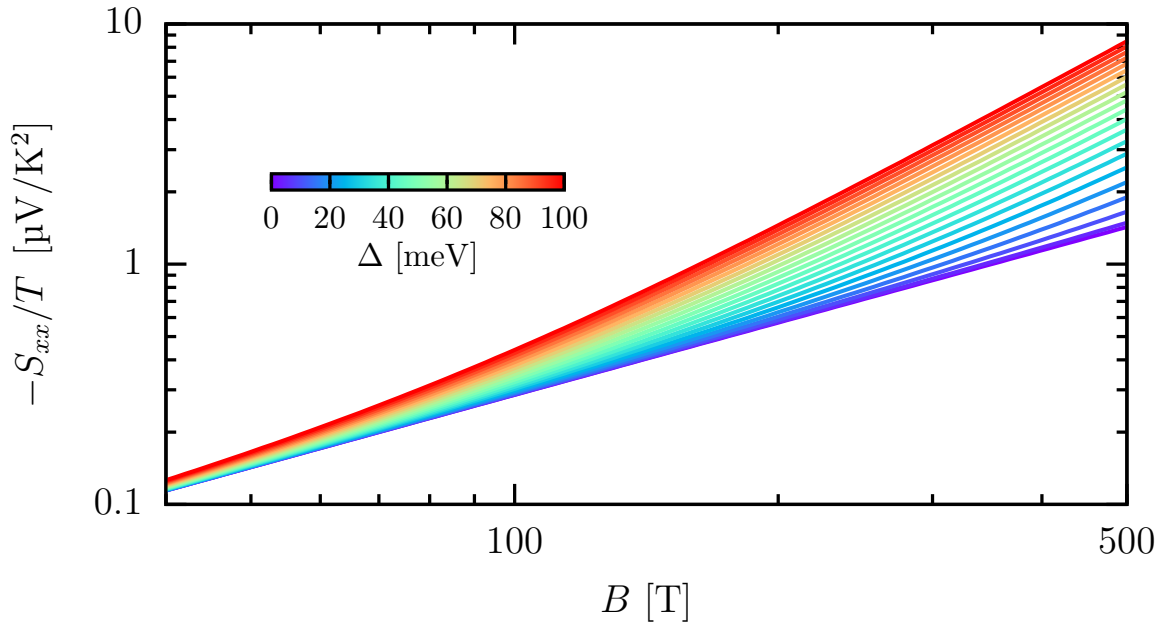

Figure 5.16: The Seebeck coefficient in the quantum limit (5.4.4) as a function of the magnetic field using different mass terms. The parameters used are: $n_c = 10^{18}\mathrm{cm}^{-3}$ and $v = 10^6 \mathrm{m\,s}^{-1}$.

The Nernst-coefficient can be divided in two terms as:

$$S_{xy} = \underbrace{S_{xx}\frac{\sigma_{xx}}{\sigma_{xy}}}_{S_{xy}^{(1)}} + \underbrace{T\frac{\pi^2}{3e}\frac{\partial_\mu \sigma_{xx}}{\sigma_{xy}}}_{S_{xy}^{(2)}} . \tag{5.4.5}$$

As we showed in previous sections $\sigma_{xx} \propto \sigma_{xy}$ at high fields, this means that the magnetic field dependence of $S_{xy}^{(1)}$ is qualitatively the same as S_{xx}. For the second term we need to evaluate $\partial_\mu \sigma_{xx}$. Since the chemical potential dependence affects many components of the conductivity through Δ_B in Eq. (5.3.13), we calculate the derivative numerically. The conductivity as a function of the chemical potential can be seen in Fig. 5.17.

In the massless case the conductivity is almost independent of the chemical potential, but in the massive case we can see that the dependence becomes very strong close to the bottom of the Landau level, caused by the diverging density of states. Using the numerical derivative for the conductivity we can calculate $S_{xy}^{(2)}$. The results for the two components of the Nernst coefficient can be seen on Fig. 5.18.

The first component is very similar to the Seebeck coefficient, but it is suppressed

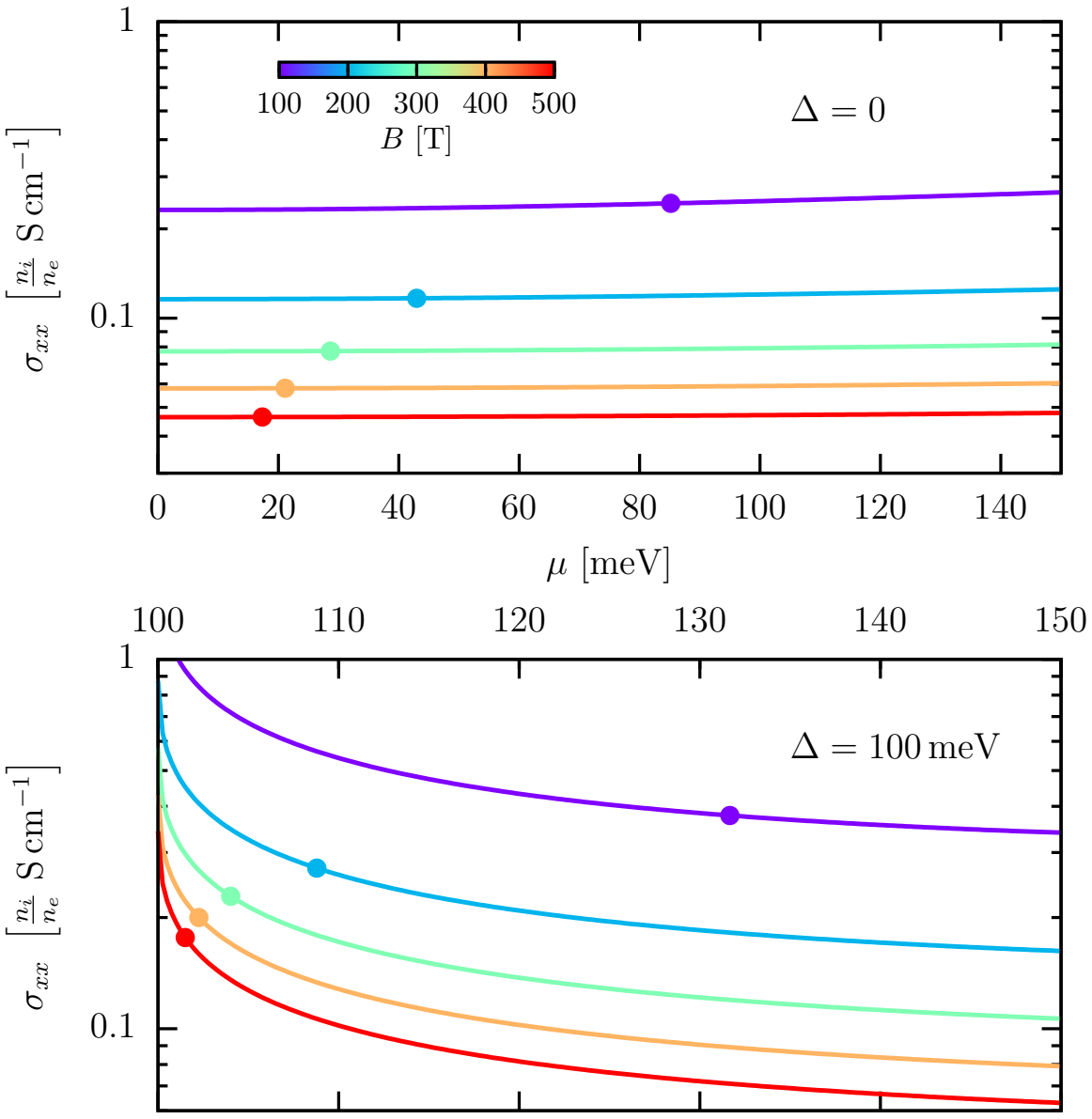

Figure 5.17: The conductivity in the quantum limit (5.3.13) as a function of the chemical potential at different magnetic fields. The mass term is $\Delta = 0$ (top plot) and $\Delta = 100\,\text{meV}$ (bottom plot). The solid circles show the values of the chemical potential when $n_c = 10^{18}\text{cm}^{-3}$ at the given magnetic fields, which is the point where the derivative in Eq. (5.4.5) has to be evaluated.

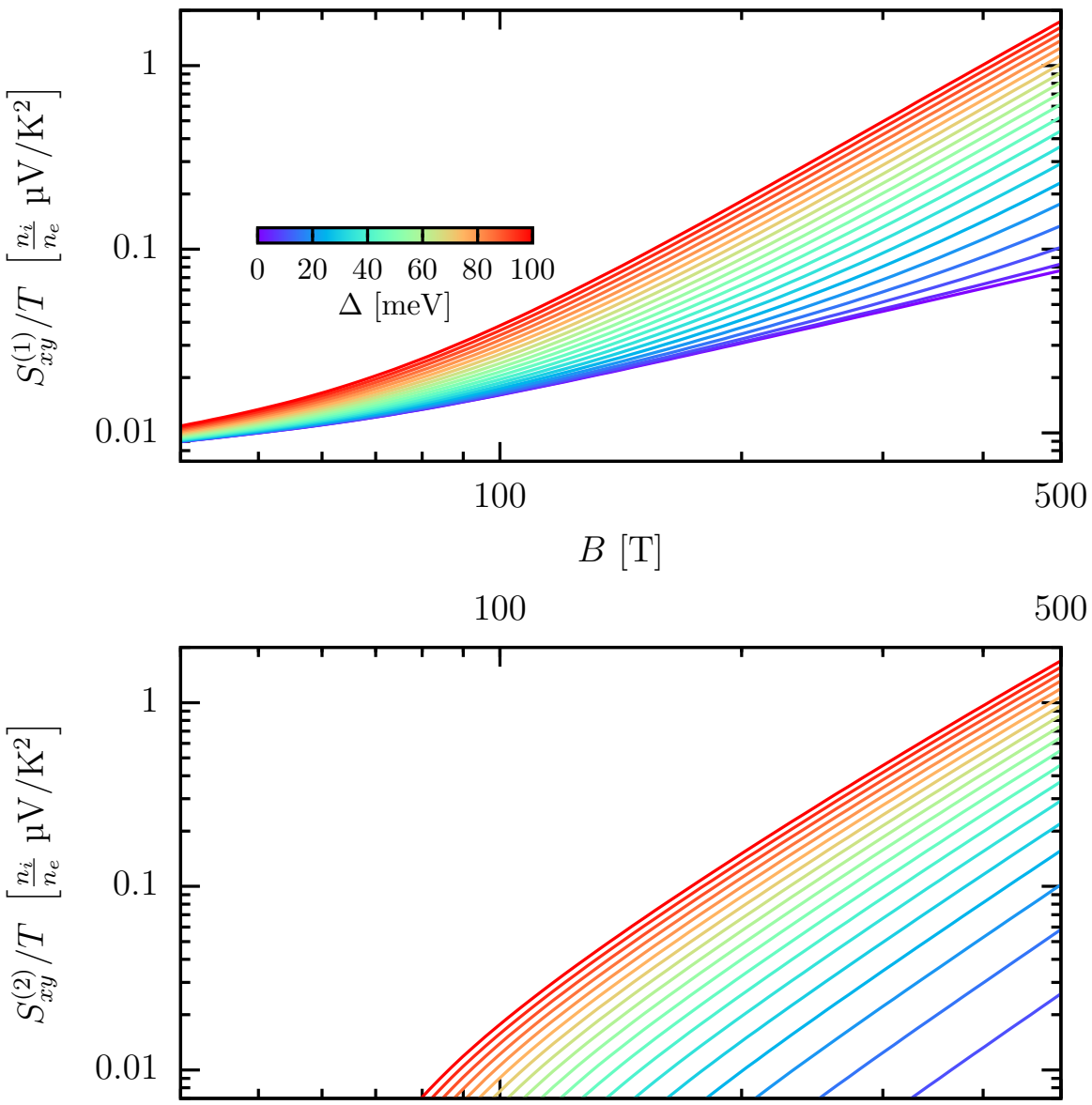

Figure 5.18: The two components of the Nernst coefficient in the quantum limit (5.4.5) as a function of the magnetic field using different mass terms. The parameters used are: $n_c = 10^{18}\mathrm{cm}^{-3}$ and $v = 1 \times 10^6\,\mathrm{m\,s}^{-1}$

by $\cot\vartheta_H$. The second component is very small (at certain regions even negative) at low fields and low mass terms. At higher fields in the case of finite mass term it has the same dependence as $S_{xy}^{(1)}$ and roughly the same value.

The total Nernst coefficient can be seen in Fig. 5.19. The dependence is very

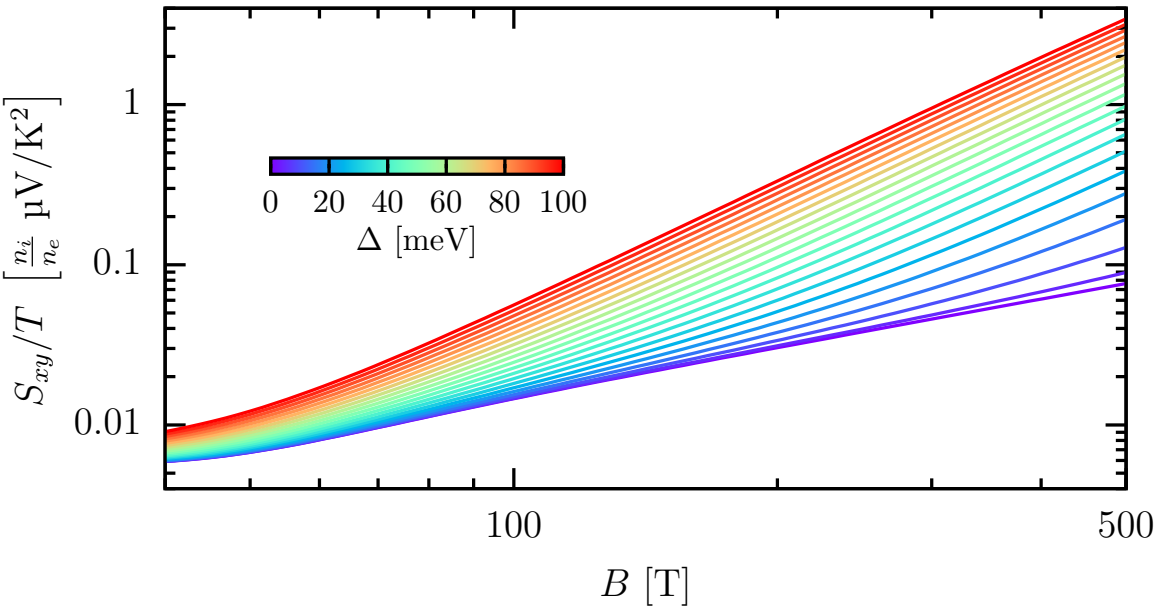

Figure 5.19: The Nernst coefficient in the quantum limit (5.4.5) as a function of the magnetic field using different mass terms. The parameters used are: $n_c = 10^{18}\mathrm{cm}^{-3}$ and $v = 10^6\mathrm{m\,s}^{-1}$.

similar to that of the Seebeck coefficient. The main difference is at lower fields where σ_{xx} differs from the asymptotic behavior.

5.5 Summary

In this final section the most important results of this chapter are summarized. We studied the transport coefficients of a three-dimensional relativistic electron gas in high magnetic fields. The used model is the Dirac Hamiltonian in a constant magnetic field. This model is a generalization of the Weyl Hamiltonian used in Refs. [43] and [114], and can be used as a continuum model for massive Dirac materials.

We calculated the chemical potential fixing the charge carrier density, the screening wavenumber using the random phase approximation, and the scattering rate using the first Born approximation. At high magnetic fields we show the analytic asymptotic

behavior of these. The important energy scale is $\Delta_B = 2\pi^2 n_c \ell_B^2$ and the mass term Δ becomes relevant when $\Delta_B < \Delta$. For realistic systems this happens at high fields which are hard to realize experimentally. In order to be able to see the effects of the mass term, materials with smaller charge carrier density or larger mass term need to be studied. The asymptotic behavior can be summarized as:

$$\mu \propto B^{-1} \qquad \kappa^2 \propto B \qquad \Gamma \propto B^{-1} \qquad \Delta_B \gg \Delta\,, \tag{5.5.1a}$$

$$\mu \sim \Delta \qquad \kappa^2 \propto B^2 \qquad \Gamma \propto B^{-2} \qquad \Delta_B \ll \Delta\,. \tag{5.5.1b}$$

At lower magnetic fields the effect of the mass term is negligible and all quantities show SdH oscillations. For the $\Delta = 0$ case our results are consistent with studies on the Weyl Hamiltonian [43, 114].

Using the formalism described in Chapter 3 we calculated the transport coefficients in a magnetic field. We studied the magnetoconductivity and magnetothermopower in the transverse plane of the magnetic field. At high magnetic fields we got analytic results for these quantities which is the main result of this chapter, and it can be summarized as:

$$\sigma_{xx} \propto \frac{n_i}{B} \qquad S_{xx} \propto \frac{TB}{n_c} \qquad \Delta_B \gg \Delta\,, \tag{5.5.2a}$$

$$\sigma_{xx} \propto \frac{n_i}{B} \qquad S_{xx} \propto \frac{TB^2\Delta}{n_c^2} \qquad \Delta_B \ll \Delta\,, \tag{5.5.2b}$$

$$\sigma_{xy} \propto \frac{n_c}{B} \qquad S_{xy} \propto \frac{n_i TB}{n_c^2} \qquad \Delta_B \gg \Delta\,, \tag{5.5.2c}$$

$$\sigma_{xy} \propto \frac{n_c}{B} \qquad S_{xx} \propto \frac{n_i TB^2\Delta}{n_c^3} \qquad \Delta_B \ll \Delta\,. \tag{5.5.2d}$$

The different scalings of the transport coefficients obtained in this chapter are consistent with other experimental and theoretical studies found in the literature. These related studies are summarized in Tab. 5.1. In the following, we give a detailed description of our results and explain what is new and how they are connected to the studies found in the literature.

First, we discuss the magnetoconductivity. This was previously studied in the massless case using the 2×2 Weyl Hamiltonian [43, 114–116]. The finite mass results shown in this dissertation are new results.

We showed that the Hall conductivity in the clean limit is inversely proportional

Scaling	Mass term	Experimental studies	Theoretical studies
$\sigma_{xx} \propto B^{-1}$	$\Delta_B \gg \Delta$	[68, 69, 81, 90–92, 95]	[43, 114–116]
$\sigma_{xy} \propto B^{-1}$			
$S_{xx} \propto B$		[80, 83, 96]	[117]
$S_{xy} \propto B$			present study
$\sigma_{xx} \propto B^{-1}$	$\Delta_B \ll \Delta$	not studied yet	present study
$\sigma_{xy} \propto B^{-1}$			
$S_{xx} \propto B^2$			
$S_{xy} \propto B^2$			

Table 5.1: A review of the previous experimental and theoretical results found in the literature and the new results of the present dissertation for the scaling of the transport coefficients.

to the magnetic field and it is independent of the mass term and temperature. This magnetic field dependence was shown previously in the massless case.

In the case of σ_{xx} impurities are necessary to get a non-zero result. We have shown that the magnetic field dependence of the scattering rate directly affects the magnetic field dependence of the conductivity. The screened charged impurities are necessary to reproduce the B^{-1} dependence of the conductivity and thus the linear magnetoresistance, consistently with previous studies in the massless case [43, 114–116]. We calculated the vertex correction and showed that it is negligible for realistic parameter regimes, which justifies the assumptions in previous studies. In the case of finite mass term we showed that the high field limit is qualitatively the same as in the massless case i.e. proportional to B^{-1} but with different numerical prefactors.

We calculated the magnetoresistance and recovered the linear magnetoresistance observed in many experimental studies [68, 69, 81, 90–92, 95]. At low fields, ϱ_{xx} for the massive and massless cases behave very similarly. In addition to the SdH oscillations, ϱ_{xx} is proportional to B if we assume a phenomenological scattering rate as $\Gamma \propto B$. On the other hand, if we use the scattering rate calculated from the Born approximation

we get $\varrho_{xx} \propto B^{1/3}$ as in Ref. [114].

We have seen that the temperature dependence is not so relevant. It decreases the SdH oscillations but it does not affect the overall magnetic field dependence. This is consistent with experimental results [68, 90–92]. The temperature dependence in the experimental results is mainly caused by the normalization using the zero field conductivity, which is strongly temperature dependent.

Finally, we discuss the magnetothermopower. This was discussed previously in the massless case using a theory where the entropy density is used to calculate the Seebeck coefficient in a magnetic field [117]. A microscopic description using linear response theory employed in this dissertation was not discussed before in the literature.

Using the Mott-formula we studied the Seebeck and Nernst coefficients. We assumed that the Hall conductivity is larger than the diagonal conductivity, and thus the Hall-angle is large. This is a reasonable assumption if the impurity density is low and it is consistent with experimental results [95]. With this S_{xx} is linear in the massless case consistently with Ref. [117]. In contrast, in the massive case the Seebeck coefficient increases quadratically with the magnetic field. This is also consistent with the experimental result for massive Dirac electrons [80, 83, 96], where they found the thermopower to be linear, since the magnetic field is not high enough in the experiment to see the different behavior. While the qualitative difference does not appear in the conductivity, we see it in the Seebeck coefficient, but only at very high fields. As we saw the Nernst coefficient behaves very similarly to the Seebeck coefficient. This is mainly caused by the fact that the Hall angle saturates at high fields, which makes $S_{xy} \propto S_{xx}$.

Chapter 6

Summary and outlook

We presented a microscopic formalism based on linear response theory to calculate magnetotransport in solid state systems. We studied both the low magnetic field and high magnetic field cases. As we saw the formalism and approximations used are very different for the two cases. We applied these methods to study Dirac systems in magnetic fields. In the following we review the most important results presented in the previous chapters. Furthermore, we present some unsolved problems and future prospects.

In Chapter 4 we studied the low magnetic field dependence of the magnetoconductivity. We expressed the Hall conductivity (4.2.9) and longitudinal magnetoconductivity (4.2.14) up to linear order of the magnetic field assuming small scattering rates. These expressions were not derived using a microscopic theory so far and are new results in this dissertation. The magnetoconductivity is expressed in terms of energy derivatives, the Berry curvature, and the orbital magnetic moment. The terms containing the Berry curvature were previously explained using the semiclassical Boltzmann theory using the anomalous velocity, but the term containing the orbital magnetic moment is not present in these previous studies.

We discussed that in systems where the time reversal symmetry is broken it is possible to produce a linear longitudinal magnetoconductivity. As a simple example where this effect is present we studied tilted Weyl semimetals. This system was studied previously using the Boltzmann transport theory. We reproduced the semiclassical result (4.3.8a) with our microscopic theory and showed that the linear longitudinal magnetoconductivity has corrections connected to the orbital magnetic moment (4.3.8b). The main finding of this chapter is the extra term in the magnetoconductivity related to the orbital magnetic moment and the effect of it in the case of tilted Weyl semimetals.

This term does not affect the qualitative behavior but modifies the quantitative value of the magnetoconductivity.

Our formalism is general and can easily be applied to any system and can be generalized to thermoelectric transport or higher orders of the magnetic field. This opens a new pathway to theoretically study low magnetic field magnetotransport.

In Chapter 5 we studied the thermoelectric transport coefficients of a massive Dirac fermion gas in high magnetic fields using the formalism described in Chapters 2 and 3.

The novel results of this chapter are connected to the finite mass term, which was not studied in the high magnetic fields. We showed that the mass term becomes relevant at high fields or low carrier densities and the energy scale that the mass term has to be compared to is $\Delta_B = 2v\hbar^2\pi^2 n_e/eB$.

We calculated the transverse magnetoconductivity and transverse magnetothermopower and gave analytic scalings (5.5.2) for these as a function of the magnetic field, which is the main result of this chapter. These results and their connection to previous findings are summarized in Tab. 5.1.

We found that the transverse magnetoconductivity is inversely proportional to the magnetic field. This is consistent with the linear magnetoresistance observed in experiments. The finite mass term does not cause a qualitatively different result and the scaling remains B^{-1} for finite mass terms. In the case of the transverse magnetothermopower at high magnetic fields a qualitatively different behavior occurs between the massless and massive cases. In the massless case we got a linear increase while in the massive case the increase is quadratic.

We showed that the temperature range where the low temperature approximation can be applied expands with increasing magnetic fields. This means that at high magnetic fields, the temperature dependence of the magnetoconductivity is negligible. And in the case of the thermoelectric transport coefficients, the linear temperature dependence persists to higher temperatures when a magnetic field is applied.

The formalism described by us works very well at high magnetic fields. It is completely general and it can be used to study other topological systems in the quantum limit, and gives a robust method to study the high field magnetotransport in solid state materials.

In the following we discuss some future problems, that are beyond the scope of this dissertation. The low magnetic field formalism was developed for the linear order

of the magnetic field. Our plan for the future is to extend the formalism to higher orders of the magnetic field. The higher order we study the more complicated the formalism becomes (e.g. in the quadratic order there will be six Green's functions and six current operators), which makes the problem very challenging. The formalism can also be extended to study thermoelectric components, and it could be used to study non-trivial effects in the Seebeck and Nernst coefficients.

In the high magnetic field description we needed several assumptions in order to be able to calculate the transport coefficients. The general problem is very complicated with many multivariate integrations, but in order to better study the low magnetic field behavior a more accurate calculation for the scattering rate and impurity potential is needed.

At lower magnetic fields we saw very strong oscillations in the scattering rate, which are caused by only using the first Born approximation. An important improvement would be the self-consistent Born approximation, which is a numerically very challenging problem. Furthermore, using the static and long-wave limit in the random phase approximation is the simplest way to include the electron-electron interaction for the screening. An improvement would be to take into account the frequency and momentum dependence of the polarization function and thus the screening wavenumber. The assumption of a simple screened Coulomb potential might not be sufficient to describe all the effects properly.

The ultimate goal of the theoretical study of magnetotransport is to connect the low field and high field descriptions with a continuous curve and have a consistent description that works for any system. This is a very challenging task with still a lot of unsolved problems and inconsistencies. All things considered, the formalisms presented in this dissertation bring us one step closer to achieve this goal, and help to deepen our understanding of thermoelectric transport in magnetic fields.

Appendix A

Matsubara summations

A.1 Matsubara summation with branch cuts

The Matsubara summations in this dissertation are mainly in the form of:

$$C(i\omega_\lambda) = -\frac{1}{\beta}\sum_n g(i\varepsilon_n, i\varepsilon_n + i\omega_\lambda)\,, \tag{A.1.1}$$

where the function g contains Green's functions with arguments $i\varepsilon_n$ or $i\varepsilon_n + i\omega_\lambda$. A simple example is (this appears in Sec. 3.2.1):

$$g(i\varepsilon_n, i\varepsilon_n + i\omega_\lambda) = G_a(i\varepsilon_n)G_b(i\varepsilon_n + i\omega_\lambda)\,. \tag{A.1.2}$$

In general there can be any number of Green's functions with any kind of indices. Because of the sign changing properties of the scattering rate at $\mathrm{Im}\{\varepsilon\} = 0$, g has two branch cuts and this type of summation can be transformed to four ordinary integrals using the residue theorem [19]. We first show this on the example given in Eq. (A.1.2). The Matsubara summation can be transformed into a contour integral as shown in the left side of Fig. A.1:

$$C(i\omega_\lambda) = -\frac{1}{\beta}\sum_n G_b(i\omega_n + i\omega_\lambda)G_a(i\omega_n) = \oint_{\mathcal{C}} \frac{\mathrm{d}z}{2\pi i} G_b(z + i\omega_\lambda)G_a(z)f(z)\,, \tag{A.1.3}$$

where $f(z)$ is the Fermi-Dirac function:

$$f(z) = \frac{1}{\mathrm{e}^{\beta z} + 1}\,, \qquad \operatorname*{Res}_{z=i\omega_n}[f(z)] = -\frac{1}{\beta}\,. \tag{A.1.4}$$

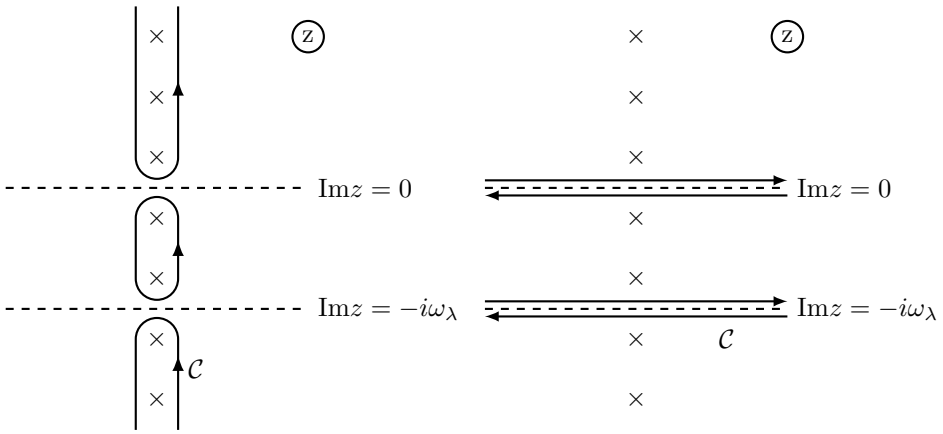

Figure A.1: The left side shows the contour integral equivalent to the Matsubara summation. The right side shows this same integral transformed to four ordinary integrals. The crosses show the singularities of the Fermi-Dirac distribution. The dashed lines show the branch cuts of g in Eq. (A.1.1).

The contour integral can be transformed to four line integrals as show in the right side of Fig. A.1:

$$\begin{aligned} C^R(\omega) = \int_{-\infty}^{\infty} \frac{\mathrm{d}\varepsilon}{2\pi i} f(\varepsilon) \Big[\; & G_b(\varepsilon+\omega, +\Gamma_b(\varepsilon+\omega)) G_a(\varepsilon, +\Gamma_a(\varepsilon)) - \\ & - G_b(\varepsilon+\omega, +\Gamma_b(\varepsilon+\omega)) G_a(\varepsilon, -\Gamma_a(\varepsilon)) + \\ & + G_b(\varepsilon, +\Gamma_b(\varepsilon)) G_a(\varepsilon-\omega, -\Gamma_a(\varepsilon-\omega)) - \\ & - G_b(\varepsilon, -\Gamma_b(\varepsilon)) G_a(\varepsilon-\omega, -\Gamma_a(\varepsilon-\omega)) \Big] , \end{aligned} \tag{A.1.5}$$

where:

$$G_a(z, \pm\Gamma_a(z)) := \frac{1}{z + \mu - E_a \pm i\Gamma_a(z)} , \tag{A.1.6}$$

and we performed the analytic continuation in the frequency $i\omega_\lambda \to \omega + i0^+$. It is useful to shift ε by the chemical potential, and define the retarded and advanced Green's functions:

$$G_a^R(\varepsilon) := \frac{1}{\varepsilon - E_a + i\Gamma_a(\varepsilon)} , \qquad G_a^A(\varepsilon) := \frac{1}{\varepsilon - E_a - i\Gamma_a(\varepsilon)} . \tag{A.1.7}$$

With this the Matsubara summation becomes:

$$C^R(\omega) = \int_{-\infty}^{\infty} \frac{\mathrm{d}\varepsilon}{2\pi i} f(\varepsilon-\mu)\Big[G_b^R(\varepsilon+\omega)G_a^R(\varepsilon) - G_b^R(\varepsilon+\omega)G_a^A(\varepsilon) + \\ + G_b^R(\varepsilon)G_a^A(\varepsilon-\omega) - G_b^A(\varepsilon)G_a^A(\varepsilon-\omega)\Big]. \tag{A.1.8}$$

This same derivation works for any number of Green's function, and the general Matsubara summation can be expressed as:

$$C^R(\omega) = \int_{-\infty}^{\infty} \frac{\mathrm{d}\varepsilon}{2\pi i} f(\varepsilon-\mu)\left[g^{RR}(\varepsilon,\varepsilon+\omega) - g^{AR}(\varepsilon,\varepsilon+\omega) + \right. \\ \left. + g^{AR}(\varepsilon-\omega,\varepsilon) - g^{AA}(\varepsilon-\omega,\varepsilon)\right], \tag{A.1.9}$$

where the upper indices of g show the retardedness of the Green's function with the corresponding argument. In our previous example:

$$g^{XY}(\varepsilon,\varepsilon+\omega) = G_a^X(\varepsilon)G_b^Y(\varepsilon+\omega). \tag{A.1.10}$$

In the case of the conductivity only the $\omega \to 0$ limit is important. Since in Eq. (3.2.5a) we have to divide by ω, the limit we are interested in is $C = \lim_{\omega\to 0} \frac{C^R(\omega)}{\omega}$:

$$C = \int_{-\infty}^{\infty} \frac{\mathrm{d}\varepsilon}{2\pi i} f'(\varepsilon-\mu)\left[g^{AR}(\varepsilon,\varepsilon) - g^{AA}(\varepsilon,\varepsilon)\right] + \\ + f(\varepsilon-\mu)\partial_\omega\left[g^{RR}(\varepsilon,\varepsilon+\omega) - g^{AA}(\varepsilon,\varepsilon+\omega)\right]\big|_{\omega=0}. \tag{A.1.11}$$

A.2 Integrals of Green's functions

From now on we assume $\Gamma_a(\varepsilon) \equiv \Gamma$ and $\Gamma \to 0$. This means that we only keep the highest order terms in Γ and neglect anything $\mathcal{O}(\Gamma^0)$. We substitute the infinite integral in Eq. (A.1.11) with a contour integral on the upper complex plane as in Fig. A.2. The integrand will have several poles coming from the Fermi-Dirac distribution and poles coming from the advanced Green's functions inside the contour. After collecting the residues coming from the Fermi-distribution and performing the $\Gamma \to 0$, limit we

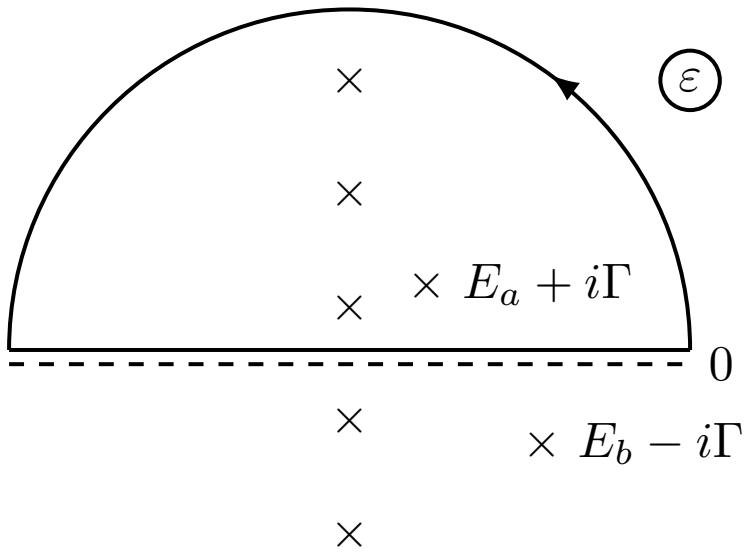

Figure A.2: Contour integration on the upper half plane. The crosses show the singularities of the Fermi-Dirac distribution and the Green's functions.

see that these contributions disappear since for $\Gamma = 0$ the difference between advanced and retarded Green's functions disappears, thus in the combination $g^{AR} - g^{AA}$ and $g^{RR} - g^{AA}$ the singularities coming from the Fermi-Dirac distribution can be neglected in the order of $\mathcal{O}(\Gamma^0)$. This means that the integral can be substituted with the residues coming only from the advanced Green's functions in the upper plane[1].

This means immediately that the term g^{RR} can be neglected. It can also be shown that g^{AA} can only have contributions of $\mathcal{O}(\Gamma^0)$. In order to have a higher order term two poles with the same energy but with different retardednesses are necessary. In this case in the residue a $1/(E_a - E_a + 2i\Gamma)$ type of term appears which is of $\mathcal{O}(\Gamma^{-1})$. With higher order poles higher orders of Γ^{-1} can also appear. Since in g^{AA} all the poles are on one side the contribution is $\mathcal{O}(\Gamma^0)$.

This way C can be calculated as:

$$C = \sum_i \mathrm{Res}\{f'(\varepsilon) g^{AR}(\varepsilon, \varepsilon), \varepsilon_i\}\,, \tag{A.2.1}$$

where ε_i are the singular points on the upper half plane of only g^{AR}. Taking our simple

[1]This same argument can be done with the lower half plane and retarded Green's functions, and the results do not change.

example in the case of $b = a$:

$$C = \mathrm{Res}\big\{ f'(\varepsilon) G_a^A(\varepsilon) G_a^R(\varepsilon), E_a + i\Gamma \big\} = \frac{f'(E_a)}{2i\Gamma} \,. \tag{A.2.2}$$

This is exactly the same result as using the usual $G_a^A(\varepsilon)G_a^R(\varepsilon) = \pi\delta(\varepsilon - E_a)/\Gamma$ approximation. But in cases where there are more Green's functions, this approximation can not always be used. Our method provides a systematic approach to evaluate these types of integrals. It is important to note that here $f'(E_a + i\Gamma) \approx f'(E_a)$ was used since we are neglecting terms of $\mathcal{O}(\Gamma^0)$. In cases with more Green's functions the Taylor expansion of f is necessary to get a proper result as we will see in the following section.

A.3 Summations in Chapter 4

In this section we give the results of the summations present in Eqs. (4.2.3) and (4.2.11). We detail C_{aaaa} and list the rest of the results. The g^{AR} in this case is:

$$g^{AR} = G_a^R G_a^A (G_a^A G_a^A - G_a^R G_a^R) \,. \tag{A.3.1}$$

using Eq. (A.2.2):

$$\begin{aligned} C_{aaaa} &= \frac{1}{2} \left(f' G_a^R \right)'' \Big|_{\varepsilon = E_a + i\Gamma} - f' \left(G_a^R \right)^3 \Big|_{\varepsilon = E_a + i\Gamma} = -f'' \left(G_a^R \right)^2 \Big|_{\varepsilon = E_a + i\Gamma} + \frac{1}{2} f''' G^R \Big|_{\varepsilon = E_a + i\Gamma} = \\ &= \frac{f''(E_a + i\Gamma)}{4\Gamma^2} + \frac{f'''(E_a + i\Gamma)}{4i\Gamma} \approx \frac{f''(E_a)}{4\Gamma^2} + \frac{f'''(E_a) i\Gamma}{4\Gamma^2} + \frac{f'''(E_a)}{4i\Gamma} = \frac{f''(E_a)}{4\Gamma^2} \,. \end{aligned} \tag{A.3.2}$$

All the other summations can be done in a similar way. Here are the results for the C summations in Eq. (4.2.3):

$$C_{aaaa} = \frac{f_a''}{4\Gamma^2} + \mathcal{O}\big(\Gamma^0\big) \,, \tag{A.3.3a}$$

$$C_{abba} = \mathcal{O}\big(\Gamma^0\big) \,, \tag{A.3.3b}$$

$$C_{aabb} = \frac{1}{2i\Gamma} \frac{f_a' - f_b'}{(E_a - E_b)^2} + \mathcal{O}\big(\Gamma^0\big) \,, \quad C_{abab} = C_{aabb} \,, \tag{A.3.3c}$$

$$C_{aaab} = \frac{1}{4\Gamma^2} \frac{f_a'}{E_a - E_b} + \frac{i}{4\Gamma} \left[\frac{2 f_a'}{(E_a - E_b)^2} - \frac{f_a''}{E_a - E_b} \right] + \mathcal{O}\big(\Gamma^0\big), C_{baaa} = C_{aaab}^*, \tag{A.3.3d}$$

$$C_{abaa} = \frac{1}{2\Gamma^2} \frac{f_a'}{E_a - E_b} + \mathcal{O}\big(\Gamma^0\big) \,, \quad C_{aaba} = C_{abaa} \,, \tag{A.3.3e}$$

$$C_{aacb} = \frac{f'_a}{2i\Gamma}\frac{1}{E_a - E_b}\frac{1}{E_a - E_c} + \mathcal{O}\big(\Gamma^0\big)\,, \quad C_{aacb} = C_{abac} = -C_{cbaa} = -C_{baca}\,, \tag{A.3.3f}$$

$$C_{abca} = \mathcal{O}\big(\Gamma^0\big)\,, \quad C_{caab} = \mathcal{O}\big(\Gamma^0\big)\,, \tag{A.3.3g}$$

$$C_{abcd} = \mathcal{O}\big(\Gamma^0\big)\,. \tag{A.3.3h}$$

And here are the results for the D summations in Eq. (4.2.11):

$$C_{aaaa} = D_{aaaa} - \tilde{D}_{aaaa}\,, \tag{A.3.4a}$$

$$D_{abba} = \frac{1}{2i\Gamma}\frac{f'_a}{(E_a - E_b)^2} + \mathcal{O}\big(\Gamma^0\big)\,, \quad D_{abba} = \tilde{D}_{abba} = D_{aabb} = \tilde{D}_{aabb} = D_{abab} = \tilde{D}_{abab}\,, \tag{A.3.4b}$$

$$D_{baaa} = \mathcal{O}\big(\Gamma^0\big)\,, \quad \tilde{D}_{baaa} = \mathcal{O}\big(\Gamma^0\big)\,, \tag{A.3.4c}$$

$$D_{aaab} = C_{aaab}\,, \quad \tilde{D}_{aaba} = -D^*_{aaba}\,, \quad D_{aaab} = D_{aaba} = D_{abaa}\,, \quad \tilde{D}_{aaab} = \tilde{D}_{aaba} = \tilde{D}_{abaa}\,, \tag{A.3.4d}$$

$$D_{aacb} = C_{aacb}\,, \quad D_{aacb} = \tilde{D}_{aacb} = D_{abca} = \tilde{D}_{abca} = D_{abac} = \tilde{D}_{abac}\,, \tag{A.3.4e}$$

$$D_{cbaa} = \mathcal{O}\big(\Gamma^0\big)\,, \quad \tilde{D}_{cbaa} = \mathcal{O}\big(\Gamma^0\big)\,, \quad D_{caab} = \mathcal{O}\big(\Gamma^0\big)\,, \quad \tilde{D}_{caab} = \mathcal{O}\big(\Gamma^0\big)\,, \tag{A.3.4f}$$

$$D_{baca} = \mathcal{O}\big(\Gamma^0\big)\,, \quad \tilde{D}_{baca} = \mathcal{O}\big(\Gamma^0\big)\,, \quad D_{abcd} = \mathcal{O}\big(\Gamma^0\big)\,, \quad \tilde{D}_{abcd} = \mathcal{O}\big(\Gamma^0\big)\,. \tag{A.3.4g}$$

Appendix B

Low field magnetoconductivity

B.1 Low magnetic field approximation

In this appendix we show how the formula for the current-current correlation function in Eqs. (4.2.1a) and (4.2.1b) is calculated based on the microscopic formalism developed by Fukuyama [30, 31].

We start by taking a general relativistic Hamiltonian[1] as in Eq. (2.1.2):

$$\mathbb{H}(\mathbf{p},\mathbf{x}) = \frac{(\mathbf{p}+e\mathbf{A})^2}{2m} + V + \frac{\hbar}{4m^2c^2}\boldsymbol{\sigma}\cdot[\boldsymbol{\nabla}V\times(\mathbf{p}+e\mathbf{A})] + \frac{\hbar^2}{8m^2c^2}\nabla^2 V\,. \tag{B.1.1}$$

The conductivity tensor is obtained using the current-current correlation as:

$$\sigma_{\mu\nu} = \lim_{\omega\to 0}\frac{ie^2}{\omega}\Pi^R_{\mu\nu}(\omega)\,. \tag{B.1.2}$$

the Matsubara current-current correlation function at finite q momentum is calculated as:

$$\Pi_{\mu\nu}(\mathbf{q}, i\omega_\lambda) = -\frac{1}{V}\int_0^\beta \mathrm{d}\tau\, \mathrm{e}^{i\omega_\lambda\tau}\left\langle \mathcal{J}_{\mathbf{q}\alpha}(\tau)\mathcal{J}_{\mathbf{0}\beta}(0)\right\rangle\,, \tag{B.1.3}$$

where $\mathcal{J}_{\mathbf{q}\alpha}$ is the Fourier transform of the current density operator defined as:

$$\mathcal{J}_{\boldsymbol{q}\mu}(\tau) := \int \mathrm{d}^3 r\, \mathcal{J}_\mu(\boldsymbol{r},\tau)e^{-i\boldsymbol{q}\boldsymbol{r}}. \tag{B.1.4}$$

The current operator was derived in Sec. 2.1.3. Here we need the current density operator, which in the case of the Eq. (B.1.1) Hamiltonian can be divided into two

[1] We only focus on the orbital contribution and neglect the Zeeman term.

contributions $\boldsymbol{\mathcal{J}}(\boldsymbol{r}) = \boldsymbol{\mathcal{J}}^{\mathrm{para}}(\boldsymbol{r}) + \boldsymbol{\mathcal{J}}^{\mathrm{dia}}(\boldsymbol{r})$ where the paramagnetic current is

$$\boldsymbol{\mathcal{J}}^{\mathrm{para}}(\boldsymbol{r}) = -\frac{i\hbar}{2m}\left(\boldsymbol{\Psi}^{\dagger}\boldsymbol{\nabla}\boldsymbol{\Psi} - \boldsymbol{\nabla}\boldsymbol{\Psi}^{\dagger}\cdot\boldsymbol{\Psi}\right) + \frac{\hbar}{4m^2c^2}\boldsymbol{\Psi}^{\dagger}(\boldsymbol{\sigma}\times\boldsymbol{\nabla}V)\boldsymbol{\Psi}\,, \tag{B.1.5}$$

and the diamagnetic current is

$$\boldsymbol{\mathcal{J}}^{\mathrm{dia}}(\boldsymbol{r}) = \frac{e}{m}\boldsymbol{A}(\boldsymbol{r})\varrho(\boldsymbol{r})\,, \tag{B.1.6}$$

where $\varrho(\boldsymbol{r})$ is the density operator, $\varrho(\boldsymbol{r}) = \boldsymbol{\Psi}^{\dagger}(\boldsymbol{r})\boldsymbol{\Psi}(\boldsymbol{r})$.

We will calculate $\sigma_{\mu\nu}$ up to the first order with respect to the magnetic field. For this it is useful to express the vector potential $\boldsymbol{A}(\boldsymbol{x})$ using a plane wave (similarly to Refs. [30] and [34]) as:

$$\boldsymbol{A}(\boldsymbol{x}) = -i\boldsymbol{A}_{\boldsymbol{q}}\mathrm{e}^{i\boldsymbol{q}\boldsymbol{x}}\,. \tag{B.1.7}$$

With this vector potential, the magnetic field $\mathbf{B} = \boldsymbol{\nabla}\times\mathbf{A}$ becomes:

$$\boldsymbol{B}(\boldsymbol{r}) = \mathbf{q}\times\boldsymbol{A}_{\boldsymbol{q}}e^{i\boldsymbol{q}\boldsymbol{x}}\,. \tag{B.1.8}$$

In the $\mathbf{q}\to\mathbf{0}$ limit we get the constant magnetic field as $\mathbf{B} = \mathbf{q}\times\boldsymbol{A}_{\boldsymbol{q}}$. If the magnetic field points in the z direction:

$$q_{\mu}A_{\mathbf{q},\nu} - q_{\nu}A_{\mathbf{q},\mu} = \varepsilon_{\mu\nu z}B\,. \tag{B.1.9}$$

To get a first order expression in the magnetic field, $\Pi_{\mu\nu}(\boldsymbol{q}, i\omega_{\lambda})$ has to be expressed up to the first order with respect to both $\boldsymbol{A}_{\boldsymbol{q}}$ and $\boldsymbol{q}$.

In the zeroth order the current-current correlation function $\Pi_{\mu\nu}(\boldsymbol{q}, i\omega_{\lambda})$ in Eq. (B.1.3) becomes:

$$\Pi^{(0)}_{\mu\nu}(\boldsymbol{q}, i\omega_{\lambda}) = -\frac{1}{V}\int_0^{\beta} d\tau\,\left\langle \mathcal{J}^{\mathrm{para}}_{\boldsymbol{q}\mu}(\tau)\mathcal{J}^{\mathrm{para}}_{\mathbf{0}\nu}(0)\right\rangle_0 e^{i\omega_{\lambda}\tau}\,, \tag{B.1.10}$$

where the thermal average is taken at zero magnetic field. This gives the zero field conductivity discussed in Sec. 4.1.

In the first order with respect to the magnetic field, we have two contributions to

$\Pi^{(1)}_{\mu\nu}(\boldsymbol{k}, i\omega_\lambda)$. These are expressed as:

$$\Pi^{\mathrm{dia}}_{\mu\nu}(\boldsymbol{q}, i\omega_\lambda) = -\frac{1}{V}\int_0^\beta d\tau \Big(\left\langle \mathcal{J}^{\mathrm{para}}_{\boldsymbol{q}\mu}(\tau)\mathcal{J}^{\mathrm{dia}}_{\boldsymbol{0}\nu}(0)\right\rangle_0 + \left\langle \mathcal{J}^{\mathrm{dia}}_{\boldsymbol{q}\mu}(\tau)\mathcal{J}^{\mathrm{para}}_{\boldsymbol{0}\nu}(0)\right\rangle_0 \Big) e^{i\omega_\lambda \tau}\,, \tag{B.1.11a}$$

$$\Pi^{\mathrm{para}}_{\mu\nu}(\boldsymbol{q}, i\omega_\lambda) = \frac{1}{V}\int_0^\beta d\tau \int_0^\beta d\tau_1 \left\langle T_\tau \mathcal{J}^{\mathrm{para}}_{\boldsymbol{q}\mu}(\tau)\mathcal{J}^{\mathrm{para}}_{\boldsymbol{0}\nu}(0)\mathcal{H}_1(\tau_1)\right\rangle_0 e^{i\omega_\lambda\tau}, \tag{B.1.11b}$$

where $\mathcal{H}_1$ is the first-order Hamiltonian with respect to the vector potential:

$$\mathcal{H}_1 = \sum_\alpha \int \mathrm{d}^3x\, \boldsymbol{\Psi}(\mathbf{x}) \frac{\partial \mathbb{H}_0}{\partial p_\alpha} e A_\alpha \boldsymbol{\Psi}(\mathbf{x})\,, \tag{B.1.12}$$

where $\mathbb{H}_0$ is the Hamiltonian at zero magnetic field.

B.2 Luttinger-Kohn representation

In a periodic potential the Hamiltonian can be described with the (2.1.3) Bloch Hamiltonian:

$$\mathbb{H}_{\mathbf{k}}(\mathbf{p}, \mathbf{x}) = \frac{(\mathbf{p}+\mathbf{k})^2}{2m} + V + \frac{\hbar}{4m^2c^2}\boldsymbol{\sigma}\cdot[\boldsymbol{\nabla}V \times (\mathbf{p}+\mathbf{k})] + \frac{\hbar^2}{8m^2c^2}\nabla^2 V\,. \tag{B.2.1}$$

This Hamiltonian acts on Bloch wave functions as:

$$\mathbb{H}_{\mathbf{k}}(\mathbf{p}, \mathbf{x})\mathbf{u}_{a\mathbf{k}}(\mathbf{x}) = E_{a\mathbf{k}}\mathbf{u}_{a\mathbf{k}}(\mathbf{x})\,. \tag{B.2.2}$$

In the Luttinger-Kohn representation [135], the electron field operator is expressed using Bloch wave functions as:

$$\boldsymbol{\Psi}(\mathbf{x}) = \sum_{a,\mathbf{k}} \mathrm{e}^{i\mathbf{k}\mathbf{x}}\mathbf{u}_{a\mathbf{k}_0}(\mathbf{x})c_{a\mathbf{k}}\,, \tag{B.2.3}$$

where $\mathbf{k}_0$ is a fixed momentum chosen conveniently for the later calculations. In this

representation the current density operator and the density operator is written as:

$$\begin{aligned} \mathcal{J}^{\text{para}}_{\boldsymbol{q}\mu} &= \sum_{a,b,\boldsymbol{k}} \int \mathrm{d}^3x\, \mathbf{u}^{\dagger}_{a\mathbf{k}_0} \mathbb{J}_{\mathbf{k},\mu} \mathbf{u}_{b\mathbf{k}_0}\; c^{\dagger}_{a,\boldsymbol{k}-\frac{\boldsymbol{q}}{2}} c_{b,\boldsymbol{k}+\frac{\boldsymbol{q}}{2}}\,, \\ \varrho_{\boldsymbol{q}} &= \sum_{a,\boldsymbol{k}} c^{\dagger}_{a,\boldsymbol{k}-\frac{\boldsymbol{q}}{2}} c_{a,\boldsymbol{k}+\frac{\boldsymbol{q}}{2}}\,, \end{aligned} \tag{B.2.4}$$

with

$$\mathbb{J}_{\mathbf{k},\mu} := \frac{\partial \mathbb{H}_{\boldsymbol{k}}}{\partial \boldsymbol{k}} = \frac{\hbar^2}{m}(\mathbf{k}+\mathbf{p}) + \frac{\hbar^2}{4m^2c^2}\boldsymbol{\sigma}\times\boldsymbol{\nabla}V. \tag{B.2.5}$$

Using the Eq. (B.1.7) form of the vector potential the Fourier component of the diamagnetic current becomes:

$$\boldsymbol{\mathcal{J}}^{\text{dia}}_{\boldsymbol{q}} = -i\frac{e}{m}\boldsymbol{A}_{\boldsymbol{q}}\varrho_{\mathbf{0}}\,, \qquad\qquad \boldsymbol{\mathcal{J}}^{\text{dia}}_{\mathbf{0}} = -i\frac{e}{m}\boldsymbol{A}_{\boldsymbol{q}}\varrho_{-\boldsymbol{q}}\,. \tag{B.2.6}$$

The first order Hamiltonian (B.1.12) can be expressed using the paramagnetic current and the vector potential as:

$$\mathcal{H}_1 = -ie\boldsymbol{\mathcal{J}}^{\text{para}}_{-\boldsymbol{q}}\cdot\boldsymbol{A}_{\boldsymbol{q}}\,. \tag{B.2.7}$$

B.3 Current-current correlation

Using thermal Green's functions, the first contribution to $\Pi_{\mu\nu}(\boldsymbol{q}, i\omega_\lambda)$ in Eq. (B.1.11b) denoted as $\Pi^{\text{dia}}_{\mu\nu}(\boldsymbol{q}, i\omega_\lambda)$ becomes[2]:

$$\Pi^{\text{dia}}_{\mu\nu}(\boldsymbol{q}, i\omega_\lambda) = -\frac{1}{\beta V}\sum_{n,\boldsymbol{k}}\frac{ie}{m}\mathrm{Tr}\Big[\mathbb{J}_{\mathbf{k},\mu}\mathbb{G}_{\boldsymbol{k}_+}(i\varepsilon_n + i\omega_\lambda)\mathbb{G}_{\boldsymbol{k}_-}(i\varepsilon_n)\Big]A_{\boldsymbol{q},\nu}\,, \tag{B.3.1}$$

where $\boldsymbol{k}_\pm = \boldsymbol{k} \pm \boldsymbol{q}/2$, and $\mathbb{G}_{\boldsymbol{k}}(i\varepsilon_n)$ is the thermal Green's function in the momentum representation defined in Eq. (2.1.8).

[2] In the $\mathbf{q}\to\mathbf{0}$ limit the $\mathcal{O}(q^0)$ terms will vanish, so we neglected the terms independent of $\mathbf{q}$.

The second term $\Pi^{\text{para}}_{\mu\nu}(\boldsymbol{q}, i\omega_\lambda)$ has two contributions:

$$\Pi^{\text{para}}_{\mu\nu}(\boldsymbol{q}, i\omega_\lambda) = \frac{-1}{\beta V}\sum_{n,\alpha,\boldsymbol{k}} \frac{ie}{\hbar^3}\text{Tr}\left[\mathbb{J}_{\boldsymbol{k},\mu}\mathbb{G}_{\boldsymbol{k}_+}(i\varepsilon_n + i\omega_\lambda)\mathbb{J}_{\boldsymbol{k}_+,\nu}\mathbb{G}_{\boldsymbol{k}_+}(i\varepsilon_n)\mathbb{J}_{\boldsymbol{k},\alpha}\mathbb{G}_{\boldsymbol{k}_-}(i\varepsilon_n)\right]A_{\boldsymbol{q},\alpha} + \\ + \text{Tr}\left[\mathbb{J}_{\boldsymbol{k},\mu}\mathbb{G}_{\boldsymbol{k}_+}(i\varepsilon_n + i\omega_\lambda)\mathbb{J}_{\boldsymbol{k},\alpha}\mathbb{G}_{\boldsymbol{k}_-}(i\varepsilon_n + i\omega_\lambda)\mathbb{J}_{\boldsymbol{k}_-,\nu}\mathbb{G}_{\boldsymbol{k}_-}(i\varepsilon_n)\right]A_{\boldsymbol{q},\alpha}\,. \tag{B.3.2}$$

Next, we calculate the linear order in $\boldsymbol{q}$ of the total $\Pi^{(1)}_{\mu\nu}(\boldsymbol{q}, i\omega_\lambda)$. Defining the following differential operator

$$D_q := \sum_\mu q_\mu \frac{\partial}{\partial k_\mu}\,, \tag{B.3.3}$$

the thermal Green's function can be expanded as:

$$\mathbb{G}_{\boldsymbol{k}_+}(i\varepsilon_n) = \mathbb{G}_{\boldsymbol{k}}(i\varepsilon_n) + \frac{1}{2}D_q\mathbb{G}_{\boldsymbol{k}}(i\varepsilon_n) + O(q^2)\,. \tag{B.3.4}$$

In the following, we use these abbreviations: $\mathbb{J}_{\boldsymbol{k},\mu} \to \mathbb{J}_\mu$, $\mathbb{G}_{\boldsymbol{k}}(i\varepsilon_n) \to \mathbb{G}$, and $\mathbb{G}_{\boldsymbol{k}}(i\varepsilon_n + i\omega_\lambda) \to \mathbb{G}_+$. Using the previously defined D_q operator, we get:

$$\Pi^{(1)}_{\mu\nu}(\boldsymbol{q}, i\omega_\lambda) = -\frac{1}{\beta V}\sum_{n,\boldsymbol{k}}\frac{ie}{2m\hbar}\Big\{\text{Tr}\big[\mathbb{J}_\mu D_q\mathbb{G}_+\mathbb{G}\big]A_{\boldsymbol{q},\nu} - \text{Tr}\big[\mathbb{J}_\mu\mathbb{G}_+D_q\mathbb{G}\big]A_{\boldsymbol{q},\nu}\Big\} - \\ -\frac{1}{\beta V}\sum_{n,\alpha,\boldsymbol{k}}\frac{ie^3}{2\hbar^3}A_{\boldsymbol{q},\alpha}\big\{\text{Tr}\left[\mathbb{J}_\mu D_q\mathbb{G}_+\mathbb{J}_\nu\mathbb{G}\mathbb{J}_\alpha\mathbb{G}\right] + \text{Tr}\left[\mathbb{J}_\mu\mathbb{G}_+D_q\mathbb{J}_\nu\mathbb{G}\mathbb{J}_\alpha\mathbb{G}\right] + \\ + \text{Tr}\left[\mathbb{J}_\mu\mathbb{G}_+\mathbb{J}_\nu D_q\mathbb{G}\mathbb{J}_\alpha\mathbb{G}\right] - \text{Tr}\left[\mathbb{J}_\mu\mathbb{G}_+\mathbb{J}_\nu\mathbb{G}\mathbb{J}_\alpha D_q\mathbb{G}\right] + \\ + \text{Tr}\left[\mathbb{J}_\mu D_q\mathbb{G}_+\mathbb{J}_\alpha\mathbb{G}_+\mathbb{J}_\nu\mathbb{G}\right] - \text{Tr}\left[\mathbb{J}_\mu\mathbb{G}_+\mathbb{J}_\alpha D_q\mathbb{G}_+\mathbb{J}_\nu\mathbb{G}\right] \\ - \text{Tr}\left[\mathbb{J}_\mu\mathbb{G}_+\mathbb{J}_\alpha\mathbb{G}_+D_q\mathbb{J}_\nu\mathbb{G}\right] - \text{Tr}\left[\mathbb{J}_\mu\mathbb{G}_+\mathbb{J}_\alpha\mathbb{G}_+\mathbb{J}_\nu D_q\mathbb{G}\right]\big\}\,. \tag{B.3.5}$$

Using the definition of the Green's function the following Ward identity can be shown to hold:

$$\mathbb{G}\mathbb{J}_\mu\mathbb{G} = \frac{\partial}{\partial k_\mu}\mathbb{G}\,. \tag{B.3.6}$$

Furthermore, from the definition of $\mathbb{J}_\mu$ in Eq. (B.2.5), we can see that:

$$D_q\mathbb{J}_\mu = \frac{\hbar^2}{m}q_\mu\,. \tag{B.3.7}$$

Using these identities we can get an expression for the current-current correlation function that is proportional to the gauge invariant combination $q_\alpha A_{\mathbf{q},\beta} - q_\beta A_{\mathbf{q},\alpha}$:

$$\begin{aligned}\Pi^{(1)}_{\mu\nu} = &-\frac{ie}{2m\hbar}\frac{1}{\beta V}\sum_{n,\mathbf{k},\alpha}\mathrm{Tr}[\mathbb{J}_\mu\mathbb{G}_+\mathbb{J}_\alpha\mathbb{G}_+\mathbb{G} - \mathbb{J}_\mu\mathbb{G}_+\mathbb{G}\mathbb{J}_\alpha\mathbb{G}](q_\alpha A_{\mathbf{q},\nu} - q_\nu A_{\mathbf{q},\alpha}) - \\ &-\frac{ie^3}{2\hbar^3}\frac{1}{\beta V}\sum_{n,\mathbf{k},\alpha,\beta}(q_\alpha A_{\mathbf{q},\beta} - q_\beta A_{\mathbf{q},\alpha})\times \\ \times&\left\{\mathrm{Tr}[\mathbb{J}_\mu\mathbb{G}_+\mathbb{J}_\alpha\mathbb{G}_+\mathbb{J}_\nu\mathbb{G}\mathbb{J}_\beta\mathbb{G}] + \mathrm{Tr}[\mathbb{J}_\mu\mathbb{G}_+\mathbb{J}_\nu\mathbb{G}\mathbb{J}_\alpha\mathbb{G}\mathbb{J}_\beta\mathbb{G}] + \mathrm{Tr}[\mathbb{J}_\mu\mathbb{G}_+\mathbb{J}_\alpha\mathbb{G}_+\mathbb{J}_\beta\mathbb{G}_+\mathbb{J}_\nu\mathbb{G}]\right\}.\end{aligned} \tag{B.3.8}$$

In this final expression we can substitute $q_\alpha A^q_\beta - q_\beta A^q_\alpha$ with $\varepsilon_{\alpha\beta z}B$ as explained in Eq. (B.1.9).

To get the expressions in the main part of the dissertation in Eqs. (4.2.1a) and (4.2.1b) some transformations are needed. Using the Ward identity and partial integrations, for example, the following identity holds:

$$\sum_{\mathbf{k}}\mathbb{J}_x\mathbb{G}_+\mathbb{J}_y\mathbb{G}\mathbb{J}_x\mathbb{G}\mathbb{J}_y\mathbb{G} = -\sum_{\mathbf{k}}\frac{\hbar^2}{m}\mathbb{J}_x\mathbb{G}_+\mathbb{G}\mathbb{J}_x\mathbb{G} + \mathbb{J}_x\mathbb{G}_+\mathbb{J}_y\mathbb{G}_+\mathbb{J}_y\mathbb{G}\mathbb{J}_x\mathbb{G} + \mathbb{J}_x\mathbb{G}_+\mathbb{J}_y\mathbb{G}\mathbb{J}_y\mathbb{G}\mathbb{J}_x\mathbb{G}\,. \tag{B.3.9}$$

Using other similar identities to this one, we get a more compact expression for the Hall conductivity and longitudinal conductivity:

$$\Pi^{(1)}_{xy}(i\omega_\lambda) = -\frac{ieB}{\beta V}\sum_{n,\mathbf{k}}\mathrm{Tr}[\mathbb{J}_x\mathbb{G}_+\mathbb{J}_y\mathbb{G}\mathbb{J}_x\mathbb{G}\mathbb{J}_y\mathbb{G} - \mathbb{J}_x\mathbb{G}_+\mathbb{J}_y\mathbb{G}_+\mathbb{J}_x\mathbb{G}_+\mathbb{J}_y\mathbb{G}]\,, \tag{B.3.10a}$$

$$\Pi^{(1)}_{zz}(i\omega_\lambda) = -\frac{ieB}{\beta V}\sum_{n,\mathbf{k}}\mathrm{Tr}[\mathbb{J}_z\mathbb{G}_+\mathbb{J}_z\mathbb{G}\mathbb{J}_x\mathbb{G}\mathbb{J}_y\mathbb{G} - \mathbb{J}_z\mathbb{G}_+\mathbb{J}_y\mathbb{G}_+\mathbb{J}_x\mathbb{G}_+\mathbb{J}_z\mathbb{G}]\,. \tag{B.3.10b}$$

Bibliography

[1] L. Boltzmann, "Weitere Studien über das Wärmegleichgewicht unter Gasmolekülen," Sitz.-Ber. Akad. Wiss. Wien (II) **66**, 275–370 (1872).

[2] J. Sólyom, *Electronic Properties*, Fundamentals of the Physics of Solids, Vol. II. (Springer, 2009).

[3] M. V. Berry, "Quantal phase factors accompanying adiabatic changes," Proc. R. Soc. London. A. Math. Phys. Sci. **392**, 45–57 (1984).

[4] M. C. Chang and Q. Niu, "Berry phase, hyperorbits, and the Hofstadter spectrum," Phys. Rev. Lett. **75**, 1348–1351 (1995).

[5] M.-C. Chang and Q. Niu, "Berry phase, hyperorbits, and the Hofstadter spectrum: Semiclassical dynamics in magnetic Bloch bands," Phys. Rev. B **53**, 7010–7023 (1996).

[6] G. Sundaram and Q. Niu, "Wave-packet dynamics in slowly perturbed crystals: gradient corrections and Berry-phase effects," Phys. Rev. B **59**, 14915–14925 (1999).

[7] M.-C. Chang and Q. Niu, "Berry curvature, orbital moment, and effective quantum theory of electrons in electromagnetic fields," Journal of Physics: Condensed Matter **20**, 193202 (2008).

[8] D. Xiao, M.-C. Chang, and Q. Niu, "Berry phase effects on electronic properties," Rev. Mod. Phys. **82**, 1959–2007 (2010).

[9] T. Jungwirth, Q. Niu, and A. H. MacDonald, "Anomalous Hall Effect in Ferromagnetic Semiconductors," Phys. Rev. Lett. **88**, 4 (2002).

[10] N. Nagaosa, J. Sinova, S. Onoda, A. H. MacDonald, and N. P. Ong, "Anomalous Hall effect," Rev. Mod. Phys. **82**, 1539–1592 (2010).

[11] D. Xiao, J. Shi, and Q. Niu, "Berry phase correction to electron density of states in solids," Phys. Rev. Lett. **95**, 137204 (2005).

[12] K.-S. Kim, H.-J. Kim, and M. Sasaki, "Boltzmann equation approach to anomalous transport in a Weyl metal," Phys. Rev. B **89**, 195137 (2014).

[13] S. K. Yip, "Kinetic equation and magneto-conductance for Weyl metal in the clean limit," (2015), arXiv:1508.01010 .

[14] T. Morimoto, S. Zhong, J. Orenstein, and J. E. Moore, "Semiclassical theory of nonlinear magneto-optical responses with applications to topological Dirac/Weyl semimetals," Phys. Rev. B **94**, 245121 (2016).

[15] Y. Gao, S. A. Yang, and Q. Niu, "Intrinsic relative magnetoconductivity of nonmagnetic metals," Phys. Rev. B **95**, 165135 (2017).

[16] S. Nandy, A. Taraphder, and S. Tewari, "Berry phase theory of planar Hall effect in topological insulators," Sci. Rep. **8**, 1–9 (2018).

[17] H.-P. Sun and H.-Z. Lu, "Quantum transport in topological semimetals under magnetic fields (II)," Front. Phys. **14**, 33405 (2019).

[18] G. D. Mahan, *Many-Particle Physics* (Springer US, 2000).

[19] H. Bruus and K. Flensberg, *Many-Body Quantum Theory in Condensed Matter Physics: An Introduction* (Oxford University Press, 2004).

[20] R. Kubo, "Statistical-Mechanical Theory of Irreversible Processes. I. General Theory and Simple Applications to Magnetic and Conduction Problems," J. Phys. Soc. Jpn. **12**, 570–586 (1957).

[21] J. M. Luttinger, "Theory of Thermal Transport Coefficients," Phys. Rev. **135**, A1505–A1514 (1964).

[22] L. Smrčka and P. Středa, "Transport coefficients in strong magnetic fields," J. Phys. C Solid State Phys. **10**, 2153–2161 (1977).

[23] T. Qin, Q. Niu, and J. Shi, "Energy magnetization and the thermal Hall effect," Phys. Rev. Lett. **107**, 1–5 (2011).

[24] M. Ogata and H. Fukuyama, "Range of Validity of Sommerfeld-Bethe Relation Associated with Seebeck Coefficient and Phonon Drag Contribution," J. Phys. Soc. Japan **88**, 74703 (2019).

[25] H. Matsuura, H. Maebashi, M. Ogata, and H. Fukuyama, "Effect of Phonon Drag on Seebeck Coefficient Based on Linear Response Theory: Application to $FeSb_2$," J. Phys. Soc. Japan **88**, 74601 (2019).

[26] M. Jonson and G. D. Mahan, "Mott's formula for the thermopower and the Wiedemann-Franz law," Phys. Rev. B **21**, 4223–4229 (1980).

[27] H. Kontani, "General formula for the thermoelectric transport phenomena based on Fermi liquid theory: Thermoelectric power, Nernst coefficient, and thermal conductivity," Phys. Rev. B **67**, 014408 (2003).

[28] R. Karplus and J. M. Luttinger, "Hall Effect in Ferromagnetics," Phys. Rev. **95**, 1154–1160 (1954).

[29] N. A. Sinitsyn, A. H. MacDonald, T. Jungwirth, V. K. Dugaev, and J. Sinova, "Anomalous Hall effect in a two-dimensional Dirac band: The link between the Kubo-Streda formula and the semiclassical Boltzmann equation approach," Phys. Rev. B **75**, 045315 (2007).

[30] H. Fukuyama, H. Ebisawa, and Y. Wada, "Theory of Hall Effect. I," Prog. Theor. Phys. **42**, 494–511 (1969).

[31] H. Fukuyama, "Theory of Hall Effect. II," Prog. Theor. Phys. **42**, 1284–1303 (1969).

[32] L. Landau, "Diamagnetismus der Metalle," Z. Phys. **64**, 629–637 (1930).

[33] R. Peierls, "Zur Theorie des Diamagnetismus von Leitungselektronen," Z. Phys. **80**, 763–791 (1933).

[34] J. E. Hebborn, J. M. Luttinger, E. H. Sondheimer, and P. J. Stiles, "The orbital diamagnetic susceptibility of Bloch electrons," J. Phys. Chem. Solids **25**, 741–749 (1964).

[35] H. Fukuyama and R. Kubo, "Interband Effect on Magnetic Susceptibility. I. a Simple Two-Band Model," J. Phys. Soc. Jpn. **27**, 604–614 (1969).

[36] H. Fukuyama and R. Kubo, "Interband Effects on Magnetic Susceptibility. II. Diamagnetism of Bismuth," J. Phys. Soc. Jpn. **28**, 570–581 (1970).

[37] H. Fukuyama, "Theory of Orbital Magnetism of Bloch Electrons: Coulomb Interactions," Prog. Theor. Phys. **45**, 704–729 (1971).

[38] M. Ogata and H. Fukuyama, "Orbital Magnetism of Bloch Electrons I. General Formula," J. Phys. Soc. Jpn. **84**, 124708 (2015).

[39] M. Ogata, "Orbital magnetism of Bloch electrons: II. Application to single-band models and corrections to Landau-Peierls susceptibility," J. Phys. Soc. Jpn. **85**, 064709 (2016).

[40] M. Ogata, "Orbital magnetism of Bloch electrons: III. Application to graphene," J. Phys. Soc. Jpn. **85**, 104708 (2016).

[41] L. D. Landau and E. M. Lifshitz, *Quantum Mechanics: Non-Relativistic Theory* (Pergamon Press, 1965).

[42] N. H. Shon and T. Ando, "Quantum Transport in Two-Dimensional Graphite System," J. Phys. Soc. Japan **67**, 2421–2429 (1998).

[43] A. A. Abrikosov, "Quantum magnetoresistance," Phys. Rev. B **58**, 2788–2794 (1998).

[44] P. A. M. Dirac, "The Quantum Theory of the Electron," Proc. R. Soc. A Math. Phys. Eng. Sci. **117**, 610–624 (1928).

[45] H. Weyl, "Elektron und Gravitation. I," Z. Phys. **56**, 330–352 (1929).

[46] K. S. Novoselov, A. K. Geim, S. Morozov, D. Jiang, Y. Zhang, S. V. Dubonos, I. V. Grigorieva, and A. A. Firsov, "Electric Field Effect in Atomically Thin Carbon Films," Science **306**, 666–669 (2004).

[47] J. Wang, S. Deng, Z. Liu, and Z. Liu, "The rare two-dimensional materials with Dirac cones," Natl. Sci. Rev. **2**, 22–39 (2015).

[48] S. M. Young, S. Zaheer, J. C. Y. Teo, C. L. Kane, E. J. Mele, and A. M. Rappe, "Dirac Semimetal in Three Dimensions," Phys. Rev. Lett. **108**, 140405 (2012).

[49] Z. Wang, H. Weng, Q. Wu, X. Dai, and Z. Fang, "Three-dimensional Dirac semimetal and quantum transport in Cd_3As_2," Phys. Rev. B **88**, 125427 (2013).

[50] B. J. Yang and N. Nagaosa, "Classification of stable three-dimensional Dirac semimetals with nontrivial topology," Nat. Commun. **5**, 4898 (2014).

[51] N. P. Armitage, E. J. Mele, and A. Vishwanath, "Weyl and Dirac semimetals in three-dimensional solids," Rev. Mod. Phys. **90**, 015001 (2018).

[52] A. Bernevig, H. Weng, Z. Fang, and X. Dai, "Recent Progress in the Study of Topological Semimetals," J. Phys. Soc. Japan **87**, 041001 (2018).

[53] C.-K. Chiu, J. C. Y. Teo, A. P. Schnyder, and S. Ryu, "Classification of topological quantum matter with symmetries," Rev. Mod. Phys. **88**, 035005 (2016).

[54] P. Wolff, "Matrix elements and selection rules for the two-band model of bismuth," J. Phys. Chem. Solids **25**, 1057–1068 (1964).

[55] Y. Fuseya, M. Ogata, and H. Fukuyama, "Transport Properties and Diamagnetism of Dirac Electrons in Bismuth," J. Phys. Soc. Japan **84**, 012001 (2015).

[56] T. Kariyado and M. Ogata, "Three-Dimensional Dirac Electrons at the Fermi Energy in Cubic Inverse Perovskites: Ca_3PbO and Its Family," J. Phys. Soc. Japan **80**, 083704 (2011).

[57] T. Kariyado and M. Ogata, "Low-Energy Effective Hamiltonian and the Surface States of Ca_3PbO," J. Phys. Soc. Japan **81**, 064701 (2012).

[58] T. Kariyado and M. Ogata, "Evolution of band topology by competing band overlap and spin-orbit coupling: Twin Dirac cones in Ba_3SnO as a prototype," Phys. Rev. Mater. **1**, 061201 (2017).

[59] M. Orlita, B. Piot, G. Martinez, N. S. Kumar, C. Faugeras, M. Potemski, C. Michel, E. Hankiewicz, T. Brauner, Č. Drašar, S. Schreyeck, S. Grauer, K. Brunner, C. Gould, C. Brüne, and L. Molenkamp, "Magneto-Optics of Massive Dirac Fermions in Bulk Bi_2Se_3," Phys. Rev. Lett. **114**, 186401 (2015).

[60] Z.-G. Chen, R. Y. Chen, R. D. Zhong, J. Schneeloch, C. Zhang, Y. Huang, F. Qu, R. Yu, Q. Li, G. D. Gu, and N. L. Wang, "Spectroscopic evidence for bulk-band inversion and three-dimensional massive Dirac fermions in $ZrTe_5$," Proc. Natl. Acad. Sci. U. S. A. **114**, 816–821 (2017).

[61] B. Fu, H. W. Wang, and S. Q. Shen, "Quantum magnetotransport in massive Dirac materials," Phys. Rev. B **101**, 125203 (2020).

[62] P. R. Wallace, "The band theory of graphite," Phys. Rev. **71**, 622–634 (1947).

[63] M. Neupane, S. Y. Xu, R. Sankar, N. Alidoust, G. Bian, C. Liu, I. Belopolski, T. R. Chang, H. T. Jeng, H. Lin, A. Bansil, F. Chou, and M. Z. Hasan, "Observation of a three-dimensional topological Dirac semimetal phase in high-mobility Cd_3As_2," Nat. Commun. **5**, 3786 (2014).

[64] S. Borisenko, Q. Gibson, D. Evtushinsky, V. Zabolotnyy, B. Büchner, and R. J. Cava, "Experimental realization of a three-dimensional dirac semimetal," Phys. Rev. Lett. **113**, 027603 (2014).

[65] H. Yi, Z. Wang, C. Chen, Y. Shi, Y. Feng, A. Liang, Z. Xie, S. He, J. He, Y. Peng, X. Liu, Y. Liu, L. Zhao, G. Liu, X. Dong, J. Zhang, M. Nakatake, M. Arita, K. Shimada, H. Namatame, M. Taniguchi, Z. Xu, C. Chen, X. Dai, Z. Fang, and X. J. Zhou, "Evidence of topological surface state in three-dimensional dirac semimetal Cd_3As_2," Sci. Rep. **4**, 6106 (2014).

[66] Z. K. Liu, J. Jiang, B. Zhou, Z. J. Wang, Y. Zhang, H. M. Weng, D. Prabhakaran, S.-K. S.-K. Mo, H. Peng, P. Dudin, T. Kim, M. Hoesch, Z. Fang, X. Dai, Z. X. Shen, D. L. Feng, Z. Hussain, and Y. L. Chen, "A stable three-dimensional topological Dirac semimetal Cd_3As2," Nat. Mater. **13**, 677–681 (2014).

[67] S. Jeon, B. B. Zhou, A. Gyenis, B. E. Feldman, I. Kimchi, A. C. Potter, Q. D. Gibson, R. J. Cava, A. Vishwanath, and A. Yazdani, "Landau quantization and quasiparticle interference in the three-dimensional Dirac semimetal Cd_3As_2," Nat. Mater. **13**, 851–856 (2014).

[68] L. P. He, X. C. Hong, J. K. Dong, J. Pan, Z. Zhang, J. Zhang, and S. Y. Li, "Quantum Transport Evidence for the Three-Dimensional Dirac Semimetal Phase in Cd_3As_2," Phys. Rev. Lett. **113**, 246402 (2014).

[69] T. Liang, Q. Gibson, M. N. Ali, M. Liu, R. J. Cava, and N. P. Ong, "Ultrahigh mobility and giant magnetoresistance in the Dirac semimetal Cd_3As_2," Nat. Mater. **14**, 280–284 (2015).

[70] I. Crassee, R. Sankar, W.-L. Lee, A. Akrap, and M. Orlita, "3D Dirac semimetal Cd_3As_2: A review of material properties," Phys. Rev. Mater. **2**, 120302 (2018).

[71] Z. Wang, Y. Sun, X. Q. Chen, C. Franchini, G. Xu, H. Weng, X. Dai, and Z. Fang, "Dirac semimetal and topological phase transitions in A_3Bi (A=Na, K, Rb)," Phys. Rev. B **85**, 195320 (2012).

[72] Z. K. Liu, B. Zhou, Y. Zhang, Z. J. Wang, H. M. Weng, D. Prabhakaran, S.-K. Mo, Z. X. Shen, Z. Fang, X. Dai, Z. Hussain, and Y. L. Chen, "Discovery of a three-dimensional topological Dirac semimetal, Na_3Bi." Science **343**, 864–7 (2014).

[73] S. Y. Xu, C. Liu, S. K. Kushwaha, R. Sankar, J. W. Krizan, I. Belopolski, M. Neupane, G. Bian, N. Alidoust, T. R. Chang, H. T. Jeng, C. Y. Huang, W. F. Tsai, H. Lin, P. P. Shibayev, F. C. Chou, R. J. Cava, and M. Z. Hasan, "Observation of Fermi arc surface states in a topological metal," Science **347**, 294–298 (2015).

[74] S. K. Kushwaha, J. W. Krizan, B. E. Feldman, A. Gyenis, M. T. Randeria, J. Xiong, S. Y. Xu, N. Alidoust, I. Belopolski, T. Liang, M. Zahid Hasan, N. P. Ong, A. Yazdani, and R. J. Cava, "Bulk crystal growth and electronic characterization of the 3D Dirac semimetal Na_3Bi," APL Mater. **3**, 041504 (2015).

[75] B. Q. Lv, H. M. Weng, B. B. Fu, X. P. Wang, H. Miao, J. Ma, P. Richard, X. C. Huang, L. X. Zhao, G. F. Chen, Z. Fang, X. Dai, T. Qian, and H. Ding, "Experimental discovery of weyl semimetal TaAs," Phys. Rev. X **5**, 031013 (2015).

[76] S.-Y. Xu, I. Belopolski, N. Alidoust, M. Neupane, G. Bian, C. Zhang, R. Sankar, G. Chang, Z. Yuan, C.-C. Lee, S.-M. Huang, H. Zheng, J. Ma, D. S. Sanchez, B. Wang, A. Bansil, F. Chou, P. P. Shibayev, H. Lin, S. Jia, and M. Z. Hasan, "Discovery of a Weyl fermion semimetal and topological Fermi arcs," Science **349**, 613–617 (2015).

[77] S. Y. Xu, N. Alidoust, I. Belopolski, Z. Yuan, G. Bian, T. R. Chang, H. Zheng, V. N. Strocov, D. S. Sanchez, G. Chang, C. Zhang, D. Mou, Y. Wu, L. Huang,

C. C. Lee, S. M. Huang, B. Wang, A. Bansil, H. T. Jeng, T. Neupert, A. Kaminski, H. Lin, S. Jia, and M. Z. Hasan, "Discovery of a Weyl fermion state with Fermi arcs in niobium arsenide," Nat. Phys. **11**, 748–754 (2015).

[78] H. Xiong, J. A. Sobota, S. L. Yang, H. Soifer, A. Gauthier, M. H. Lu, Y. Y. Lv, S. H. Yao, D. Lu, M. Hashimoto, P. S. Kirchmann, Y. F. Chen, and Z. X. Shen, "Three-dimensional nature of the band structure of $ZrTe_5$ measured by high-momentum-resolution photoemission spectroscopy," Phys. Rev. B **95**, 195119 (2017).

[79] B. Xu, L. X. Zhao, P. Marsik, E. Sheveleva, F. Lyzwa, Y. M. Dai, G. F. Chen, X. G. Qiu, and C. Bernhard, "Temperature-Driven Topological Phase Transition and Intermediate Dirac Semimetal Phase in $ZrTe_5$," Phys. Rev. Lett. **121**, 187401 (2018).

[80] W. Zhang, P. Wang, B. Skinner, R. Bi, V. Kozii, C. W. Cho, R. Zhong, J. Schneeloch, D. Yu, G. Gu, L. Fu, X. Wu, and L. Zhang, "Observation of a thermoelectric Hall plateau in the extreme quantum limit," Nat. Commun. **11**, 1–5 (2020).

[81] S. Suetsugu, K. Hayama, A. W. Rost, J. Nuss, C. Mühle, J. Kim, K. Kitagawa, and H. Takagi, "Magnetotransport in Sr_3PbO antiperovskite," Phys. Rev. B **98**, 115203 (2018).

[82] P. Dziawa, B. J. Kowalski, K. Dybko, R. Buczko, A. Szczerbakow, M. Szot, E. Łusakowska, T. Balasubramanian, B. M. Wojek, M. H. Berntsen, O. Tjernberg, and T. Story, "Topological crystalline insulator states in $Pb_{1-x}Sn_xSe$," Nat. Mater. **11**, 1023–1027 (2012).

[83] T. Liang, Q. Gibson, J. Xiong, M. Hirschberger, S. P. Koduvayur, R. Cava, and N. Ong, "Evidence for massive bulk Dirac fermions in $Pb_{1-x}Sn_xSe$ from Nernst and thermopower experiments," Nat. Commun. **4**, 2696 (2013).

[84] J. Hu, S.-Y. Xu, N. Ni, and Z. Mao, "Transport of Topological Semimetals," Annu. Rev. Mater. Res. **49**, 207–252 (2019).

[85] S. Wang, B.-C. Lin, A.-Q. Wang, D.-P. Yu, and Z.-M. Liao, "Quantum transport in Dirac and Weyl semimetals: a review," Adv. Phys. X **2**, 518–544 (2017).

[86] H. Nielsen and M. Ninomiya, "The Adler-Bell-Jackiw anomaly and Weyl fermions in a crystal," Phys. Lett. B **130**, 389–396 (1983).

[87] S. L. Adler, "Axial-vector vertex in spinor electrodynamics," Phys. Rev. **177**, 2426–2438 (1969).

[88] J. S. Bell and R. Jackiw, "A PCAC puzzle: $\pi^0 \to \gamma\gamma$ in the σ-model," Nuovo Cim. A **60**, 47–61 (1969).

[89] X. Huang, L. Zhao, Y. Long, P. Wang, D. Chen, Z. Yang, H. Liang, M. Xue, H. Weng, Z. Fang, X. Dai, and G. Chen, "Observation of the Chiral-Anomaly-Induced Negative Magnetoresistance in 3D Weyl Semimetal TaAs," Phys. Rev. X **5**, 031023 (2015).

[90] A. C. Niemann, J. Gooth, S. C. Wu, S. Bäßler, P. Sergelius, R. Hühne, B. Rellinghaus, C. Shekhar, V. Süß, M. Schmidt, C. Felser, B. Yan, and K. Nielsch, "Chiral magnetoresistance in the Weyl semimetal NbP," Sci. Rep. **7**, 3–8 (2017).

[91] A. Narayanan, M. D. Watson, S. F. Blake, N. Bruyant, L. Drigo, Y. L. Chen, D. Prabhakaran, B. Yan, C. Felser, T. Kong, P. C. Canfield, and A. I. Coldea, "Linear magnetoresistance caused by mobility fluctuations in n-doped Cd_3As_2," Phys. Rev. Lett. **114**, 117201 (2015).

[92] J. Feng, Y. Pang, D. Wu, Z. Wang, H. Weng, J. Li, X. Dai, Z. Fang, Y. Shi, and L. Lu, "Large linear magnetoresistance in Dirac semimetal Cd_3As_2 with Fermi surfaces close to the Dirac points," Phys. Rev. B **92**, 081306 (2015).

[93] M. Novak, S. Sasaki, K. Segawa, and Y. Ando, "Large linear magnetoresistance in the Dirac semimetal TlBiSSe," Phys. Rev. B **91**, 041203 (2015).

[94] Y. Zhao, H. Liu, C. Zhang, H. Wang, J. Wang, Z. Lin, Y. Xing, H. Lu, J. Liu, Y. Wang, S. M. Brombosz, Z. Xiao, S. Jia, X. C. Xie, and J. Wang, "Anisotropic fermi surface and quantum limit transport in high mobility three-dimensional dirac semimetal Cd_3As_2," Phys. Rev. X **5**, 031037 (2015).

[95] I. A. Leahy, Y.-P. Lin, P. E. Siegfried, A. C. Treglia, J. C. W. Song, R. M. Nandkishore, and M. Lee, "Nonsaturating large magnetoresistance in semimetals," Proc. Natl. Acad. Sci. **115**, 10570–10575 (2018).

[96] F. Han, N. Andrejevic, T. Nguyen, V. Kozii, Q. Nguyen, Z. Ding, R. Pablo-Pedro, S. Parjan, B. Skinner, A. Alatas, E. Alp, S. Chi, J. Fernandez-Baca, S. Huang, L. Fu, and M. Li, "Discovery of Giant, Non-saturating Thermopower in Topological Semimetal at Quantum Limit," (2019), arXiv:1904.03179 .

[97] H. Wang, X. Luo, K. Peng, Z. Sun, M. Shi, D. Ma, N. Wang, T. Wu, J. Ying, Z. Wang, and X. Chen, "Magnetic Field-Enhanced Thermoelectric Performance in Dirac Semimetal Cd_3As_2 Crystals with Different Carrier Concentrations," Adv. Funct. Mater. **29**, 1902437 (2019).

[98] T. Liang, J. Lin, Q. Gibson, T. Gao, M. Hirschberger, M. Liu, R. J. Cava, and N. P. Ong, "Anomalous Nernst Effect in the Dirac Semimetal Cd_3As_2," Phys. Rev. Lett. **118**, 136601 (2017).

[99] F. Caglieris, C. Wuttke, S. Sykora, V. Süss, C. Shekhar, C. Felser, B. Büchner, and C. Hess, "Anomalous Nernst effect and field-induced Lifshitz transition in the Weyl semimetals TaP and TaAs," Phys. Rev. B **98**, 201107 (2018).

[100] J. S. Xiang, S. L. Hu, M. Lyu, W. L. Zhu, C. Y. Ma, Z. Y. Chen, F. Steglich, G. F. Chen, and P. J. Sun, "Large transverse thermoelectric figure of merit in a topological Dirac semimetal," Sci. China Physics, Mech. Astron. **63**, 1–7 (2020).

[101] G. Sharma, P. Goswami, and S. Tewari, "Nernst and magnetothermal conductivity in a lattice model of Weyl fermions," Phys. Rev. B **93**, 035116 (2016).

[102] G. Sharma, C. Moore, S. Saha, and S. Tewari, "Nernst effect in Dirac and inversion-asymmetric Weyl semimetals," Phys. Rev. B **96**, 195119 (2017).

[103] R. Lundgren, P. Laurell, and G. A. Fiete, "Thermoelectric properties of Weyl and Dirac semimetals," Phys. Rev. B **90**, 165115 (2014).

[104] E. V. Gorbar, V. A. Miransky, I. A. Shovkovy, and P. O. Sukhachov, "Anomalous thermoelectric phenomena in lattice models of multi-Weyl semimetals," Phys. Rev. B **96**, 1–20 (2017).

[105] E. V. Gorbar, V. A. Miransky, I. A. Shovkovy, and P. O. Sukhachov, "Anomalous transport properties of Dirac and Weyl semimetals (Review Article)," Low Temp. Phys. **44**, 487–505 (2018).

[106] K. Das and A. Agarwal, "Linear magnetochiral transport in tilted type-I and type-II Weyl semimetals," Phys. Rev. B **99**, 085405 (2019).

[107] D. Ma, H. Jiang, H. Liu, and X. C. Xie, "Planar Hall effect in tilted Weyl semimetals," Phys. Rev. B **99**, 115121 (2019).

[108] T. M. McCormick, R. C. McKay, and N. Trivedi, "Semiclassical theory of anomalous transport in type-II topological Weyl semimetals," Phys. Rev. B **96**, 235116 (2017).

[109] Y. Ferreiros, A. A. Zyuzin, and J. H. Bardarson, "Anomalous Nernst and thermal Hall effects in tilted Weyl semimetals," Phys. Rev. B **96**, 115202 (2017).

[110] S. Saha and S. Tewari, "Anomalous Nernst effect in type-II Weyl semimetals," Eur. Phys. J. B **91**, 4 (2018).

[111] G. Sharma and S. Tewari, "Transverse thermopower in Dirac and Weyl semimetals," Phys. Rev. B **100**, 195113 (2019).

[112] H. Fukuyama, "Anomalous orbital magnetism and hall effect of massless fermions in two dimension," J. Phys. Soc. Jpn. **76**, 043711 (2007).

[113] T. Ando, "Formula of weak-field magnetoresistance in graphene," J. Phys. Soc. Jpn. **88**, 014704 (2019).

[114] X. Xiao, K. T. Law, and P. A. Lee, "Magnetoconductivity in Weyl semimetals: Effect of chemical potential and temperature," Phys. Rev. B **96**, 165101 (2017).

[115] J. Klier, I. V. Gornyi, and A. D. Mirlin, "Transversal magnetoresistance in Weyl semimetals," Phys. Rev. B **92**, 205113 (2015).

[116] J. Klier, I. V. Gornyi, and A. D. Mirlin, "Transversal magnetoresistance and Shubnikov-de Haas oscillations in Weyl semimetals," Phys. Rev. B **96**, 214209 (2017).

[117] B. Skinner and L. Fu, "Large, nonsaturating thermopower in a quantizing magnetic field," Sci. Adv. **4**, eaat2621 (2018).

[118] V. Canuto and C. Chiuderi, "Transverse Electrical Conductivity of a Relativistic Gas in an Intense Magnetic Field," Phys. Rev. D **1**, 2219–2226 (1970).

[119] A. D. Kaminker and D. G. Yakovlev, "Description of a relativistic electron in a quantizing magnetic field. Transverse transport coefficients of an electron gas," Theor. Math. Phys. **49**, 1012–1020 (1981).

[120] H.-W. Wang, B. Fu, and S.-Q. Shen, "Intrinsic magnetoresistance in three-dimensional Dirac materials with low carrier density," Phys. Rev. B **98**, 081202 (2018).

[121] I. Proskurin, M. Ogata, and Y. Suzumura, "Longitudinal conductivity of a three-dimensional Dirac electron gas in magnetic field," J. Phys. Conf. Ser. **603**, 012009 (2015).

[122] V. Könye and M. Ogata, "Microscopic theory of magnetoconductivity at low magnetic fields in terms of Berry curvature and orbital magnetic moment," (2020), arXiv:2006.15882 .

[123] V. Könye and M. Ogata, "Magnetoresistance of a three-dimensional Dirac gas," Phys. Rev. B **98**, 195420 (2018).

[124] V. Könye and M. Ogata, "Thermoelectric transport coefficients of a Dirac electron gas in high magnetic fields," Phys. Rev. B **100**, 155430 (2019).

[125] L. L. Foldy and S. A. Wouthuysen, "On the dirac theory of spin 1/2 particles and its non-relativistic limit," Phys. Rev. **78**, 29–36 (1950).

[126] M. Jonson and G. D. Mahan, "Electron-phonon contribution to the thermopower of metals," Phys. Rev. B **42**, 9350–9356 (1990).

[127] S. Balasubramanian, "A note on the generalized Hellmann-Feynman theorem," Am. J. Phys. **58**, 1204–1205 (1990).

[128] A. A. Zyuzina and R. P. Tiwari, "Intrinsic anomalous Hall effect in type-II Weyl semimetals," JETP Lett. **103**, 717–722 (2016).

[129] S. Katayama, A. Kobayashi, and Y. Suzumura, "Pressure-induced zero-gap semiconducting state in organic conductor α-(BEDT-TTF)$_2$I$_3$ salt," J. Phys. Soc. Japan **75**, 054705 (2006).

[130] A. Kobayashi, Y. Suzumura, and H. Fukuyama, "Hall effect and orbital diamagnetism in zerogap state of molecular conductor α-(BEDT-TTF)$_2$I$_3$," J. Phys. Soc. Japan **77**, 064718 (2008).

[131] M. O. Goerbig, J. N. Fuchs, G. Montambaux, and F. Piéchon, "Tilted anisotropic Dirac cones in quinoid-type graphene and α- (BEDT-TTF)$_2$I$_3$," Phys. Rev. B **78**, 045415 (2008).

[132] A. A. Soluyanov, D. Gresch, Z. Wang, Q. Wu, M. Troyer, X. Dai, and B. A. Bernevig, "Type-II Weyl semimetals," Nature **527**, 495–498 (2015).

[133] P. E. C. Ashby and J. P. Carbotte, "Theory of magnetic oscillations in Weyl semimetals," Eur. Phys. J. B **87**, 92 (2014).

[134] D. H. D. Bailey and P. P. N. Swarztrauber, "A Fast Method for the Numerical Evaluation of Continuous Fourier and Laplace Transforms," SIAM J. Sci. Comput. **15**, 1–8 (1994).

[135] J. M. Luttinger and W. Kohn, "Motion of Electrons and Holes in Perturbed Periodic Fields," Phys. Rev. **97**, 869–883 (1955).